Aviation Induced Tropospheric Ozone

Sartaj Singh

Delft University of Technology

TU Delft

Aviation Induced Tropospheric Ozone

by

Sartaj Singh

in partial fulfillment of the requirements for the degree of

Master of Science

in Aerospace Engineering

at the Delft University of Technology,

to be defended publicly on Thursday October 9th 2025.

Student number:	4660951	
Project duration:	February 24, 2025 – September 10, 2025	
Equivalent Word Count:	43742 Words	
Thesis committee:	Dr. M. Mertens,	TU Delft, supervisor
	Prof. dr. V. Grewe,	TU Delft
	Dr. F. de Domenico	TU Delft

An electronic version of this thesis is available at http://repository.tudelft.nl/.

Cover: Image generated by Sartaj Singh using OpenAI's DALLE model

TU Delft

Preface

This thesis is written to obtain my master's degree in Aerospace Engineering from the Delft University of Technology. As a student in the track Flight Performance and Propulsion, I was always strongly interested in learning about the various climate effects of aviation. Thus, I am happy to having gotten the opportunity to work with climate chemistry model data provided by the German Aerospace Center (DLR). Learning about aviation NO_x emissions has been eye opening and has given me the pleasure to learn about the complex chemistry and physics which drive the presence of greenhouse gases globally.

I would like to express my gratitude towards Volker and Mariano, for allowing me to conduct this research under their supervision. It was an honour to work with and learn from both of my supervisors. I would also like to thank all of my friends and family for their constant support across my many years of studying at the TU Delft. Nearing my graduation, I look forward to finishing my studies and starting the next phase of my life!

Sartaj Singh
Delft, September 2025

Summary

In recent years, mitigation of the anthropogenic climate impact has become increasingly more important. Over the past decades, the aviation industry has grown significantly, making it a large contributor to greenhouse gases in the atmosphere. One such greenhouse gas is Ozone (O_3) in the troposphere, which has a warming effect on the global climate. Aviation Nitrogen Oxides (NO_x) emissions play a role in the formation and loss of O_3 in the troposphere, however, the chemistry is highly non-linear which makes mitigation more complex. To gain a better understanding of the contribution of aviation to tropospheric O_3, this thesis looks at how aviation's tropospheric O_3 contribution varies and how the Ozone Burden Efficiency (OBE) metric can be used to better explain these global variations. The OBE is a metric which quantifies the efficiency of the background chemistry and the global transportation phenomena to promote the net formation of O_3. To conduct this research, chemistry climate simulation results of the ECHAM/MESSy Atmospheric Chemistry (EMAC) model were used for a period of 2003 to 2018.

The analysis showed that across the simulated time period aviation's contribution to tropospheric O_3 increased from about 1.6% to approximately 1.9%. Looking at the vertical spread of the aviation induced O_3 showed that downwards transport of O_3 drives global distributions, creating large O_3 mixing ratios in the free troposphere under the flight altitudes. Furthermore, the analysis of the vertical spread showed that the percentage contribution of aviation to local O_3 mixing ratios is larger at ground level than at flight altitudes, showing that aviation induced O_3 also contributes to air quality.

Analysing the OBE, showed that the OBE of aviation for the whole troposphere is about 4.5 Tg $(O_3) \cdot$ Tg^{-1} (NO_x). Further analysis showed that the OBE in the planetary boundary layer is about 2.5 Tg $(O_3) \cdot$ Tg^{-1} (NO_x), whereas the OBE at flight altitudes is about 1.3 Tg $(O_3) \cdot$ Tg^{-1} (NO_x). The larger OBE at ground level is caused by the large scale downward transport of the formed O_3 and the low amount of local NO_x emissions, whereas at flight altitudes, the local NO_x emissions are not as small compared to the local O_3 burden. Furthermore, analysis of the OBE metric also shows that the OBE of aviation is largest in the free troposphere below the flight altitudes, where it is estimated to be around 8 Tg $(O_3) \cdot$ Tg^{-1} (NO_x). This result highlights the large amount of O_3 which is transported downwards to lower altitudes from the flight levels. Overall, the analysis using the OBE metric shows that it is most useful for emission sectors where the emissions are dominated by NO_x emissions rather than carbon species which also contribute towards the production of O_3. However, this attribute of the OBE metric makes it difficult to use OBE values to compare different emissions sources.

Contents

List of Figures

List of Symbols

Chemical Species

Ar	Argon
C_2H_6	Ethane
C_3H_6	Propene
CH_3O_2	Methy Peroxy Radical
CH_3OOH	Methyl Hydroperoxide
CH_3O	Methoxy Radical
CH_3	Methyl Radical
CH_4	Methane
CO_2	Carbon Dioxide
CO	Carbon Monoxide
H_2O_2	Hydrogen Peroxide
H_2O	Water
HCHO	Formaldehyde
HNO_3	Nitric Acid
HO_2	Hydroperoxyl Radical
HO_x	Hydrogen Oxides (HO_x = HO_2 + OH)
N_2	Molecular Nitrogen
NO_2	Nitrogen Dioxide
NO_3	Nitrate Radical
NO_x	Nitrogen Oxides (NO_x = NO_2 + NO)
NO	Nitric Oxide
O_2	Molecular Oxygen
O_3	Ozone
OH	Hydroxyl Radical
$O(^1D)$	Excited Oxygen Atom
SO_2	Sulfur Dioxide

Other symbols

Λ	Longitude
λ	Climate Sensitivity Parameter
μ	Mass Mixing Ratio
Ω	Earth's Angular Velocity
ρ	Mass Density
θ	Wavelength
φ	Latitude
$\vec{\tau}$	Shear Stress Tensor
$\vec{g}$	Gravitational Acceleration
$\vec{v}$	Wind Velocity Vector
c_p	Specific Heat at Constant Pressure
c_v	Specific Heat at Constant Volume
E_a	Activation Energy
N_A	Avogadro's constant
T_s	Global Mean Surface Temperature
[X]	Concentration of Species X
A	Pre-Exponential Factor
C	Volume or Molar Mixing Ratio
k	Rate Constant of the Reaction
L	Rate of Loss/Depletion of a Species
M	Molar Mass
M	Third Body Reactant
n	Number Density of a Species
P	Rate of Production of a Species
p	Pressure
R	Universal Gas Constant
r	Distance to Centre of the Earth
s	Local Source Term
T	Temperature
t	Time
VMR	Molar Mixing Ratio

List of Abbreviations

CAM4 Community Atmosphere Model version 4 with Chemistry.

CAMS Copernicus Atmosphere Monitoring Service.

CCMI2 Chemistry Climate Model Initiative Phase 2.

CEDS Community Earth atmospheric Data System.

CESM Community Earth System Model.

CMIP6 Coupled Model Intercomparison Project Phase 6.

DLR German Aerospace Center.

ECMWF European Centre for Medium-Range Weather Forecasts.

EMAC ECHAM/MESSy Atmospheric Chemistry Model.

GFED Global Fire Emissions Database.

GISS Goddard Institute for Space Studies.

ITCZ Intertropical Convergence Zone.

MECCA Module Efficiently Calculating the Chemistry of the Atmosphere.

MESSy Modular Earth Submodel System.

NMHC Non Methane Hydrocarbons.

OBE Ozone Burden Efficiency.

OPE Ozone Production Efficiency.

PMO Primary Mode Ozone.

STE Stratosphere - Troposphere Exchange.

SWV Stratospheric Water Vapor.

TOAR Tropospheric Ozone Assessment Report.

VOC Volatile Organic Compounds.

1

Introduction

In recent years more focus has been shifting towards anthropogenic emissions and the impact that they have on the Earth's climate. Climate change and its consequences have been becoming perceptibly more noticeable with 2024 being the warmest year on record since 1880[1]. This has led to increasingly more initiatives by governments to employ mitigation policies that can address climate change. However, to implement and apply the right mitigation strategies, understanding of the different emission sectors and the different species emitted is required. One of the biggest emission sectors worldwide is the transportation sector, which consists of road traffic, shipping and aviation. Aviation, especially, has been growing very quickly over the past few years, with the emergence of budget airlines such as Ryanair, who offer flights at low prices. This fast growth of the aviation industry has meant that in 2022 aviation accounted for approximately 4% of EU emissions of greenhouse gases. Furthermore, it is estimated that aviation generated approximately 14% of transport emissions, making it the second largest source of greenhouse gases after road transport[2]. This means that understanding how exactly Aviation emissions contribute towards climate change is vital, especially when governing bodies are trying to develop climate change mitigation strategies.

Most aircraft engines are air-breathing jet engines which use air and kerosene as their combustion reactants. The chemical species in the atmosphere take part in the combustion reaction with kerosene and impact the climate effect of aviation. For example, atmospheric Nitrogen (N_2) dissociates in the jet engines due to the high temperatures and reacts with Oxygen (O_2) to form Nitrogen Oxides (NO_x). The primary emissions from aviation are Carbon Dioxide (CO_2) and Water (H_2O) vapour, which are the hydrocarbon complete combustion products. In addition, the combustion reaction also leads to the emissions of species such as NO_x, Sulfur Dioxide (SO_2), Carbon Monoxide (CO), soot and other particulate matter.

The different processes by which aviation contributes to the climate system are shown in Figure 1.1. Figure 1.1 shows that the CO_2 and H_2O vapour emitted by aircraft act as greenhouse gases, leading to an overall warming effect. When aircraft fly through cold and humid air at high altitudes, the interaction of the hot engine exhaust with the surrounding cold air can lead to the formation of contrails, which trap heat within the earth system as shown in Figure 1.1. Finally, NO_x emissions lead to the formation of Ozone (O_3) which is a greenhouse gas, but at the same time NO_x emissions also play a role in reducing

[1] https://climate.nasa.gov/vital-signs/global-temperature/?intent=121#:~:text=Overall%2C%20Earth%20was%20about%202.65,change%20in%20global%20surface%20temperatures. Date accessed 10th August 2025

[2] https://climate.ec.europa.eu/eu-action/transport-decarbonisation/reducing-emissions-aviation_en Date accessed 10th August

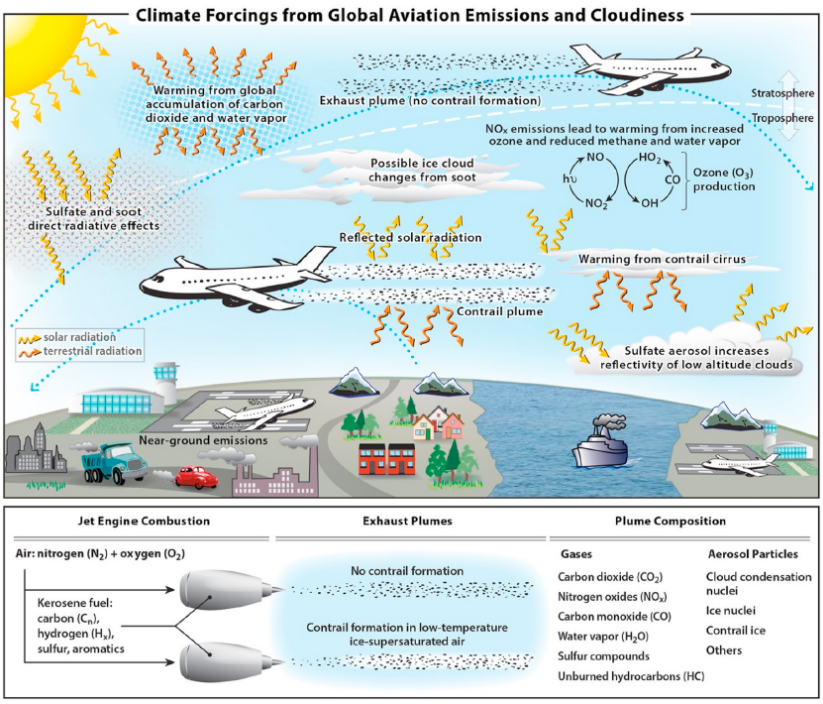

Figure 1.1: Schematic overview of the different processes by which aviation emissions and aviation induced cirrus cloudiness impact the climate system (Lee et al., 2021).

Methane (CH_4) and stratospheric water vapor (SWV) concentrations.

The largest contribution to anthropogenic climate change across all different sectors comes from the production and increase in concentration of CO_2, which is seen as the primary cause of the observed global warming in recent times (IPCC, 2013, 2018). Similarly for aviation the biggest individual climate impact comes from the CO_2 emissions. However, Lee et al. (2021) show that about 66% of the climate impact from aviation comes from non-CO_2 effects, despite this, the impact of non-CO_2 effects is still not fully understood. One of the biggest contributors towards the non-CO_2 effects is the emission of NO_x and its contribution to tropospheric O_3. The chemistry that leads from NO_x emissions to the formation of O_3 in the atmosphere is complex and non-linear. To be able to effectively mitigate the climate impact that arises from increased O_3 concentrations due to aviation NO_x emissions, having an understanding of how aviation contributes to tropospheric O_3 is very important.

Nitrogen oxides (NO_x) emitted from aircraft at an altitude of 10 km or even more, have a large impact on the concentration of tropospheric ozone O_3. The chemistry that leads from NO_x emissions to O_3 burdens is complex and highly non-linear. Depending on the existing background NO_x levels, increases in NO_x concentrations can either lead to O_3 formation or loss, with the rate of change in concentration also being highly variable based on the amount of background NO_x. Combining this background NO_x level effect with atmospheric transport and the Earth's climate response leads to spatial variations across the globe.

Many researchers refer to an Ozone Production Efficiency (OPE), which relates the rate of O_3 production to the precursor emissions. However, Gilmore et al. (2013) have shown that the variation in the OPE does not match the variation in the O_3 perturbation response and that the Ozone Burden Efficiency (OBE) metric could much better explain trends in the O_3 concentrations (Mertens et al., 2024). Unlike the OPE, the OBE does not only account for production of O_3, but it also accounts for all chemical loss pathways. This way, the OBE as a metric can be used to better explain trends and variations in the global O_3 concentrations. Despite this, there is limited literature that looks at the variations in the OBE

in detail and tries to use these variations to explain variations in O_3 concentrations. Thus, the objective of this thesis is as follows:

> *To determine the spatial and temporal variations of ozone burden efficiency and to find relationships between these variations and the variability of ozone due to aviation nitrogen oxides to enhance the understanding of the spatial and temporal patterns of tropospheric ozone.*

To meet the research objective above, the following research questions will be answered throughout this thesis:

Q1 How do aviation NO_x emissions contribute towards tropospheric O_3 levels?

Q2 How does the ozone burden efficiency of aviation emissions vary in the troposphere?

Q3 Can the ozone burden efficiency trends be used to describe trends in tropospheric O_3 levels?

To achieve the research aim and to answer the research questions, this thesis first looks at the composition of the atmosphere and explains how transport processes are driven in Chapter 2. This is followed by a detailed explanation of the NO_x - O_3 chemistry, which dictates the O_3 levels in the troposphere in Chapter 3. Using this background knowledge, trends and variations found in the contribution and impact of aviation emissions on O_3 are looked at in Chapter 4, focussing on the findings of past literature. The methodology used to undertake the analysis in this thesis is explained Chapter 5. The subsequent results from the analysis are discussed in Chapter 6, Chapter 7 and Chapter 8, which leads to the final conclusions and recommendations in Chapter 9.

2

The Atmosphere and atmospheric transport

To answer the research questions in this thesis, having an understanding of the structure and the constituents of the atmosphere is vital. The atmosphere heavily contributes towards the transport of chemical species and emissions across the globe, which drives the heterogeneous distribution of greenhouse gases such as O_3 and their precursors. This chapter describes the atmosphere, its constituents and layers in Section 2.1 and the atmospheric transport mechanisms in Section 2.2. The content in this chapter, is primarily based on the work by Seinfeld (2016).

2.1 The atmosphere and its layers

Earth's atmosphere primarily consists of the Nitrogen (N_2 - 78%), Oxygen (O_2 - 21%) and Argon (Ar - 1%) (Seinfeld, 2016). Water vapour (H_2O) is the next most abundant constituent and is primarily found in the lower atmosphere, but its concentration varies highly, with local concentrations ranging up to 3%. Trace gases are the remaining constituents which represent less than 1% of the atmosphere. However, these trace gases play a crucial role in the Earth's radiative balance and in the chemical properties of the atmosphere. In the atmosphere, solar light is the driving force for chemical processes. This solar radiation interacts with many molecules in the atmosphere and is a major source of atmospheric free radicals. These free radicals may exist in small trace amount but they act to transform most species in the atmosphere, playing a major role in atmospheric chemistry.

In the most high level terms, the atmosphere is divided into lower and upper regions, with the lower atmosphere extending to the top of the stratosphere up to an altitude of abut 50 km. The temperature and pressure of the atmosphere vary with altitude and the average temperature variation is used to distinguish the different layers of the atmosphere, which are shown in Figure 2.1.

The lowest layer of the atmosphere is the troposphere, which ranges from the Earth's surface up to the tropopause. The troposphere only accounts for a small fraction of the atmosphere's total height, but it accounts for 80% of the atmosphere's mass (Seinfeld, 2016). The troposphere can be further divided into the planetary boundary layer which extends from the surface up to an altitude of about 1 km and the free troposphere, which extends from from the planetary boundary layer up to the tropopause.

The tropopause is the layer between the troposphere and the stratosphere. Over the equator the

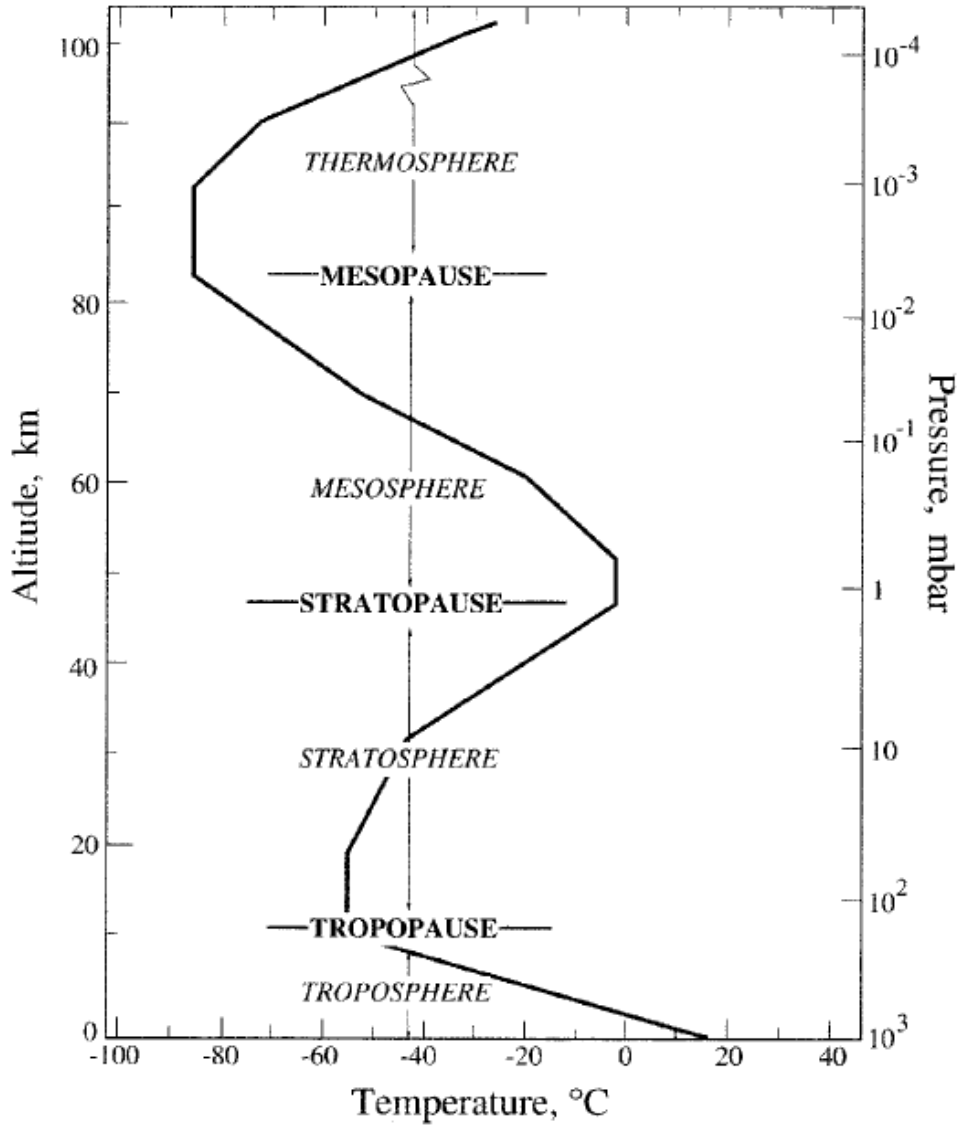

Figure 2.1: The Layers of the atmosphere and the variation in the atmospheric temperature and pressure with increasing altitude (Seinfeld, 2016)

altitude of the tropopause is about 16 km whereas over the polar regions it is at an altitude of about 8 km (Seinfeld, 2016). The tropopause is specifically defined as the lowest altitude at which the rate of decrease in temperature with increasing altitude is $\leq$ 2 K/km.

The stratosphere is characterised by an isothermal region at an altitude range of about 11 km to 20 km. Beyond this isothermal region, the temperature of the atmosphere increases with increasing altitude and this trend is a a result of the absorption of the solar ultraviolet light by O_3 in the stratosphere.

The atmosphere is a very dynamic system with its constituents being exchanged with vegetation, bodies of water and biological organisms. Gases are produced by chemical processes within the atmosphere, biological activity, and human industrial (anthropogenic) activities. These gases are also removed from the atmosphere by chemical processes, biological activities, physical processes in the atmosphere and by deposition. Most of the species considered air pollutants have natural as well as anthropogenic sources.

As chemical species are transported throughout the atmosphere, they participate in various chemical reactions, unless the chemical species are very inert. The chemical reactions change the chemical composition and physical properties of the species to form new chemical products. Chemical species are continuously added and removed from the atmosphere across large spatial and temporal scales. The spatial scales are caused by a combination of the chemical lifetimes of the species along with the large scale transport which occurs in the atmosphere. This is summarized in Figure 2.2, which shows that with each chemical lifetime a spatial transport scale is associated. For example, chemical species with long lifetimes undergo atmospheric transport on a larger scale, such that the concentrations of these species are more uniform across the globe. On the other hand, chemical species with short lifetimes travel smaller distances which leads to more localised concentrations.

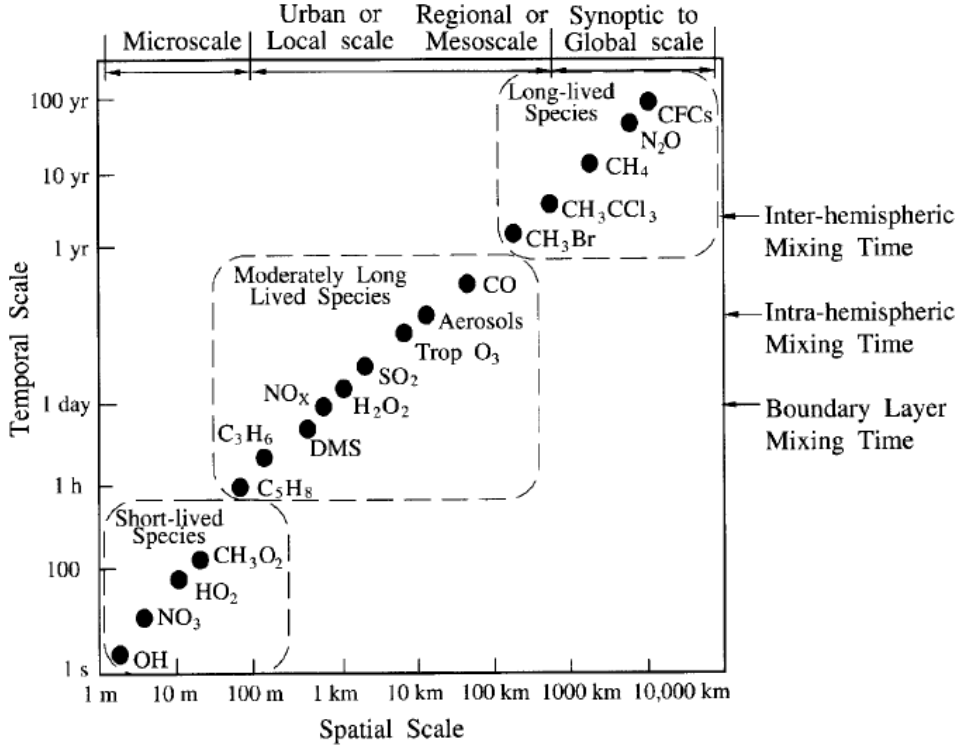

Figure 2.2: Variation of spatial and temporal scales of species in the atmosphere (Seinfeld, 2016)

2.2 Atmospheric Transport

Atmospheric transport is fundamentally driven by the uneven heating of the Earth's surface by the sun. The total energy that is received by the Earth, is balanced out by the total energy radiated back into space by the Earth's surface. However, on a local scale this balance does not hold for each specific location. For example, in the tropics close to the equator more energy is received than radiated out, while in the polar regions more energy is radiated out than received. This trend is more specifically shown in Figure 2.3. This variation in the local energy balance across the different latitudes has the impact that the warm air tends to travel towards the polar regions and cold air travels towards the equator.

The ideal global atmospheric transport can be represented by three specific cells; the Hadley Cell, the Ferrel Cell and the Polar Cell as depicted in Figure 2.4. The Hadley cell extends from the equator to approximately 30° latitude in both hemispheres. The Ferrel cell lies between the Hadley cell and the Polar cell, extending from about 30° latitude to 60° latitude in both hemispheres. The Polar cell extends from 60° latitude to 90° latitude in both hemispheres.

In the Hadley cell warm air rises at the equator due to the intense solar heating, creating a low pressure

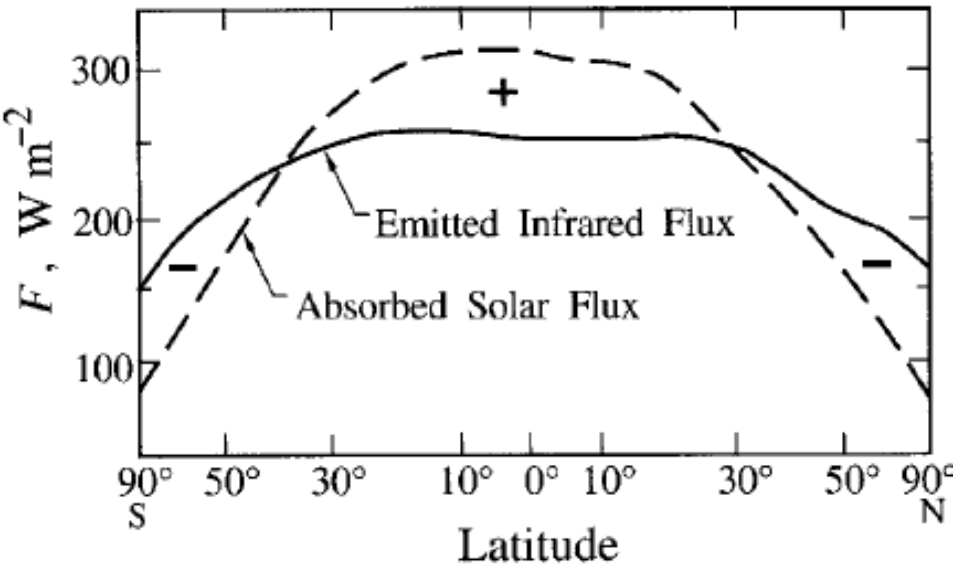

Figure 2.3: Zonally averaged absorbed solar flux and emitted infrared flux at the top of the atmosphere. The positive sign indicates a local energy gain, while the negative sign indicates a local energy loss (Seinfeld, 2016).

zone, which is also called the Intertropical Convergence Zone (ITCZ). The air rises up to the tropopause where it then moves towards the pole. As the air moves towards the pole it becomes colder and denser, sinking around 30° latitude, creating high pressure zones that are referred to as the subtropical highs. At the surface the air flows back towards the equator and due to the rotation of the earth and the induced Coriolis force, the air deflects forming the Trade Winds, which go from east to west. The ITCZ is also the area where the Trade Winds of the Northern and the Southern hemisphere meet, characterised by persistent cloud cover, thunderstorms and heavy rainfall. The Hadley cell is responsible for the formation of tropical rainforests near the equator and deserts around 30° latitude.

In the Ferrel cell, at the surface, air flows poleward from the subtropical highs at 30° latitude to the low pressure zones at 60° latitude. At 60° latitude, the warm air from the Ferrel cell meets the cold air from the polar cell, which causes the warm air to rise up to the tropopause. Here, the air then moves back towards the equatorial region at high altitudes. The Ferrel cell is primarily defined and influenced by the interactions of the Hadley and Polar cells. The air flow at the surface of the Ferrel cells leads to westerly winds in the mid-latitudes, which flow from west to east.

In the Polar cell, the cold and dense air sinks at the poles creating a high pressure zone. The cold air then flows towards the equator at the surface where it meets warmer air from the Ferrel cell, causing the warm air to rise and closing the loop. The Polar cell helps maintain the cool temperature of the polar region and the air flow towards the equator at the surface gives rise to the polar easterly winds which blow from east to west.

Another important transport phenomena is the Brewer-Dobson circulation, depicted in Figure 2.5, which is a large scale atmospheric circulation pattern which occurs in the stratosphere. At low latitudes in the tropics, the air rises up into the stratosphere due to the strong solar heating, similar to the Hadley cell. Driven by planetary and gravity waves, most of this air then moves towards the winter pole where it cools and sinks. The Brewer-Dobson circulation can be divided into two main branches. The shallow branch leads to the circulation occurring in the lower stratosphere, whereas the deep branch operates in the upper stratosphere. Thus, the deep branch takes longer to complete its cycle compared to the shallow branch. The descent at the poles is one of the few atmospheric transport mechanisms that takes place between the troposphere and the stratosphere.

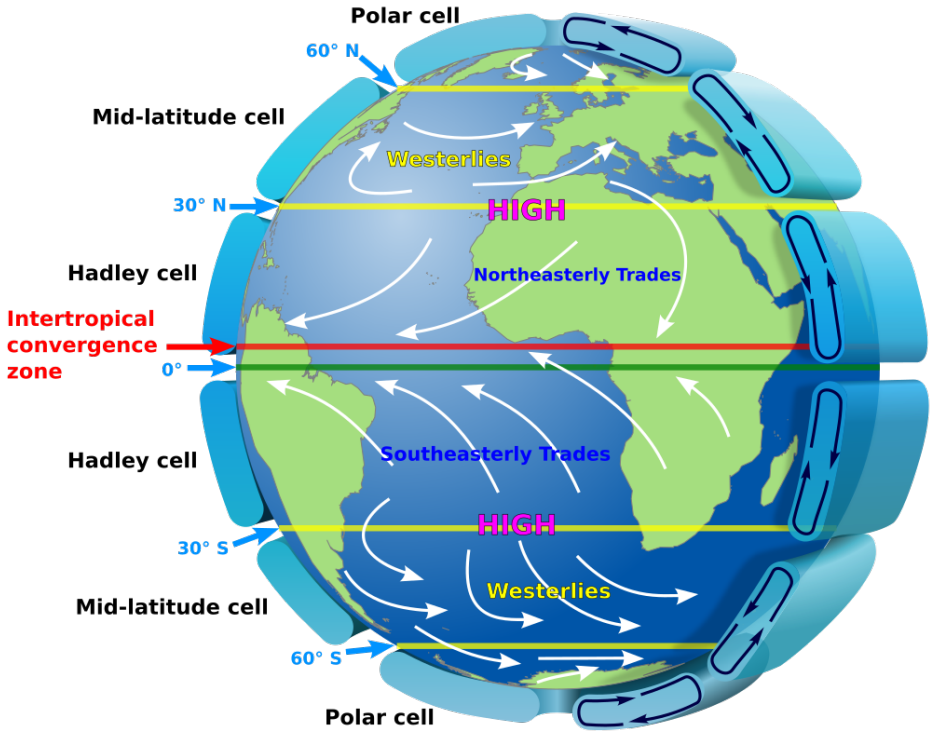

Figure 2.4: A depiction of the idealised global circulation with the Ferrel Cell labelled as the Mid Latitude Cell taken from https://en.wikipedia.org/wiki/Atmospheric_circulation

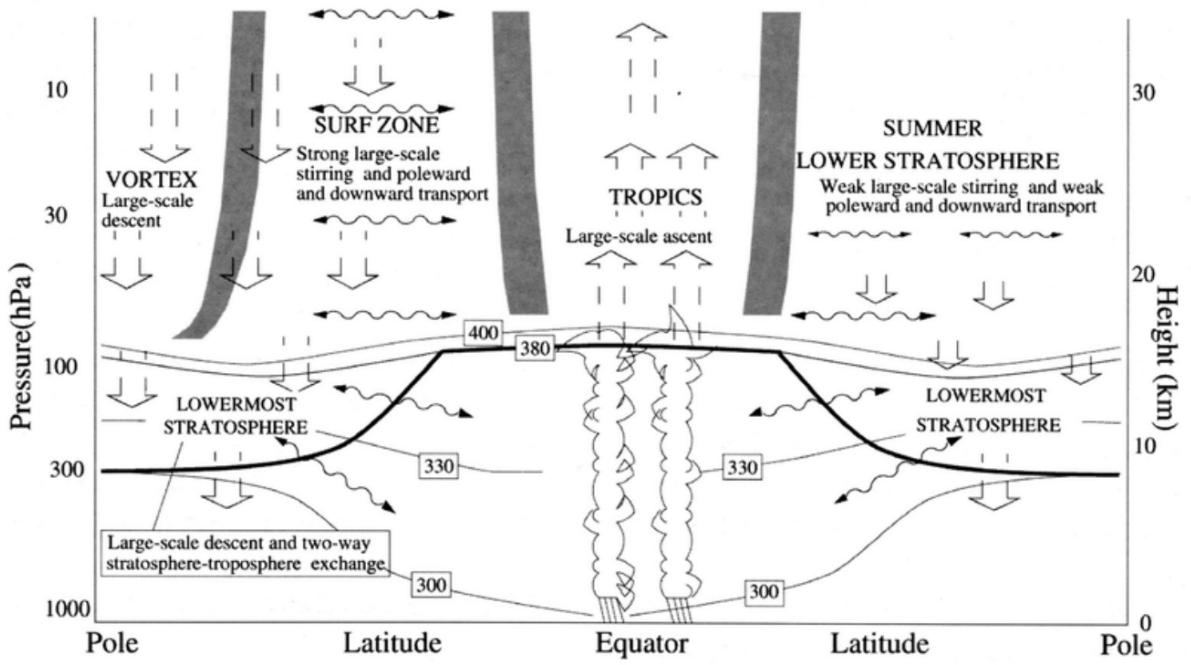

Figure 2.5: Figure depicting the Brewer Dobson Circulation, where air travels from the Troposphere to the Stratosphere at the equator, while the air travels from the Stratosphere to the Troposphere from at higher latitudes (Weidner, 2005).

3

Nitrogen Oxides and Tropospheric Ozone Chemistry

The chemistry of NO_x and O_3 is highly non-linear and driven by numerous processes involving many different species. NO_x is not only an important reactant for the formation of O_3, but also plays a vital role in the depletion of O_3. To understand the contribution of aviation NO_x emissions towards tropospheric O_3, having an understanding of the chemistry that drives the production and depletion of O_3 is vital. This chapter focuses on the chemical pathways that lead to both the formation and depletion of O_3 in the troposphere. The main NO_x-O_3 photochemical cycle is explained in Section 3.1. The formation of the Hydroxyl (OH) radical is described in Section 3.2. The impact of Carbon Monoxide (CO) on the formation and depletion of O_3 is explained in Section 3.3. The role of methane (CH_4) in the chemistry of tropospheric O_3 is described in Section 3.4. As mentioned previously, the chemistry of NO_x and O_3 is highly non-linear. This non-linear behaviour and how it impacts mitigation strategies is described in Section 3.5. The chemical mechanisms as shown in this chapter are based on the work by Seinfeld (2016).

3.1 Nitrogen Oxides and Ozone photochemical cycle

As mentioned previously, O_3 is not emitted but is purely a product of chemical reactions. In the upper troposphere O_3 is a result of the photolysis of Nitrogen Dioxide (NO_2) as shown in Reaction R1. This photolysis only occurs at wavelengths less than 424 nm (Seinfeld, 2016). The O produced in Reaction R1 is highly reactive, meaning that it instantly reacts with diatomic Oxygen (O_2) in the atmosphere to form O_3 in the presence of a gaseous third body such as N_2 (diatomic Nitrogen) as shown in Reaction R2, where M denotes this gaseous third body. In this sequence of reactions, Reaction R1 is the rate determining step, meaning that the concentration of NO_2 drives the reaction rate for the formation of O_3.

$$\mathrm{NO_2} + h\nu \longrightarrow \mathrm{NO} + \mathrm{O} \tag{R1}$$

$$\mathrm{O} + \mathrm{O_2} + \mathrm{M} \longrightarrow \mathrm{O_3} + \mathrm{M} \tag{R2}$$

However, once formed O_3 reacts with NO (Nitric Oxide) to form NO_2 as shown in Reaction R3. Reaction R3 occurs slower than Reactions R1 and R2. Thus, changes in NO_2 concentration strongly and quickly impact the production and loss of O_3, while the production of O_3 does not impact NO_2 production as quickly. Reactions R1, R2 and R3 reach a point where NO_2 is depleted and reproduced so quickly

that a steady state cycle forms. NO_x (NO_x = NO + NO_2) and specifically NO_2 is required for ozone formation to take place in the troposphere. However, most NO_x emissions are emitted in the form of NO, meaning that ozone formation is not only governed by Reactions R1, R2 and R3 but many other reactions play a role in the formation of O_3. Furthermore, the steady state mixing ratios from the O_3 - NO_x cycle are not large enough to explain atmospheric O_3 levels, further supporting the importance of the role of other reactions.

$$\mathrm{O_3 + NO \longrightarrow NO_2 + O_2} \tag{R3}$$

3.2 Hydroxyl Radical Production and Ozone Depletion

The Hydroxyl (OH) radical is the main oxidant species in the tropospheric atmosphere. Molecules such as O_2 and O_3 are abundant in the atmosphere and have strong oxidant properties, however they are very unreactive, as the chemical bonds between their atoms are very strong. OH is known as the ”detergent” of the atmosphere because it binds to many trace species and makes them soluble in water, leading to these trace species being rained out of the atmosphere. When OH reacts with these trace gases, it is often regenerated in catalytic cycles, leading to sustained concentrations of OH.

As mentioned previously, the photolysis of O_3 can lead two to options. Either R4 takes place or R5 happens followed by R6, both options leading to a null cycle in the O_3 formation.

$$\mathrm{O_3 + } h\nu \longrightarrow \mathrm{O_2 + O} \tag{R4}$$

$$\mathrm{O_3 + } h\nu \longrightarrow \mathrm{O_2 + O(^1}D\mathrm{)} \tag{R5}$$

$$\mathrm{O(^1}D\mathrm{) + M \longrightarrow O + M} \tag{R6}$$

However, some of the $\mathrm{O(^1}D\mathrm{)}$ atoms collide with water H_2O molecules leading to the formation of OH as seen in Reaction R7. OH is part of the HO_x(HO_x = OH + HO_2) family and within HO_x OH and HO_2 cycle between each other by reacting with various different reactants in the atmosphere.

$$\mathrm{O(^1}D\mathrm{) + H_2O \longrightarrow 2\,OH} \tag{R7}$$

One such reactant in the atmosphere is O_3, the depletion of which leads to the formation of OH as shown earlier, but also allows the OH and HO_2 to cycle between each other. This is shown Reactions R8 and R9.

$$\mathrm{O_3 + OH \longrightarrow HO_2 + O_2} \tag{R8}$$

$$\mathrm{O_3 + HO_2 \longrightarrow OH + 2\,O_2} \tag{R9}$$

3.3 Carbon Monoxide Chemistry and Ozone

Carbon Monoxide (CO) is also relevant towards the O_3 chemistry. CO oxidises by reacting with OH forming the hydroperoxyl radical (HO_2) as shown in Reaction R10. This HO_2 reacts with NO to form NO_2 in Reaction R11, leading to the formation of O_3 via the photolysis of NO_2 as previously shown in Reactions R1 and R2. Combining all of the aforementioned reactions leads to the net reaction shown in Reaction R12.

Reactions R10 and R11 show that reacting with NO_x and CO allows the OH and HO_2 to rapidly cycle between themselves within the HO_x family. A further rapid cycle occurs between HO_2 and OH, when HO_2 reacts with itself to form Hydrogen Peroxide (H_2O_2), the photolysis of which leads to the formation

of OH. This cycle is shown in Reactions R13 and R14 respectively. Furthermore the H_2O_2 formed in Reaction R13 can react with OH to form HO_2 and H_2O as shown in Reaction R15.

$$\mathrm{CO} + \mathrm{OH} \xrightarrow{\mathrm{O_2}} \mathrm{CO_2} + \mathrm{HO_2} \tag{R10}$$

$$\mathrm{HO_2} + \mathrm{NO} \longrightarrow \mathrm{NO_2} + \mathrm{OH} \tag{R11}$$

$$\mathrm{NO_2} + h\nu \longrightarrow \mathrm{NO} + \mathrm{O} \tag{R1}$$

$$\mathrm{O} + \mathrm{O_2} + \mathrm{M} \longrightarrow \mathrm{O_3} + \mathrm{M} \tag{R2}$$

$$\textbf{\textit{Net:}}\ \mathrm{CO} + 2\,\mathrm{O_2} \longrightarrow \mathrm{CO_2} + \mathrm{O_3} \tag{R12}$$

$$\mathrm{HO_2} + \mathrm{HO_2} \longrightarrow \mathrm{H_2O_2} + \mathrm{O_2} \tag{R13}$$

$$\mathrm{H_2O_2} + h\nu \longrightarrow \mathrm{OH} + \mathrm{OH} \tag{R14}$$

$$\mathrm{H_2O_2} + \mathrm{OH} \longrightarrow \mathrm{HO_2} + \mathrm{H_2O} \tag{R15}$$

Reactions R10 and R11 show that the formation of O_3 requires the presence of HO_x and NO_x radicals, however, when OH and NO_2 react together, they form Nitric Acid (HNO_3) as shown in Reaction R16. The HNO_3 formed is reluctant to further react in the upper atmosphere, thereby leading to the termination of the HO_x and NO_x reaction chains. Furthermore, HNO_3 is highly soluble in water, meaning that it can easily be removed from the atmosphere through not only dry but also wet deposition. In general once reactive radicals such as NO_x and HO_x start getting removed from the atmosphere and their concentrations start falling, the reaction cycles involving NO_x, HO_x and O_3 start to slow down, with reactions becoming less likely.

$$\mathrm{OH} + \mathrm{NO_2} + \mathrm{M} \longrightarrow \mathrm{HNO_3} + \mathrm{M} \tag{R16}$$

3.4 Methane Chemistry and Ozone

O_3 is produced when CH_4 oxidises. When CH_4 oxidises by reacting with OH, the reaction produces the methyl CH_3 radical as shown in Reaction R17 which instantaneously reacts with O_2 to form the methyl peroxy CH_3O_2 radical as shown in Reaction R18. The CH_3O_2 radical then reacts with NO to form the methoxy radical (CH_3O) and NO_2 as shown in Reaction R19. The CH_3O reacts with O_2 to form HCHO (formaldehyde) and HO_2 as shown in Reaction R20 and the produced HO_2 reacts with NO as shown in Reaction R11. The NO_2 formed in Reactions R19 and R11 subsequently photolyses and leads to the production of O_3 via the NO_x – O_3 photochemical cycle as shown in Reactions R1 and R2. The production of O_3 via the oxidation of CH_4 can be summarised by the net reaction in Reaction R21

$$\mathrm{CH_4} + \mathrm{OH} \longrightarrow \mathrm{CH_3} + \mathrm{H_2O} \tag{R17}$$

$$\mathrm{CH_3} + \mathrm{O_2} + \mathrm{M} \longrightarrow \mathrm{CH_3O_2} + \mathrm{M} \tag{R18}$$

$$\mathrm{CH_3O_2} + \mathrm{NO} \longrightarrow \mathrm{CH_3O} + \mathrm{NO_2} \tag{R19}$$

$$\mathrm{CH_3O} + \mathrm{O_2} \longrightarrow \mathrm{HCHO} + \mathrm{HO_2} \tag{R20}$$

$$\mathrm{HO_2} + \mathrm{NO} \longrightarrow \mathrm{NO_2} + \mathrm{OH} \tag{R11}$$

$$\mathrm{NO_2} + h\nu \longrightarrow \mathrm{NO} + \mathrm{O} \tag{R1}$$

$$\mathrm{O} + \mathrm{O_2} + \mathrm{M} \longrightarrow \mathrm{O_3} + \mathrm{M} \tag{R2}$$

$$\textbf{\textit{Net:}}\ \mathrm{CH_4} + 4\,\mathrm{O_2} \longrightarrow \mathrm{HCHO} + \mathrm{H_2O} + 2\,\mathrm{O_3} \tag{R21}$$

The chain of reactions shown above is specifically for the oxidation of CH_4, but it is also representative of the oxidation of Non Methane Hydro-Carbons (NMHC). This means that a variety of organic compounds such as Ethane (C_2H_6) or Propene (C_3H_6) consisting of just carbon and hydrogen atoms can lead to the formation of Ozone using a similar pathway to the one shown in Reaction R21. This practically means that the reaction between Carbon compounds and Oxygen in the presence of NO_x and HO_x leads to the formation of Ozone. CH_4 and HCHO are examples of VOCs (Volatile Organic Compounds). VOCs are a broad range of chemicals that exist in the atmosphere as gases and are important pre-cursors to the O_3 formation mechanism. VOCs oxidise by reacting with OH, which forms reactive free radicals such as CH_3O_2. These free radicals react with NO_x to form NO_2 which participates in the NO_x-O_3 photochemical cycle.

$$CH_3O_2 + HO_2 \longrightarrow CH_3OOH + O_2 \tag{R22}$$

Reaction R18 shows that the oxidised CH_4 in Reaction R17 eventually forms CH_3O_2. This methyl peroxy radical can react with NO (as shown in Reaction R19 to form CH_3O) or with HO_2 to form CH_3OOH (Methyl hydroperoxide) as shown in Reaction R22. CH_3O instantaneously reacts with O_2 to form HCHO, a VOC, as shown in Reaction R20, while CH_3OOH photlyses or reacts with OH to form CH_3O or CH_3O_2 which eventually leads to the formation of HCHO. This means that practically all of the CH_4 in the atmosphere is converted to HCHO as shown in the net Reaction R21, which undergoes photolysis or a reaction with OH in the atmosphere. Both of these reactions eventually lead to the formation of CO, making CO the principle product of CH_4 oxidation. This can lead to further O_3 formation while the CO is converted to CO_2 as shown in Reaction R12 in Section 3.3.

3.5 Impact of Background Nitrogen Oxides levels

From an initial look, it would seem that Equation (R1) is the rate determining step for the production of Ozone, as the photolysis of NO_2 directly precedes the formation of O_3 in the NO_x-O_3 photochemical cycle. This would mean that continuously increasing the concentration of NO_x (or NO_2 more specifically) would continuously increase the rate at which O_3 is produced in the atmosphere. However, in reality the environment is polluted and there is already an existing concentration of NO_x, hydrocarbons, VOCs and radicals. The formation and depletion of Ozone in a polluted atmosphere are dependent on numerous complex reactions throughout the atmosphere, meaning that there is not a linear increase in the rate of production of O_3 when the concentration levels of NO_x increase.

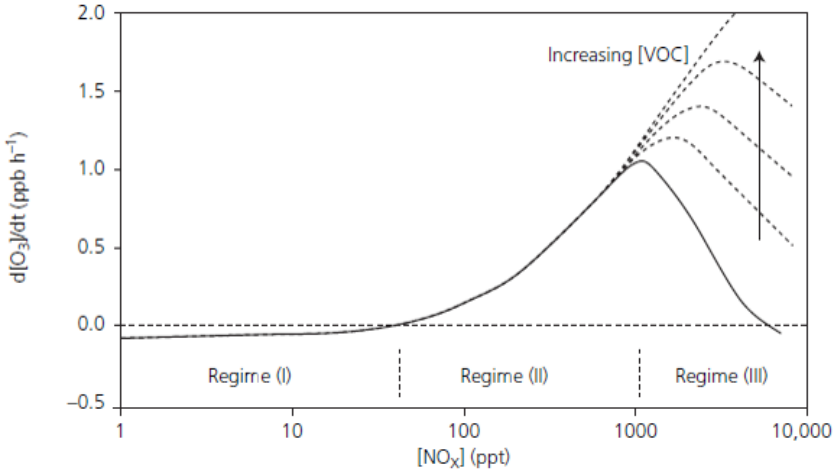

Figure 3.1: An example illustration of the NO_x dependence of the O_3 net production (Fowler, 2008)

This nonlinearity in the NO_x-O_3 chemistry is shown in Figure 3.1, which shows an illustrative example of the impact of increasing NO_x concentrations on the production rate of O_3. Three different regimes can be identified in Figure 3.1. In Regime I, the NO_x concentration is low, meaning that depletion of O_3 is dominant. With increasing NO_x concentrations the rate of production of O_3 slowly increases. At

some point due to increasing NO_x concentrations, the chemistry switches from net depletion to net production of O_3. This NO_x concentration represents the border between Regime I and Regime II. In Regime II, the NO_x concentration leads to net O_3 production and increasing rates of O_3 production with increasing NO_x concentrations. Regime II is also referred to as the NO_x limited regime. At some point in Regime II, the O_3 production rate reaches a maximum, which represents the barrier between Regime II and Regime III. In Regime III, any further increases in the NO_x concentrations lead to a decrease in the O_3 production rate and at some point in regime III, the net production becomes a net depletion.

In Figure 3.1 Regime I represents regions of the atmosphere where the NO_x levels are very low. At such low NO_x levels, very small amount of O_3 is produced due to the lack of NO_2 which can photolyse and a lack of NO which can turn into NO_2. Thus, the main reactions are the formation of OH from the photolysis of O_3 or the reactions between HO_x and O_3. The oxidation of CH_4 and CO leads to the production of species like CH_3OOH or H_2O_2 and no NO_2, leading to a net O_3 depletion.

Reactions R9 and R22 are the main reactions which compete with Reactions R11 and R19. This means that in Regime I and II when the NO_x and more specifically, when the NO concentrations increase, Reactions R1 and R2 have a higher likelihood of taking place in comparison to Reactions R9 and R22. This leads to NO_2 formation and photolysis, leading to the production of O_3. However, this is only the case while there is an abundance of VOCs. As soon as there is too much NO_x relative to VOCs in the environment, the trend shown in Regime III in Figure 3.1 takes place.

In Regime III, often referred to VOC limited, the high NO_x to VOC ratio, means that the termination reaction shown in Reaction R16 becomes more prevalent than the VOC and NMHC oxidation reactions (e.g. Reaction R17). Here it is important to again note that HNO_3 is water soluble and reluctant to interact with species in the atmosphere, leading to removal of NO_x and HO_x from the atmosphere. Thus, the concentration of reactive free radicals in the environment decreases, leading to less production of O_3. The higher the NO_x levels, the more prevalent Reaction R16 becomes and the more radicals are removed from the atmosphere leading to less O_3 being produced.

In general, this means that VOCs and NMHCs compete with NO_x to react with OH. Oxidation of VOCs and NMHCs by reacting with OH leads to the extension of the chain of radicals, which act as precursors to O_3. On the other hand, the reaction between NO_x and OH reduces OH concentrations in the atmosphere, terminating the O_3 production chain. This competing effect drives the trends seen in Figure 3.1. Furthermore, this competing effect also means that the NOx mixing ratio, where the chemical regime shifts from Regime II in Figure 3.1 to Regime III, also depends on the mixing ratios of VOCs in the atmosphere. A higher VOC mixing ratio in the atmosphere, means that a higher NO_x mixing ratio is required, before the terminating reaction between NO_2 and OH starts becoming prevalent. This impact of the changing VOC levels is shown in the top right corner of Figure 3.1, where the boundary between Regimes II and III is shown to be dependent on the VOC level.

The fact that the production of O_3 follows the trend shown in Figure 3.1, means that the O_3 formation mechanism is highly non-linear. This means that implementing counter measures to the greenhouse impact of O_3 becomes less trivial. Knowledge of the current state of background NO_x levels is required before any mitigation strategies can be deployed. For example, if the environment in a certain region is VOC limited and the local government decides to employ NO_x reducing policies, then there is a probability that these policies work towards increasing the tropospheric O_3 concentrations. This would be counterproductive, leading to larger forcings due to the increased O_3 levels and a larger anthropogenic climate impact. Knowledge of the fact that the local environment is VOC limited would mean that the mitigation strategies can take this non-linear effect into account and first carry out a trade-off on whether reducing the NO_x emissions by an achievable amount would even lead to a lower climate impact.

4

Trends and Variations in the Impact of Nitrogen Oxides

So far, Chapter 2 and Chapter 3 have explained the fundamentals behind atmospheric transport and the NO_x - O_3 chemistry. However, to apply this information it is important to look at past studies that have looked at how aviation NO_x emissions impact and contribute towards tropospheric O_3. Since the first recognition of O_3 as a pollutant by Haagen-Smit (1952), a lot of studies have been carried out looking at the different trends and variations in O_3. These studies have found that the concentrations of O_3 vary with latitude, season and altitude and these trends are described in Section 4.1, Section 4.2 and Section 4.3 respectively. On top of this, studies have found that the concentration of O_3 varies due to different Ozone efficiencies across different regions. These variations and trends are described and explained in Section 4.4.

4.1 Meridional Variations

The research carried out by Köhler et al. (2013) focuses on the meridional variation of the effect of aviation NO_x emissions on atmospheric ozone and methane and the corresponding climate metrics. Köhler et al. (2013) use a perturbation analysis with a global chemistry transport model. In this perturbation analysis, the impact of aviation emissions is studied by increasing NO_x emissions in the global chemistry transport model and comparing these to a base case, using a Taylor approximation (more details on perturbation analyses are given by Grewe et al. (2010)). The NO_x emissions are increased by $3.8 \cdot 10^{-4} Tg(N)$ per year at cruise altitude for 20° wide latitude bands. The research by Köhler et al. (2013) shows that perturbations in aviation emissions at lower latitudes cause a 6 time larger NO_x RF than emissions at higher latitudes. The overall latitudinal variation is also supported by Grewe et al. (2014), Frömming et al. (2021) and Skowron et al. (2015). Köhler et al. (2013) suggest that the largest contributor to this pattern is the higher solar irradiance at lower latitudes which leads to faster photochemical production of ozone. Frömming et al. (2021) mention that the area of jet streams or high pressure ridges have a tendency to induce a transport towards lower latitudes and altitudes. Thus any NO_x emissions in these regions can be transported to lower latitudes, enhancing the NO_x climate impact in the more chemically active regions.

In Figure 4.1 the RF due to short term formation of O_3, depletion of CH_4 and the subsequent PMO effect is shown (Köhler et al., 2013). It is important to note here that the depletion of SWV is not taken into account in the study by Köhler et al. (2013). However, as shown by the results of Lee et al. (2021), this phenomenon has a very small impact on the total RF due to aviation NO_x. Figure 4.1

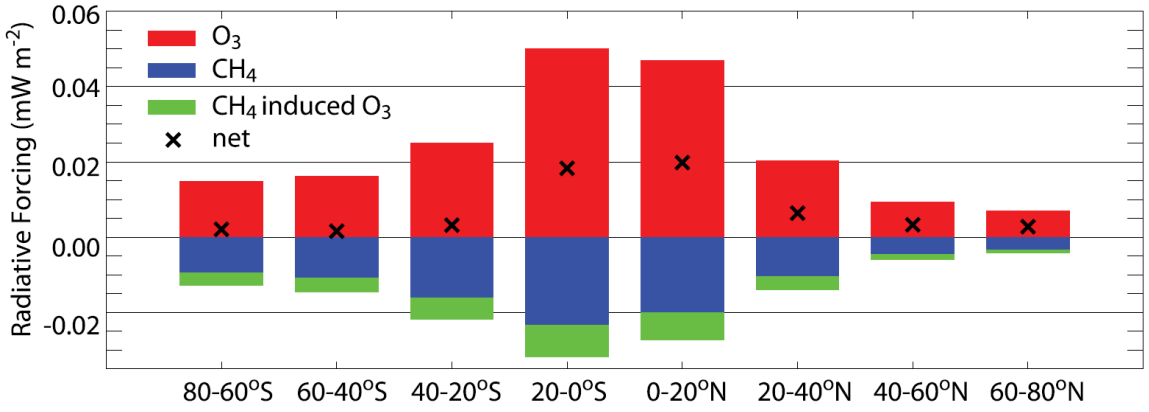

Figure 4.1: The RF response to an increase of NO_x emissions by $3.8 \cdot 10^{-4} Tg(N)$ per year at cruise altitude for 20° wide latitude bands. The individual RF components due to the formation of O_3, and depletion of CH_4 and O_3 are shown individually, with the net RF represented by the cross in the graph (Köhler et al., 2013).

clearly shows that the low latitude bands have a larger net RF and that the RF increase due to the O_3 formation and the RF decreases due to the CH_4 and O_3 depletion are also larger in magnitude in the lower latitude bands. This suggest that the higher solar irradiance leads to more O_3 formation, and more CH_4 and O_3 depletion. Another observation from Figure 4.1 is that the magnitude of the individual RF components for southern hemisphere latitude bands are larger than for their northern hemisphere counterparts. Skowron et al. (2015) shows a similar variation of the RF due to the formation of the short lived O_3. This is considered to be a consequence of the fact that the southern hemisphere has a lower background NO_x, leading to more efficient production of O_3 and thus also CH_4 depletion, but also more efficient depletion of O_3. However, Figure 4.1 shows that the net RF is not higher in the southern hemisphere, which is due to the fact that the increased RF due to O_3 formation is cancelled out by the increased negative RF due to the CH_4 and O_3 depletion.

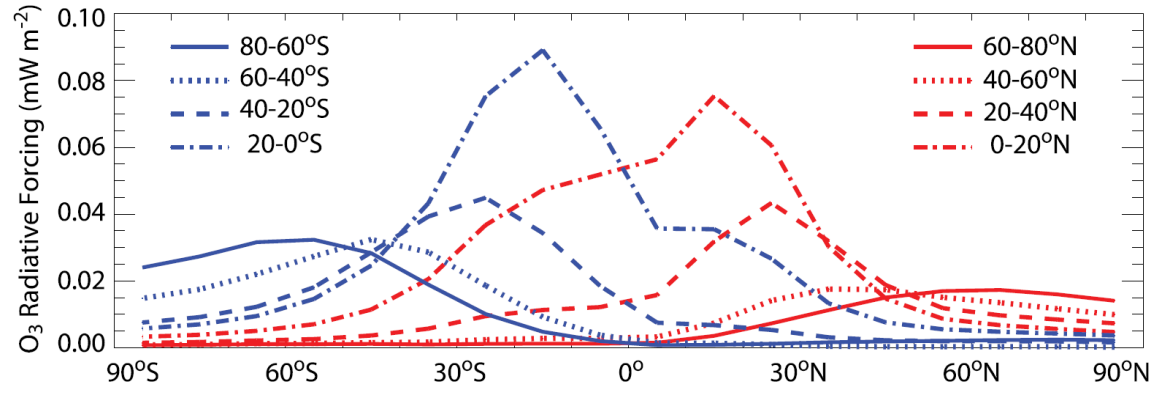

Figure 4.2: Zonal dependence of the short lived ozone RF response to an increase in NO_x by $3.8 \cdot 10^{-4} Tg(N)$ per year at cruise altitude for 20° wide latitude. The blue lines refer to the latitude bands in the southern hemisphere, whereas the red lines refer to the latitude bands in the northern hemisphere (Köhler et al., 2013)

Figure 4.2 shows the zonal dependence of the short lived ozone RF for the same latitude bands as in Figure 4.1 as presented by Köhler et al. (2013). Figure 4.2 shows that the meridional transport is larger at lower latitudes, leading to a larger geographical spread of emissions at lower latitudes. Furthermore, Figure 4.2 shows that NO_x emitted in latitude bands lower than 40° have a considerable impact on the RF close to the equator, supporting the idea of the transport of emissions towards the lower latitude bands as also presented by Skowron et al. (2015) and Frömming et al. (2021).

4.2 Seasonal Variations

The climate impact of NO_x has a dependence on the season. This is most likely due to the varying absorption of solar radiation for the different seasons as well as changing temperatures and transport patterns, as was also seen in the meridional variation, discussed in Section 4.1. The changing absorption of solar radiation impacts the photochemical activity in the atmosphere and the lifetime of its constituents. The stronger solar radiation leads to more atmospheric convection, leading to more ground level NO_x emissions to be transported up, meaning that there is a higher background NO_x concentration during the summer at cruise altitudes (Stevenson et al., 2004). In the summer, the lifetime of both NO_x and O_3 are shorter, as the higher solar radiation increases the probability that both can photolyse. The research carried out by Stevenson et al. (2004) looks at the O_3 response when aviation NO_x emissions are added during January, April, July and October in separate simulations. In the study, the amount of NO_x emitted is different for all four simulations, but the authors, normalise their results so that the results become comparable and are not dependent on the amount of NO_x emitted. Stevenson et al. (2004) find that the two effects of lifetime and background NO_x lead to the biggest O_3 concentration response from NO_x emissions in October, with the O_3 burden peak taking place a few weeks after the NO_x emissions agreeing with the results by Gilmore et al. (2013). Due to the fact that Stevenson et al. (2004) only consider 4 specific months, the resolution of their results is very coarse and full understanding of seasonal variations is lacking. In their study. Lee et al. (2010) find that across various studies the peaks usually occur in the early summer and end of spring around May, or they occur in the autumn around October, with some studies even seeing both peaks, partially agreeing with the results of Stevenson et al. (2004). Lee et al. (2010) mention that the reason for the variation in these peaks is due to the use of different models and the strong reliance of the seasonal trend on both transport and chemistry, which is also suggested by Stevenson et al. (2004). Thus, using slightly different chemistry transport models, leads to slightly different results.

The study by Stevenson et al. (2004) also looks at the RF response due to the aviation NO_x, thus also looking at the OH, CH_4 and subsequent PMO response, neglecting the SWV response. Here, the authors find that the net RF response is positive in the months of April and October and negative in the months of January and July, with the net forcing being negligible. Frömming et al. (2021) and Maruhashi et al. (2022) find in their analysis that the climate impact of NO_x aviations is higher in the summer than in the winter. However, here it is important to note that the study by Frömming et al. (2021) only considers the months of December to February and June and July, while the study by Maruhashi et al. (2022) only considers the periods of January to March and July to September.

4.3 Variation with Altitude

In the troposphere, the lifetime of both NO_x and O_3 increases with increasing altitude (Grewe et al., 2002). Grewe et al. (2002) show that decreasing the cruise altitude for aircraft by 1 km, leads to a NO_x concentration decrease of about 30% at the original cruise altitude, while leading to an increase of 5% to 10% at the lowered altitude. Grewe et al. (2002) state that due to the smaller lifetimes of the NO_x and O_3, the reduced O_3 production at the nominal cruise altitude, overcompensates the increased O_3 production at the new cruise altitude. Even taking into account, the increased fuel consumption due to the reduced aerodynamic efficiency at the lower cruise altitude, the increase in O_3 at the lower cruise altitude was shown to be overshadowed by the decrease in the O_3 production at the nominal altitude (Grewe et al., 2002). Søvde et al. (2014) and Maruhashi et al. (2024) make use of multiple models and show that lowering the flight altitude decreases the RF impact, while increasing the flight altitude, increases the RF impact. Søvde et al. (2014) suggest that this variation with altitude is mainly driven by the changes in the concentration of the short-lived ozone, which is also supported by Frömming et al. (2012).

Maruhashi et al. (2024) find that the variation based on altitude is also dependent on the season, with the variation being more pronounced in summer than winter. This means that increasing or decreasing the flight altitude in the summer has a stronger impact than doing such in the winter. However, for this

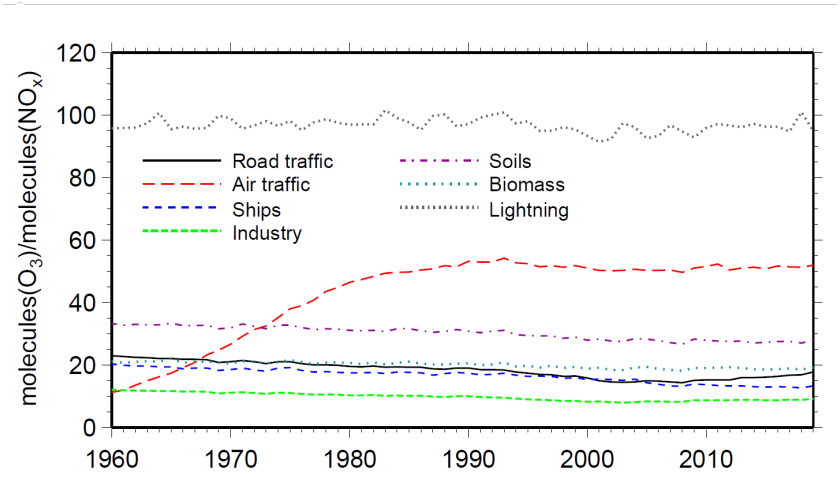

Figure 4.3: Trends between 1960 and 2019 of O_3 Production Efficiency as shown by Dahlmann et al. (2011).

effect it is important to once again note that the study Maruhashi et al. (2024) only looks at the months of January and July, meaning that a lot of details from the seasonal variation could have been lost. Furthermore, Maruhashi et al. (2024) do find that the trend of altitude and RF impact of aviation NO_x is not completely monotonic, as they find that for specific regions (Europe and North America) the trend of increasing RF with increasing cruise altitude is not true. Maruhashi et al. (2024) suggest that this may be due to background NO_x levels over these specific regions and the impact this has on the ozone production efficiency.

4.4 Variation in Ozone Production and Burden Efficiency

Across Section 4.1, Section 4.2 and Section 4.3, the variations in O_3 are partially attributed to background NO_x levels and subsequently an O_3 efficiency metric, where certain parts of the globe are more efficient at producing or creating net O_3 than others. A variation of such an efficiency metric has been part of various past studies (Dahlmann et al., 2011; Elshorbany et al., 2024; Koffi et al., 2010; S. C. Liu et al., 1987; Mertens et al., 2024). One of the first iterations of a O_3 efficiency metric was the Ozone Production Efficiency (OPE) by S. C. Liu et al. (1987), who suggested that the photochemical production of O_3 varied with the concentrations of NO_x. A detailed comparison of OPE trends is plotted by Dahlmann et al. (2011). Dahlmann et al. (2011) show that the OPE of lightning and aviation emissions are highest and these findings have also been confirmed by more recent studies using different methods (Butler et al., 2020; Nalam et al., 2025). However, here it is important to note that the values found by Butler et al. (2020) and Nalam et al. (2025) differ by a whole order of magnitude compared to the OPE results of Dahlmann et al. (2011). However, all three publications align on the findings that the high OPEs of lightning and aviation NO_x emissions are caused by the low background NO_x levels in the regions where these emissions take place. This means that NO_x is emitted by lightning and aviation in regions that are highly NO_x limited and have a high chemical efficiency to produce O_3 with little NO_x. On the other hand, land transport emissions are usually emitted in polluted urban areas, with high background NO_x, which means that formation of O_3 is not as chemically efficient.

Gilmore et al. (2013) use a perturbation analysis to look at the impact of aviation emissions on O_3 levels at flight altitudes. In their analysis, the authors look at the O_3 sensitivity, which is a metric that shows the reaction of their atmospheric chemistry model to the changes in the aviation emissions. Gilmore et al. (2013) compare this O_3 sensitivity to the OPE, the O_3 production rate and the O_3 lifetime and this figure is shown in Figure 4.4. Comparing the blue line (representing OPE) to the green one (O_3 production rate) shows, that the OPE aligns with the production rate of O_3 in terms of the seasonal trend. However, looking at the variation of the O_3 lifetime represented by the red line shows, why the OPE trend does not accurately represent trends in O_3 concentration found by Gilmore et al. (2013). When the production rate and the OPE are at their highest in the summer months (June through August), the

lifetime of O_3 is at its lowest and the opposite is true when the OPE and production rate are at their lowest during the winter months (December through February). This leads to two peaks, one in the spring months (March through May) and a stronger peak in the autumn months (September through November), with the difference in the peaks explained in Section 4.2. The misalignment between the OPE and the perturbation response confirms that only taking the production rates into account, does not allow the OPE to take into account the lifetimes of O_3.

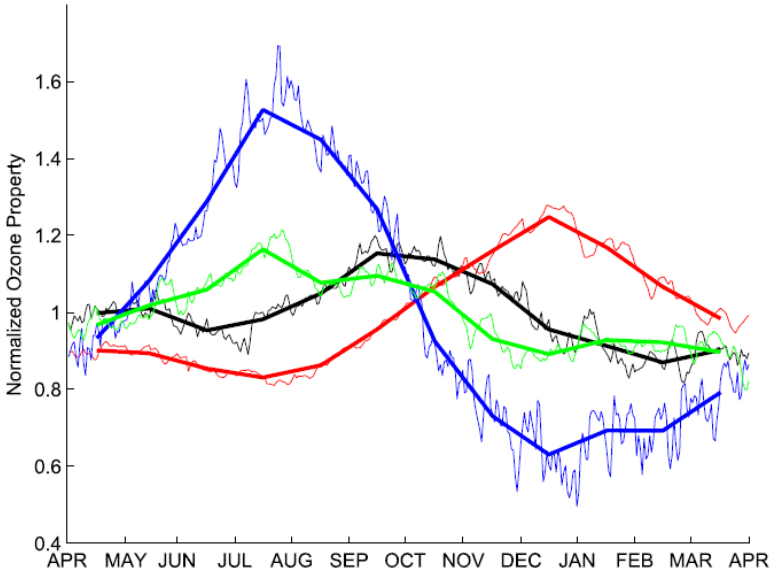

Figure 4.4: Variation of several aviation attributable Ozone metrics across a period of 12 months, where the thick lines represent the averaged quantities and the quantities are normalised using the annual mean. The black line shows the Ozone concentration response to a perturbation of 1 kg of aviation Nitrogen Oxides emissions. The blue line shows the Ozone Production Efficiency. The green line shows the Ozone production rate. The red line shows the Ozone lifetime (Gilmore et al., 2013).

Although, the OPE provides a good metric to evaluate the chemical efficiency of a region it has one drawback, which is that it only takes into account the production of O_3. In general, NO_x is just not a precursor for the formation of O_3, but it is also a precursor for the loss of O_3. How the NO_x behaves is fully dependent on the background levels of VOCs and HO_x as described in Section 3.5. This means that since the OPE metric lacks information regarding the depletion of O_3 due to NO_x, it cannot be used to fully explain trends in O_3 variations. This is clearly shown in Figure 4.4 in the misalignment between the OPE and the O_3 lifetime. On the other hand, the Ozone Burden Efficiency (OBE), defined in Equation (4.1), does take this depletion effect into account (Mertens et al., 2024). Here, $B\left(\mathrm{O_3}\right)$ is the O_3 burden and $E\left(\mathrm{NO}_x\right)$ is the emission of NO_x. The O_3 burden is the net O_3 (formation - depletion), meaning that the OBE as used by authors such as Mertens et al. (2024), is better suited to explain global trends in O_3. However, despite this, there are limited studies that look at the OBE as metric instead of the OPE. Thus, this thesis aims to add to the literature gap by expanding on the distributions in OBE and trying to link these back to O_3 mixing ratios.

$$OBE = \frac{B\left(\mathrm{O_3}\right)}{E\left(\mathrm{NO}_x\right)} \tag{4.1}$$

5

Methodology

Commonly to conduct research on the contribution of an emission sector towards tropospheric O_3, chemistry climate models are employed using a source attribution model. In the case of this thesis, the EMAC chemistry climate model is used along with a tagging method. The model and its setup are explained in Section 5.1. How the resulting data from the model is treated and used is described in Section 5.2.

5.1 The EMAC Model

To carry out the research objective, the ECHAM/MESSy Atmospheric Chemistry (EMAC) model is used. The data used for this thesis has been obtained from simulations conducted using the EMAC model by the German Aerospace Center (DLR). EMAC is a global chemistry climate model, which uses the global climate model ECHAM5 along with the Modular Earth Submodel System (MESSy) interface (Jöckel et al., 2016). These two together enable detailed simulation of the dynamics of the atmosphere and its chemical processes. Figure 5.1 shows the different atmospheric processes that are taken into account by the EMAC model[1]. As shown in Figure 5.1, the EMAC model takes emitted chemical species as inputs and models all of the different transport and chemical transformation processes that these emitted species go through, thereby modelling the interactions between the global system and the various existing chemical species.

For this thesis, the EMAC model was operated T42L90MA resolution, meaning that the horizontal grid is divided into 128 longitudes and 64 latitudes, corresponding to a resolution of approximately 2.8^o by 2.8^o. In vertical direction, the model simulates 90 distinct layers, with the top layer being situated at 0.01 hPa which corresponds to about 80 km.The model simulations are conducted for the period of 1998 to 2018, where the first two years were used as spin up years using the emissions of 2000. However, initial observation of the data showed that remnant spin-up behaviour was still present in the years from 2000 to 2002. This means that for the analysis presented in this thesis only the simulations period from 2003 to 2018 is considered. The simulation set-up is based on the CCMI2 (Chemistry Climate Model Initiative Phase 2) RD1SD-base-01_tag setup, which makes the thesis simulations comparable to the reference simulations described by Jöckel et al. (2016). However, for this thesis the TAGGING 1.0 submodel is used for source attribution as described by Grewe et al. (2017). The EMAC model used in this thesis is nudged to the European Center for Medium-Range Weather Forecasts' (ECMWF) ERA5 reanalysis and uses CCMI2 time series for the nudging of GHGs and O_3 depleting chemicals, except for CH_4 which is nudged against the Copernicus Atmosphere Monitoring Service (CAMS) v7.3 surface

[1] https://www.dlr.de/en/pa/research-transfer/research-infrastructure/models/emac Date accessed 2nd September 2025

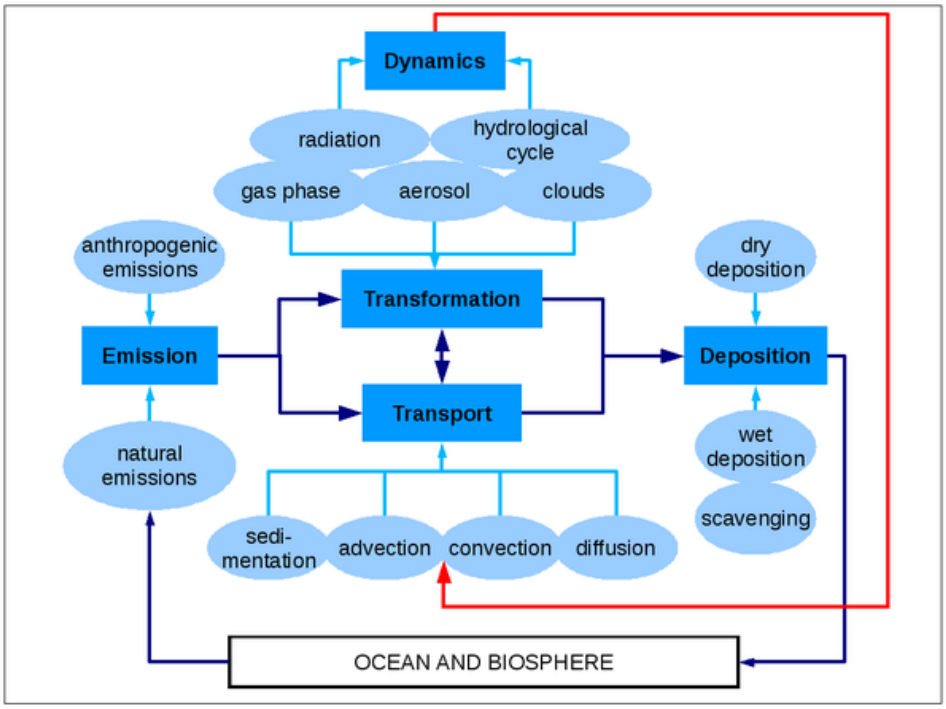

Figure 5.1: A representation of the different atmospheric processes considered by the EMAC model, along with their couplings.

mixing ratios. The CAMS-GLOB-ANT 4.2, CAMS-GLOB-SHIP 2.1 and CAMS-GLOB-AIR 2.1 emissions inventories are used for anthropogenic, shipping and aviation emissions, respectively. Biomass burning and agricultural waste burning are applied according to the CCMI2 protocol, which means that the Coupled Model Intercomparison Project Phase 6 (CMIP6) emissions are used upto 2015 and afterwards the Global Fire Emissions Database's GFED4s emissions datasets are used. Lightning NO_x emissions are parametrised according to Grewe et al. (2001) and the biogenic and soil NO_x emissions are calculated using the MESSy ONEMIS submodel as described by Kerkweg et al. (2006). The MESSy submodel Module Efficiently Calculating the Chemistry of the Atmosphere (MECCA) is used to for the calculation of the chemical kinetics (Sander et al., 2019). MECCA takes into account the gas phase chemistry, while submodel SCAV taked into accoun the aqueous phase chemistry of species in the troposphere and the stratosphere (Tost et al., 2006). The modelled species include O_3, CH_4, NO_x, HO_x, VOCs and NMHCs. However, alkynes and aromatics are not taken into account in MECCA and alkenes and alkanes are only considered up to C_4.

The goal of this thesis is to investigate how aviation emissions affect the concentration of O_3 in the troposphere. Historically, to determine how certain anthropogenic emissions affect concentrations of pollutants in the atmosphere, two major types of approaches have been used. First, is the sensitivity analysis approach which is also known as the "Perturbation approach" and the second method is source appointment method which is also knows as the "Tagging approach". For this thesis, the tagging approach is used and the method behind this approach is described in Section 5.1.1.

5.1.1. Tagging Approach

The Tagging approach aims to track all different contributions, which can either come from different sectors such as aviation, shipping, road traffic, etc. or from different regions across the globe. The tagging method labels all of the different contributions from the different sectors or regions and this label is then carried throughout the process of the simulations. This means that all NO_x emissions can then be categorised as shown in Equation (5.1), where the total NO_x emitted is the sum of the different tagged NO_x, which are denoted by i, where each tagged category is denoted with a number between 1 and N, the number of tags.

$$\mathrm{NO}_x = \mathrm{NO}_x^{\text{aviation}} + \mathrm{NO}_x^{\text{shipping}} + \mathrm{NO}_x^{\text{road traffic}} + ... = \sum_{i=1}^{N} \mathrm{NO}_x^i \tag{5.1}$$

As mentioned in Section 3.1 the formation of Ozone (O_3) in the troposphere is preceded by the photolysis of Nitrogen Dioxide (NO_2). Without this photolysis reaction O_3 cannot be formed. Before the photolysis of NO_2 can occur, the NO_2 needs to be formed, leading to the chain of reactions shown in Reactions R11, R1 and R2. Thus, in this case Reaction R11 is the rate limiting reaction (Grewe et al., 2017).

$$\mathrm{HO_2} + \mathrm{NO} \longrightarrow \mathrm{NO_2} + \mathrm{OH} \tag{R11}$$

$$\mathrm{NO_2} + h\nu \longrightarrow \mathrm{NO} + \mathrm{O} \tag{R1}$$

$$\mathrm{O} + \mathrm{O_2} + \mathrm{M} \longrightarrow \mathrm{O_3} + \mathrm{M} \tag{R2}$$

This means that the production rate of the O_3 is based on the concentrations of Nitric Oxide (NO) and Hydroperoxyl (HO_2). Thus the rate of reaction is given by Equation (5.2), where k_{R11} is the rate coefficient. Implementing the summation notation leads to Equation (5.3) and redistributing the terms leads to Equation (5.4) and Equation (5.5), which subsequently leads to Equation (5.6). Equation (5.6) shows that the rate of reaction can be broken down into the different tagged components. $P_{R11}^{\text{aviation}}$ in Equation (5.6) is the rate of production of O_3 due to NO_x and HO_2 stemming from aviation, as defined in Equation (5.8).

$$\begin{aligned}
P_{R11} &= k_{R11}\mathrm{NOHO_2} && (5.2)\\
&= k_{R11}\sum_{i=1}^{N}\mathrm{NO}^i\sum_{j=1}^{N}\mathrm{HO_2^j} && (5.3)\\
&= k_{R11}\sum_{i=1}^{N}\left(\mathrm{NO}^i\mathrm{HO_2^i} + \sum_{j\neq i}\frac{1}{2}\mathrm{NO}^i\mathrm{HO_2^j} + \sum_{j\neq i}\frac{1}{2}\mathrm{NO}^j\mathrm{HO_2^i}\right) && (5.4)\\
&= \sum_{i=1}^{N}\frac{1}{2}k_{R11}\left(\frac{\mathrm{NO}^i}{\mathrm{NO}} + \frac{\mathrm{HO_2^i}}{\mathrm{HO_2}}\right) && (5.5)\\
&= P_{R11}^{\text{aviation}} + P_{R11}^{\text{shipping}} + P_{R11}^{\text{road traffic}} + ... && (5.6)\\
&= \sum_{i=1}^{N} P_{R11}^i && (5.7)
\end{aligned}$$

It is important to mention that in Equation (5.5) and Equation (5.8), the factor of $\frac{1}{2}$ stems from the last two terms in Equation (5.4), which are the split parts of the O_3 production term for when $i \neq j$, meaning that the O_3 produced is equally attributed to both emission categories i and j. It is also important to note that the term $P_{R11}^{\text{aviation}}$ as defined in Equation (5.8) includes the reactions of all $\mathrm{NO}_x^{\text{aviation}}$ with all other HO_2 molecules and the reaction of all $\mathrm{HO_2^{aviation}}$ molecules with all NO_x molecules, without any double counting. The latter is ensured by the factor of $\frac{1}{2}$.

$$P_{R11}^{\text{aviation}} = \frac{1}{2}P_{R11}\left(\frac{\mathrm{NO}^{\text{aviation}}}{\mathrm{NO}} + \frac{\mathrm{HO_2^{aviation}}}{\mathrm{HO_2}}\right) \tag{5.8}$$

Each tagged emission sector or region then has its own differential equation as shown in Equation (5.9), where P and L represent the relevant production and loss terms. Using this approach Grewe et al. (2010) showed that the sum of all contributions adds up to the total concentration of the respective

Tag	Tag Description
str	Stratospheric Ozone
air	Aviation Emissions
land	Land Emissions
ship	Shipping Emissions
soi	Biogenic Emissions
bio	Biomass Burning
N_2O	N_2O Degradation
lig	Lightning Emissions
CH_4	CH_4 Degradation

Table 5.1: A description of the tags used for the source attribution analysis in this thesis

species such that Equation (5.1) is true for all species, including O_3. This means that the tagging approach is able to fully partition individual chemical fields into the contributions of individual emission sectors or emission regions, enabling source contribution analyses. A detailed description of how the tagging submodel is implemented in the EMAC model is given by Grewe et al. (2017).

$$\frac{d}{dt}\mathrm{O}_3^{\text{aviation}} = P^{\text{aviation}} - L^{\text{aviation}} \tag{5.9}$$

The tagged sources that are used in this thesis are summarised in Table 5.1. For these tags it is important to note that land emissions includes road emissions and anthropogenic non-traffic emissions. In literature land emissions is often referred to "anthropogenic" emissions, but at times authors also look at just road (land) transport. Furthermore, the biomass burning tag, also includes the contribution of agricultural waste burning. In the original EMAC model data, the land emissions and shipping emissions tags were further broken down into the different contributions of land and oceanic regions. However, since this thesis focuses on the contribution of aviation emissions, these different regional contributions were added up to form one land emissions tag and one shipping emissions tag.

5.1.2. Comparing Perturbation and Tagging Approaches

As mentioned previously, both perturbation and tagging approaches have historically been used to quantify the effects of emissions sources on the concentrations of pollutants. However, it is important to note that the results obtained using the different approaches vary in physical meaning.

The Perturbation approach evaluates and analyses the impact of an emission source to the atmospheric concentration of a species using two separate simulations. The first simulation is the base case and in the second simulation a perturbation (change) is made to the emission source. The goal is then to find the difference between both simulations to determine the impact of the change of the emission source. The Perturbation approach is based on using a Taylor approximation to determine the difference between the two simulations, which is described in more detail by (Grewe et al., 2010).

Grewe et al. (2012) carried out an analysis, looking at the difference between the results found using the tagging and perturbation approach. The authors looked at how the two methods provided different results in regards to the effect of road traffic NO_x emissions to the total tropospheric O_3 column. The authors showed that the two different methods have two very different use cases. The tagging approach provides information regarding the contribution of emission sources towards pollutants, whereas the perturbation approach looks at how changing concentrations of certain emission sources changes the concentrations of the pollutants. This means, that the two approaches fundamentally answer two different questions, however, these two methods are still used interchangeably by many authors. This key difference between the two methods is important to note when comparing the results of this thesis to existing literature.

5.2 Data Handling

Once the EMAC model was used with the previously described source attribution method, the resulting data had to be processed to conduct the analysis required to answer the research questions for this thesis. First, the data had to be filtered which is explained in Section 5.2.1. To get a better understanding of the spatial distributions across the horizontal and vertical grid, several altitude and regional domains were created, which are described in Section 5.2.2. Finally, the average weighted O_3 mixing ratio and the O_3 burden efficiency (OBE) were used as metrics for the analysis. How these two metrics are calculated is described in Section 5.2.3 and Section 5.2.4 respectively.

5.2.1. Filtering the Data

Initial inspection of the data showed that numerical artifacts were appearing in the results obtained from the EMAC model simulations. It is important to note that these artifacts only occurred for the tagged tracers. These artifacts occur because of the strong non-linearities in chemistry near strong sources, which cannot be captured by the simplified chemistry of the tagging sub-model. An example of these numerical artifacts can be seen in Figure 5.2, which shows the cartograph for the average aviation contribution to O_3 in 2018 at ground level. Further analysis of Figure 5.2 shows that the values of the peak $O_3{}^{air}$ values occurring over east Asia and mainland Europe are over 100 nmol $\cdot$ mol^{-1}, while everywhere else the $O_3{}^{air}$ mixing ratio is less than 3.5 nmol $\cdot$ mol^{-1}. These artifacts are most likely caused by a combination of numerical diffusion and noise from the tagging scheme. These artifacts were present in the datasets of multiple years for multiple tagged O_3 species. Due to their very large values, these numerical artifacts can have a very large impact on any averages that are computed using these values. Therefore, these artifacts had to be filtered out of the raw model results before further analysis could be conducted.

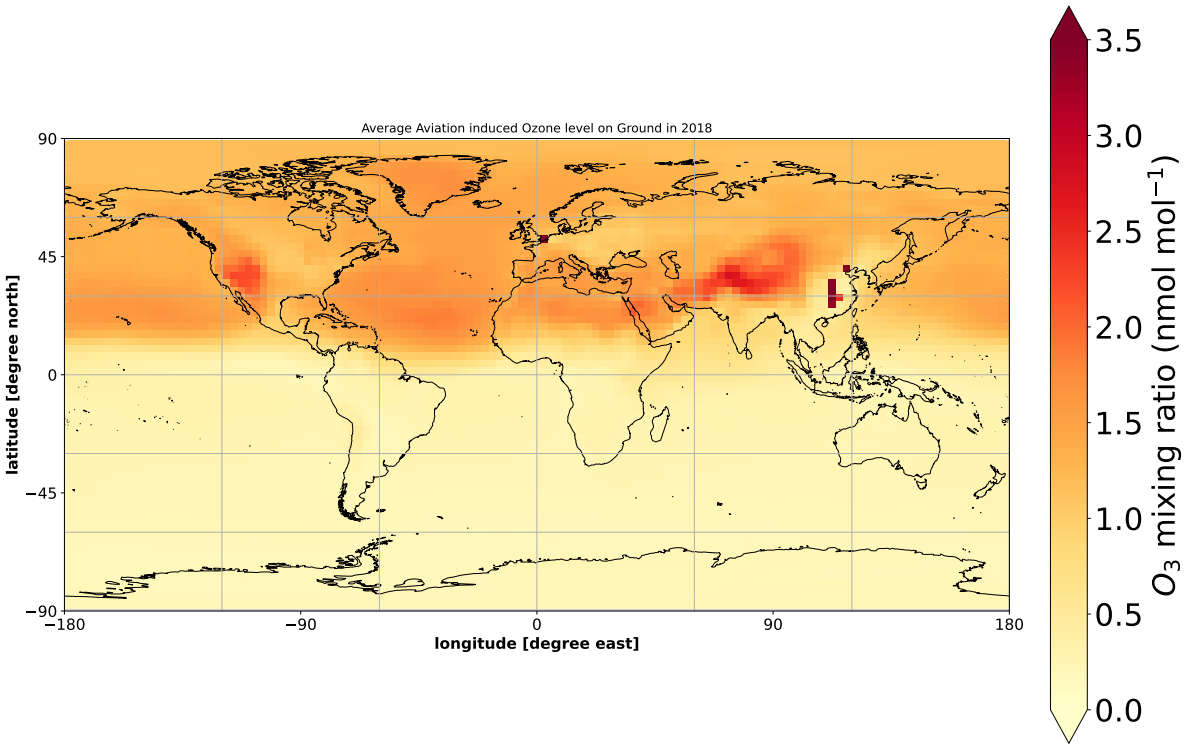

Figure 5.2: Cartograph of the average aviation contribution to O_3 on ground level for 2018 before any filtering has been applied to the data. The cartograph shows the presence of numerical artifacts over east Asia and mainland Europe.

The filtering out of the numerical artifacts was done for each tagged O_3 species at each vertical level individually. A threshold filter based on the average value of the mixing ratio at the level was implemented and values that were at least 10 times larger than the average, were discarded. This average based filtering needed to be done for each individual O_3 species and for each individual vertical level,

as the average varied for each species at each level. Increasing altitudes lead to increasing O_3 lifetimes as stated in Section 4.3, which means that with increasing altitude, O_3 concentrations increase as well. Implementing the filtering meant that the results shown in Figure 5.2 were now as shown in Figure 5.3, with the numerical artifacts being gone.

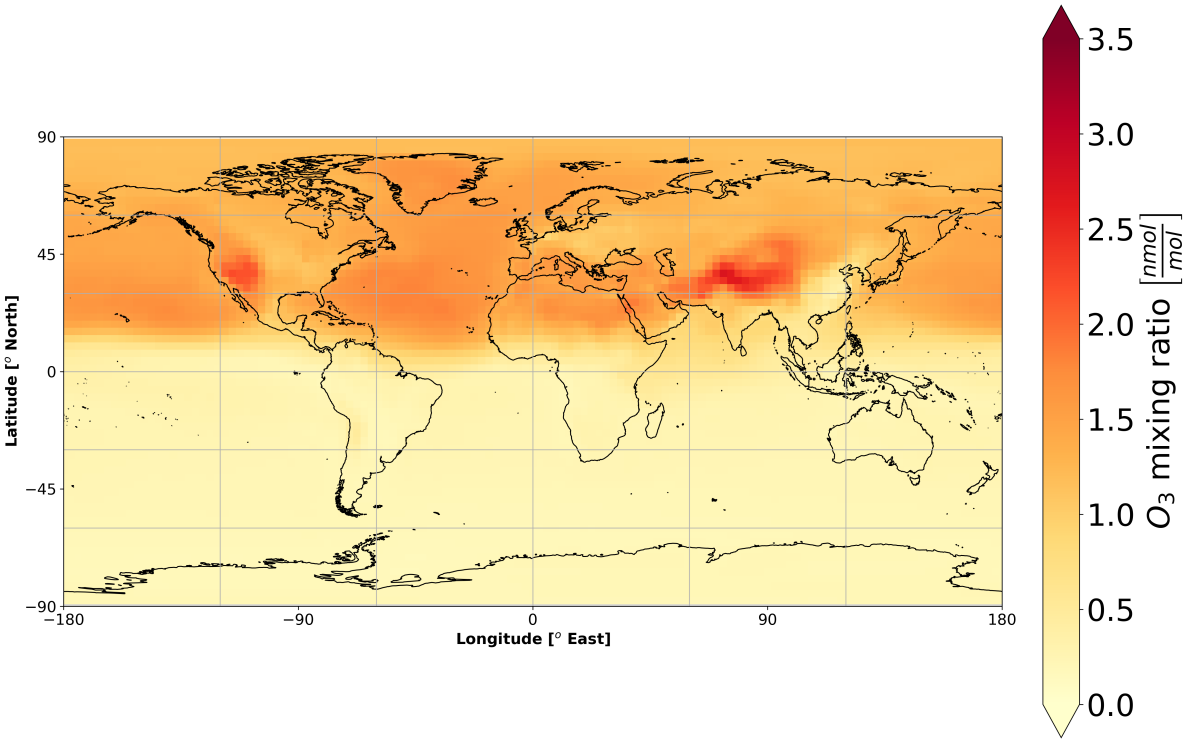

Figure 5.3: Cartograph of the average aviation contribution to O_3 on ground level for 2018 after the threshold filtering was applied to the data.

5.2.2. Definition of Altitude and Regional Domains

To better understand the spatial distribution of O_3, O_3^{air} and other O_3^{tagged}, the horizontal and vertical grid were broken down into multiple regions and altitude domains. Firstly, three altitude domains are considered; the entire troposphere ($\geq$ 150 hPa), the flight altitudes (200 hPa to 300 hPa), representing typical commercial aviation altitudes and the ground level, representing near surface conditions. However, for the analysis of the OBE, the planetary boundary layer is looked at instead of the ground level. This is due to the emissions profile of shipping, land emissions and biomass burning, as the emissions inventories for these sources are not given for model levels but heights from sea level. To include as much of these emissions grid points as possible, the planetary boundary layer is chosen to represent the lower segment of the troposphere.

The horizontal grid is broken down into several rectangles to represent the different continents. This break down of the horizontal grid is shown in Figure 5.4. To simplify the breakdown of the horizontal grid into multiple different domains, the regions considered are simple rectangles as shown in Figure 5.4. This has the effect that the exact continental borders are not held up throughout this analysis and that oceans are assumed to be part of the continents. This has the impact that for example shipping emissions are allocated to the respective regions, whereas in reality these emissions occur in the oceans.

For the regional analysis in this thesis only the regions of North America, Europe and Asia are considered. In general, literature shows that O_3 concentrations are higher in the northern Hemisphere. This primarily due to the fact that emissions in northern hemisphere are higher than in the southern hemisphere. Furthermore, analyses by Elshorbany et al. (2024), Mertens et al. (2024) and Nalam et al.

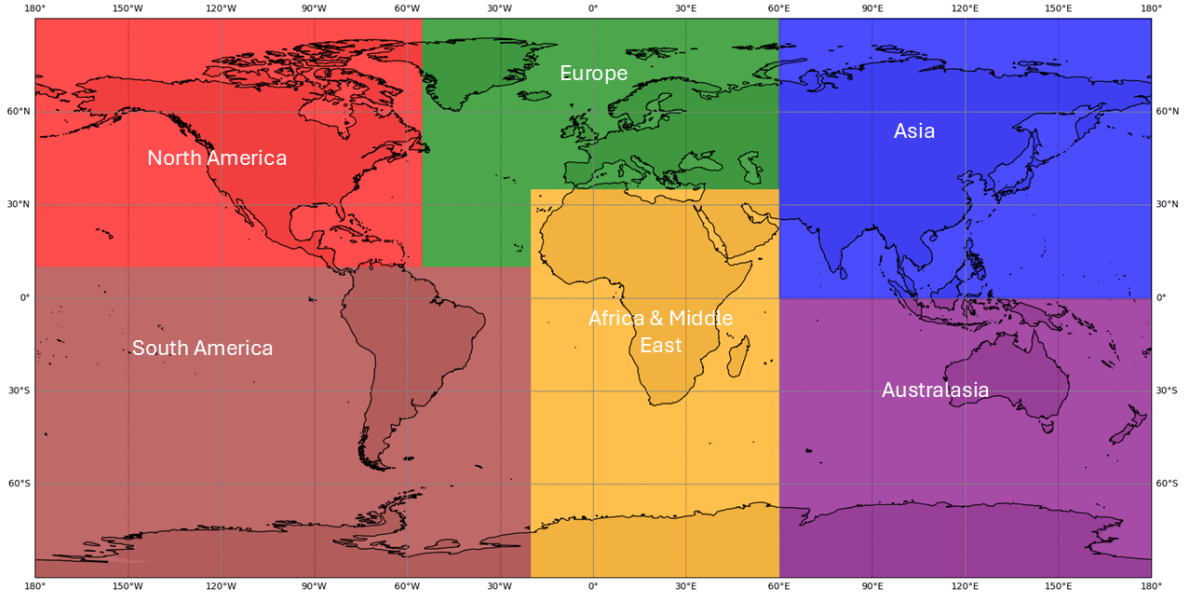

Figure 5.4: A visualisation of the different regional domains which are considered.

(2025) show that the largest O_3 concentrations are caused by Europe, North America and Asia and that these concentrations are primarily driven by the NO_x and VOC emissions in these regions. Thus, to limit the scope, but also look at the regions with the largest contributions, only Europe, Asia and North America are considered for the regional analysis in this thesis.

Here it is important to mention that the regional analysis does not use a regional tagging technique, which attributes O_3 to precursor emissions from the aforementioned geographical areas. Instead, the regional analysis in this thesis is performed by examining subsets of the model's horizontal grid to better understand trends within specific regions. In reality, horizontal transport plays a large role in the spatial distribution of O_3 and O_3 precursor concentrations. This means that for example part of the tropospheric O_3 concentration over Europe could be attributed to precursors from North America or Asia. But this attribution is not accounted for in the regional analysis in this thesis and that is something that should be kept in mind when examining the results in this thesis.

5.2.3. Average Volumetric Mixing Ratio Calculation

The O_3 molar mixing ratio results from the EMAC model vary across the horizontal grid which consists of 64 latitudes and 128 longitudes, while also varying across the 90 vertical levels. To simplify the analysis, often throughout this thesis, the average O_3 concentrations are calculated across different vertical levels or across different (or all) regions on the horizontal grid. However, calculating these averages requires a weighting. For averaging of several vertical levels, the weighting is required due to the decreasing air density with increasing altitude. For averaging across the horizontal grid, weighting is required, because of the decreasing grid box area closer to the poles, which comes from the spherical shape of the earth.

To calculate the average O_3 molar mixing ratios ($VMR_{average}$), weighting based on the dry air mass (m_{air}) is used as shown in Equation (5.10), where i represents each grid point that is part of the domain to be averaged.

$$VMR_{average} = \frac{\sum VMR_i \cdot m_i^{air}}{\sum m_i^{air}} \tag{5.10}$$

In literature the average molar mixing ratio is mostly calculated using the model grid area as a weighting to account for the curvature of the earth and thus the decreasing grid areas, at higher latitudes. However, most often, the $VMR_{average}$ is only calculated for ground level, whereas for the whole troposphere, the total burden or O_3 column are calculated. This thesis, aims to look at contributions to O_3 across altitudes and thus to carry out this comparison between the different altitude domains, a mass normalised metric is required, such as the $VMR_{average}$ as defined in Equation (5.10). On the other hand, grid area based weighting does not account for topography when looking at ground level mixing ratios and it does not account for changes in air density and mass across different altitudes.

5.2.4. Ozone Burden Efficiency Calculation

This thesis looks at the ozone burden efficiency (OBE) as a metric for the variations in O_3. As shown in Section 4.4 the OBE for a specific tagged source is defined as Equation (5.11). However, calculating the OBE for each individual grid point can lead to numerical operations that are undefined due to division by zero errors. This happens because locally no NO_x emissions occur by a certain source, or the amount of NO_x emitted is very small, falling below numerical resolution thresholds. Thus, no local OBE can be meaningfully evaluated for that specific source in that specific location. However, it is important to note that the lack of NO_x does not mean that there is also no O_3 present at this grid point. O_3 can still be present due to transport of emissions or O_3 from other grid points, or in-situ production of O_3 from other precursors.

$$OBE = \frac{B\left(\mathrm{O}_3^{\mathsf{tag}}\right)}{E\left(\mathrm{NO}_x^{\mathsf{tag}}\right)} \tag{5.11}$$

Due to these division by zero errors, this thesis only looks at global or regional values of the OBE, with the former being the OBE representing the global grid and the latter being the OBE which represents specific regions from Figure 5.4. These values are calculated by first calculating the total O_3 burden for the considered area, which is done using the VMR, the molar mass (M) of O_3 and air and the dry mass of air (m_{air}) as shown in Equation (5.12). In Equation (5.12), i represents all grid points across the horizontal and vertical grids that the OBE is being calculated for.

$$B\left(O_3^{\mathsf{tag}}\right) = \sum \mathsf{VMR}_i^{\mathsf{tag}} \cdot \frac{M_{O_3}}{M_{\mathsf{air}}} \cdot m_i^{\mathsf{air}} \tag{5.12}$$

The NO_x emissions for shipping, land emissions, biomass burning and aviation are provided as inputs for the EMAC model. These emissions are given as area (per $m^2 \cdot s$) or volume (per $m^3 \cdot s$) fluxes that vary globally over time. The fluxes for all NO_x sources are converted to masses at each grid point by multiplying by the surface area or the grid volume of the corresponding grid cell and using the molar mass of NO (Nitric Oxide). This yields the total emitted NO_x mass per grid cell, which can be integrated across the whole global or regional area by summation. This summation leads to $E\left(\mathrm{NO}_x^{\mathsf{tag}}\right)$, which along with the previously calculated $B\left(\mathrm{O}_3^{\mathsf{tag}}\right)$ leads to the OBE for the considered region in the considered altitude domain. Here it is important to note that the degradation of CH_4 and N_2O does not emit any NO_x, which means that no OBE values can be calculated for these tagged sources.

6

Ozone Levels in the Troposphere

Before trying to understand the contribution of aviation to tropospheric O_3, it is important to gain an understanding of the total O_3 levels in the troposphere. This chapter looks at the global levels of O_3 in Section 6.1 across the various altitude domains. These are then used as a basis of comparison with previously report values in literature to evaluate the EMAC model's accuracy in Section 6.2. Section 6.3 looks at the regional distribution of O_3 across the previously defined regions and Section 6.4 looks at the spatial distribution of O_3 to better understand the distributions and trends.

6.1 Global Overview of Ozone

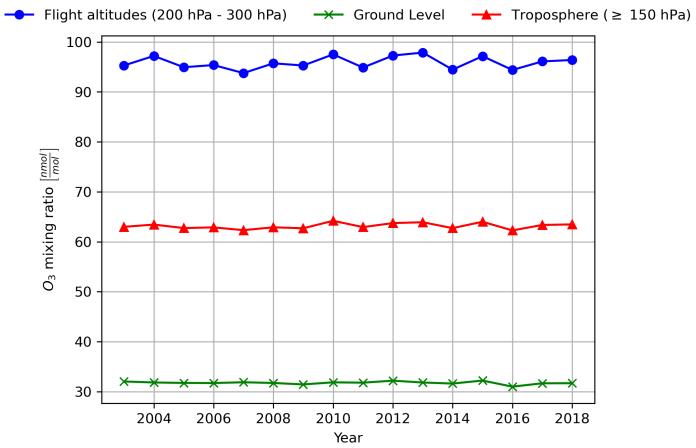

Figure 6.1: Comparison of the temporal evolution in global annual molar mixing ratio averages of O_3 of the whole troposphere, the ground level and the flight altitudes. The individual plots for the different altitudes are shown in Figure A.1, Figure A.2 and Figure A.3 respectively.

Figure 6.1 shows the temporal evolution of the global annual molar mixing ratio averages of O_3 for the whole troposphere, the ground level and the flight altitudes. Looking at Figure 6.1 shows that on average the air mass weighted O_3 mixing ratio of the troposphere is around 63 nmol $\cdot$ mol^{-1}, 95 nmol $\cdot$ mol^{-1} for the flight altitudes and around 31 nmol $\cdot$ mol^{-1} for the ground level. Similar O_3 ground level mixing ratios are reported by Butler et al. (2018), Butler et al. (2020) and Nalam et al. (2025), who use grid area based weighting for their calculations. No averaged mixing ratio values could be found for the whole troposphere or the flight altitudes in existing literature. Larger mixing ratios at the flight altitudes in comparison to the ground level are to be expected. At lower altitudes the lifetime of NO_x

is shorter, because the reactions that act as removal pathways (e.g. reaction with OH to form HNO_3 as shown in Reaction R16) for NO_x are more efficient due to higher mixing ratios of OH (Grewe et al., 2002). The higher lifetime of NO_x at higher altitudes in the troposphere, allows the NO_x to persist and take part in more O_3 forming reactions across a longer time. This effectively leads to larger O_3 levels at higher altitudes. Furthermore, O_3 also has a longer lifetime at higher altitudes. This is because at higher altitudes, the removal rates for O_3 are slower, which leads to more efficient accumulation of O_3 (Maruhashi et al., 2022). Additionally, at ground level and in the planetary boundary layer, dry deposition of O_3 acts as a major sink, whereas in the upper troposphere dry deposition of O_3 has a limited impact. This means that at lower altitudes, the dry deposition hinders the accumulation of O_3 leading to lower O_3 mixing ratios. Furthermore, the contribution of STE to O_3 also has an altitude based variability, leading to a higher contribution to O_3 mixing ratios in the upper troposphere compared to ground level (Elshorbany et al., 2024; Nalam et al., 2025).

Comparing the year on year fluctuations to the change in the O_3 mixing ratio from 2003 to 2018 in Figure A.1, Figure A.2 and Figure A.3, shows that there is no significant trend across the considered years. In all three figures, the absolute difference between the O_3 mixing ratio in 2003 and 2018 is similar to most of the year on year fluctuations, thereby suggesting that the overall change is insignificant. The existence of a trend could be further examined using statistical analysis such as the Mann Kendall test, however, this is beyond the scope of this thesis. Figure A.2 and Figure A.3 shows that the trend of the fluctuations does not always match. This means that when there is a year on year increase in the ground level O_3 mixing ratio, the O_3 mixing ratio at the flight altitudes does not necessarily increase.

The year on year fluctuations that are seen in Figure A.1, Figure A.2 and Figure A.3 could have multiple sources. Firstly, the causes could be physical, with the fluctuations occurring across the years due to changing NO_x emissions or changing background NO_x levels leading to variations in the NO_x - O_3 chemistry. Furthermore, the fluctuations in O_3 time series could also be caused by changes in contributions of different sources across the years. This could be checked with the available data, however, this is out of the scope of this thesis. The fluctuations in the O_3 time series could also be driven by changing meteorological conditions, which impact the atmospheric transport patterns and the composition of the atmosphere. Furthermore, the fluctuations could also be caused by specific events, which may have impacted the contribution of individual tagged sources.

6.2 Model Data Evaluation

Figure 6.2 shows the total O_3 burden in the troposphere, as simulated by the EMAC model. Figure 6.2 shows that the total tropospheric O_3 burden fluctuates around 454 Tg. Nalam et al. (2025) find a total tropospheric O_3 burden of 320 Tg, which represents their average value for the time period of 2000 to 2018. Similar results are found by Butler et al. (2018) and Mertens et al. (2018). These values found in literature are withing the range reported by Young et al. (2013), who find a multi-model mean tropospheric O_3 burden of around 337 Tg $\pm$ 23 Tg for the year 2000, where the latter value represents 1 standard deviation of the inter-model spread. For their analysis, Young et al. (2013) also look at results obtained using the EMAC model, which is shown to lead to an O_3 burden of around 380 Tg for the year of 2000. Comparing these literature values, to the values presented in Figure 6.2, shows that the tropospheric O_3 burden as calculated in this thesis, does not match literature findings and that it significantly overestimates the O_3 burden.

Further analysis of the results shows, that the discrepancy in the tropospheric O_3 burden comes down to the differing definitions of the troposphere that are used to simplify the calculation process. In this thesis, the troposphere is defined as air where the air pressure is $\geq$ 150 hPa, whereas in literature most authors define the troposphere as air where the O_3 mixing ratio is $\leq$ 150 nmol $\cdot$ mol^{-1}. The difference between these definitions is shown in Figure 6.3. Figure 6.3 shows that in the tropics between approximately 30^o South and approximately 30^o North, the troposphere as defined in literature accounts for a larger portion of the atmosphere compared to the troposphere as defined in this thesis. However, between approximately 30^o and 90 ^{o} in both hemispheres, the the troposphere definition used in this thesis

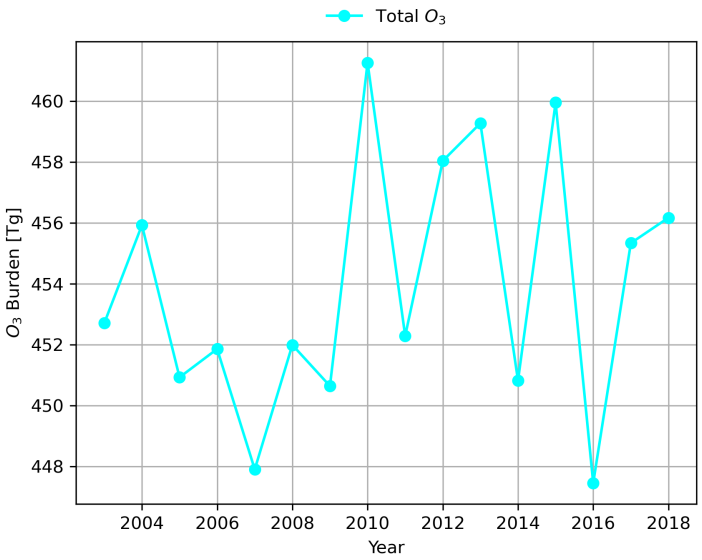

Figure 6.2: The temporal evolution in the total tropospheric O_3 burden.

accounts for a larger portion of the atmosphere compared to the troposphere definition in literature. This difference in the troposphere definitions in the mid to high latitudes leads to the strong difference between the values seen in Figure 6.2 and the ones found in literature. Figure 6.3 also shows the tropopause height as calculated by the EMAC model and it can be seen the troposphere definition as commonly used in literature matches the shape of the tropopause quite well, with some differences. In their estimates Young et al. (2013) found that these differences between the calulated tropopause and the troposphere definition leads to a discrepancy of about $\pm$ 5% in the burden and O_3 column.

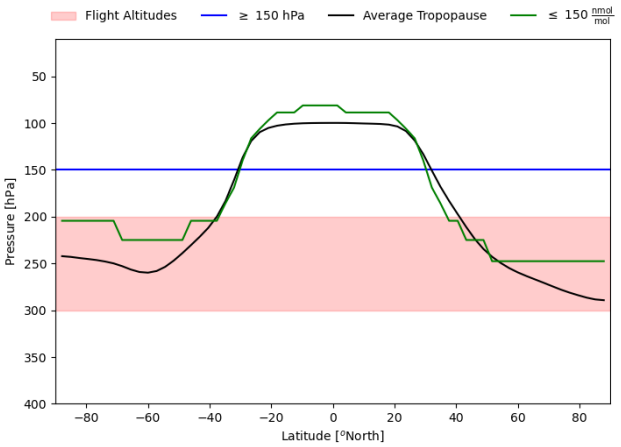

Figure 6.3: Comparison between the troposphere definition used in literature ($\leq$ 150 nmol $\cdot$ mol^{-1}), in this thesis ($\geq$ 150 hPa) and the tropopause as calculated by the EMAC model. The lines shown are averaged across the time period of 2003 to 2018. The plot also compares these tropopause definitions to the definition of the flight altitudes.

Using the troposphere definition of air where the O_3 mixing ratio is $\leq$ 150 nmol $\cdot$ mol^{-1} leads to the tropospheric O_3 burden values shown in Figure 6.4. Figure 6.4 shows that the tropospheric O_3 burden fluctuates around approximately 377 Tg, which is similar to the EMAC model reported by Young et al. (2013) for the year 2000. Furthermore, the values in Figure 6.4 also fall within two standard deviations of the inter-model spread from the multi-model mean that was reported by Young et al. (2013) and mentioned previously. Minor differences between the values in Figure 6.4 and the values found by Young et al. (2013) can be explained by the fact that different meteorologies are used, since different years are considered for the analysis along with the use of different emission inventories. Differences

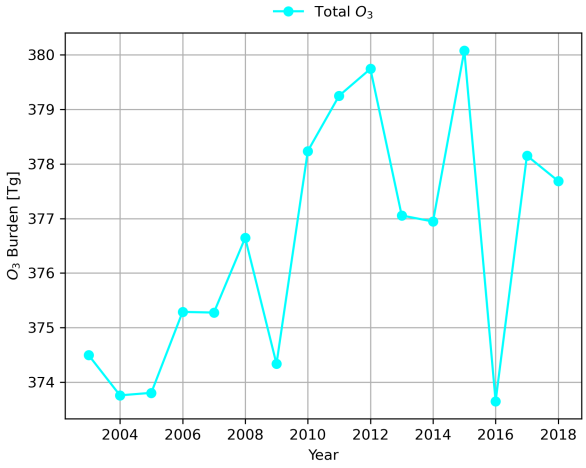

][h]

Figure 6.4: Tropospheric O_3 Burden using the troposphere definition of air where the O_3 mixing ratio is $\leq$ 150 nmol $\cdot$ mol^{-1}.

between the values seen in Figure 6.4 and the values found by Butler et al. (2020) and Nalam et al. (2025) can also be explained by the use of different emission inventories, but also by the use of different Chemistry Climate models. In general, Jöckel et al. (2016) found that the EMAC model has a strong positive O_3 bias, which explains why the tropospheric O_3 burden results found using EMAC are higher than the ones found by Butler et al. (2020) and Nalam et al. (2025), who use the Community Atmosphere Model version 4 with Chemistry (CAM4) which is a component of the Community Earth System Model (CESM).

Figure 6.5 and Figure 6.6 show the temporal evolution of production, depletion and net production rates of tropospheric O_3 using the troposphere definition of $\geq$ 150 hPa and $\leq$ 150 nmol $\cdot$ mol^{-1} respectively. As expected, the production, depletion and net production rates are larger in magnitude in Figure 6.5 compared to the rates in Figure 6.6. This is expected, because as was identified earlier, the troposphere definition based on the air pressure considers a larger portion of the stratosphere than the troposphere definition, which is based on the O_3 mixing ratio.

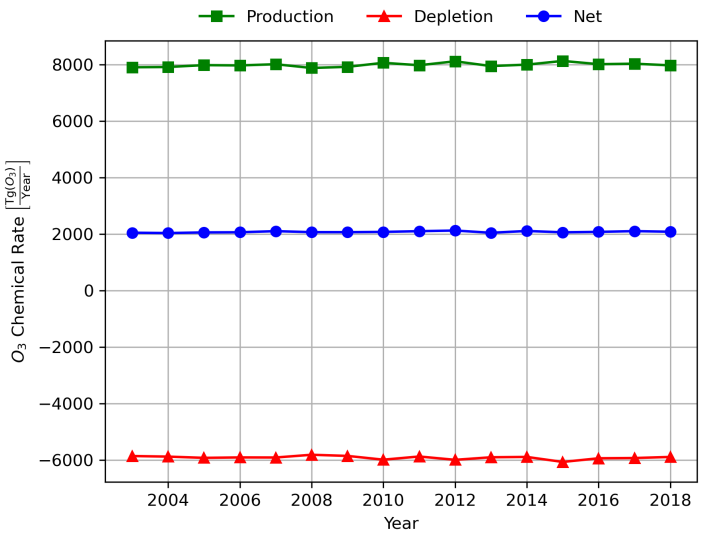

Figure 6.5: Temporal evolution of production, depletion and net production rates of tropospheric O_3, using the troposphere definition of $\geq$ 150 hPa.

Griffiths et al. (2021) find that the chemical production rate of O_3 ranges from around 4000 Tg(O_3)$\cdot$Year^{-1}

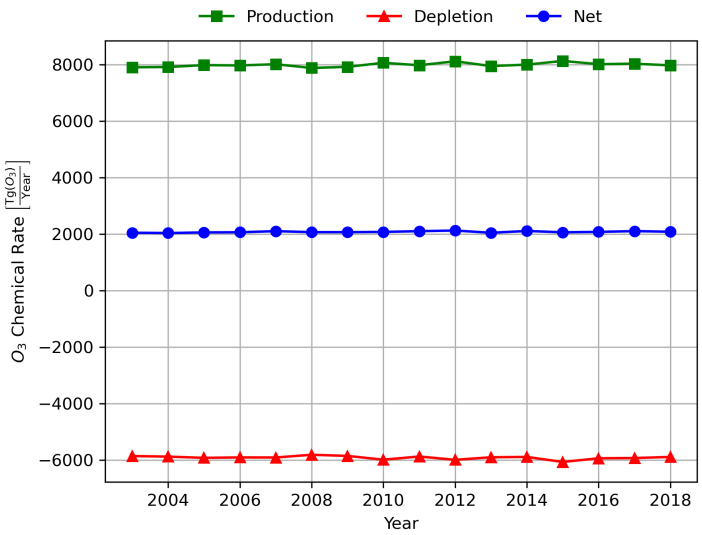

Figure 6.6: Temporal evolution of production, depletion and net production rates of tropospheric O_3, using the troposphere definition of $\leq$ 150 nmol $\cdot$ mol^{-1}.

to around 9000 Tg(O_3)·Year^{-1} for various CMIP6 models, while the depletion rate ranges from 3500 g(O_3)·Year^{-1} to around 5000 g(O_3)·Year^{-1}. For the chemical production rate, Griffiths et al. (2021) find that the Goddard Institute for Space Studies (GISS) chemistry climate model leads to the highest values, however in their analysis the GISS model did not provide the chemical depletion term. In general, Griffiths et al. (2021) find that the GISS model leads to large chemical production terms compared to the other models that are analysed, but there is good agreement across all models in terms of the O_3 burden. Similarly, it seems that the EMAC model used in this thesis, leads to high magnitudes of chemical production and depletion rates when compared to the various CMIP6 models that are analysed, however there is a good agreement with the O_3 burden values reported in Figure 6.4. It is however, important to note that Griffiths et al. (2021) use the tropopause as calculate by the models to define their troposphere, but this difference in the troposphere definition should only account for minor differences between the CMIP6 chemical rates reported by Griffiths et al. (2021) and the chemical rates seen in Figure 6.5 and Figure 6.6. The remaining difference is most likely driven by the differences in the chemical mechanisms that are considered, along with the use of different emissions inventories and the use of different meteorological data.

Overall, the analysis with the troposphere definition of air where the O_3 mixing ratio is $\leq$ 150 nmol·mol^{-1}, shows that the values found using the EMAC model used for this thesis match the values found in literature. This verifies the accuracy of the EMAC model that is used in this thesis. Additionally, it should be noted that the burden and rate contributions of the different tagged sources add up to the total O_3 burden and total O_3 net production rate, which verifies that the tagging model functions correctly. This is the case for the troposphere definition based on the air pressure as used in this thesis and the troposphere definition based on the O_3 mixing ratios as used in literature.

This analysis using the troposphere definition based on the O_3 mixing ratio highlights that the choice of the troposphere definition in this thesis is flawed. With the troposphere definition used in this thesis, parts of the stratosphere are captured by the troposphere in the mid to high latitudes as shown in Figure 6.3. Thus, in the analysis of the results in this thesis, the contribution of stratospheric O_3 to tropospheric O_3 will be overestimated, which will subsequently lead to an underestimation of the percentage contribution of different tagged sources for the whole troposphere. However, this definition of the troposphere does not impact the results that are found for ground level and the flight altitudes. However, for the latter altitude domain it is important to note that at latitudes higher than approximately 40^o in both hemispheres, the flight altitudes domain also includes a large portion of stratospheric air.

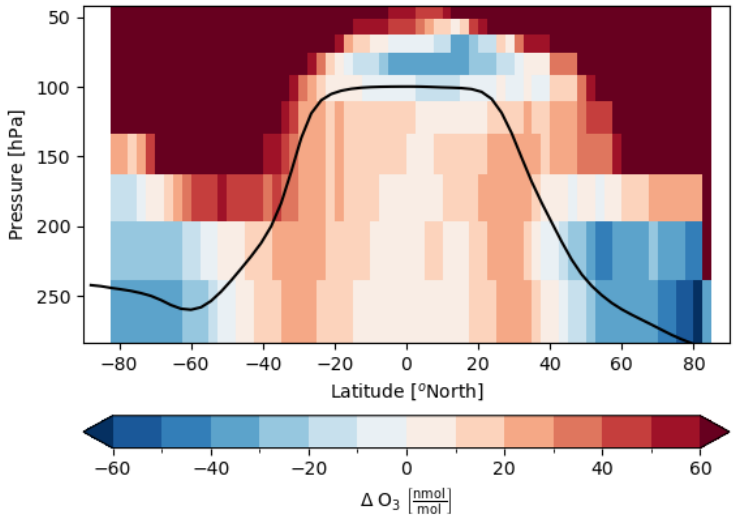

Figure 6.7: Absolute difference between the model O_3 mixing ratios and the mixing ratios of the SWOOSH data. The data is averaged for the years from 2003 to 2018. The color scale shown in the figure is optimised for tropospheric O_3. The black line in the figure represents the mean tropopause location across the years, as simulated by the EMAC model.

Figure 6.7 shows the absolute difference between the mixing ratios of the model and the mixing ratios from v2.7 of the Stratospheric Water and Ozone Satellite Homogenized (SWOOSH) dataset by Davis et al. (2016). For Figure 6.7 it is important to note that positive values represent overestimations of the EMAC model. Figure 6.7 is consistent with the findings of Jöckel et al. (2016) who show that the EMAC model has a positive O_3 bias, meaning that it overestimates the O_3 levels in the troposphere. However, as also suggested by Mertens et al. (2024), the direct comparison between the EMAC model results and the SWOOSH dataset can only be used qualitatively. Firstly, this is due to the fact that both the EMAC model data and the SWOOSH datasets have very different grid resolutions with the SWOOSH dataset having a resolution of 2.5^o and 31 levels. This means that horizontally, the SWOOSH dataset needs to be interpolated onto the coarser EMAC grid, while vertically the EMAC dataset needs to interpolated on the SWOOSH dataset. Mertens et al. (2024) also find that the peak of the upper tropospheric O_3 bias found in their comparison between EMAC model results and the SWOOSH dataset highly depend on the approach used for vertical remapping of the EMAC model. Furthermore, the averaging kernels are also not considered for the SWOOSH satellite data, which prevents the use of the SWOOSH dataset for a quantitative comparison.

In Section 6.1 it was mentioned that the ground level O_3 mixing ratio for the EMAC model was found to be about 31 nmol $\cdot$ mol^{-1} which matched the results found by Butler et al. (2018), Butler et al. (2020) and Nalam et al. (2025). Turnock et al. (2020) in their analysis show that a multi-model mean of the global O_3 mixing ratio is about 29.9 nmol $\cdot$ mol^{-1} with a standard deviation of 2.3 nmol $\cdot$ mol^{-1}. This comparison shows that the ground level results of the EMAC model used in this thesis are within one standard deviation of the multi-model mean values found by Turnock et al. (2020).

Bringing together, the comparisons between the EMAC model results, results found in literature and the SWOOSH dataset, shows that the EMAC data behaves as expected in terms of estimating O_3 mixing ratios. The simplified definition of the troposphere (air $\geq$ 150 hPa) has been shown to include a considerable amount of stratospheric air, which leads to differences in tropospherically averaged and integrated metrics such as the tropospheric O_3 burden. Implementing a more accurate troposphere definition has shown to converge to results that are found in literature, suggesting that the EMAC model used in this thesis can be confidently used to conduct an analysis of tropospheric O_3. Furthermore, the

analysis has also shown that the EMAC model used in this thesis has a positive O_3 bias when comparing it to observational data, which is consistent with the findings of Jöckel et al. (2016).

6.3 Regional Distribution and Trends

Figure 6.8, Figure 6.9 and Figure 6.10 show comparisons of the O_3 mixing ratios in Europe, Asia and North America for the complete troposphere, at flight altitudes and at ground levels respectively. Looking at the regional breakdown of the results discussed in Section 6.1, shows that even at regional scale no significant overall trend can be seen for the mixing ratio of O_3. For all three regions at all three altitude domains, there is no significant overall change in the O_3 mixing ratio between 2003 and 2018. Again, the difference between the O_3 mixing ratios in 2003 and 2018 is similar to the year on year change that is seen across the timespan of the data.

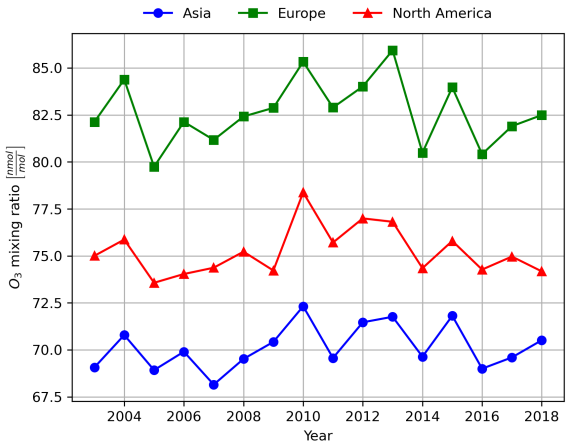

Figure 6.8: Comparison of the average annual O_3 mixing ratio for the whole Troposphere for Europe, Asia and North America

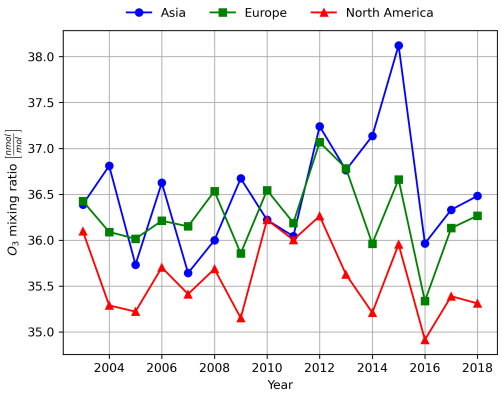

Figure 6.9: Comparison of the average annual O_3 mixing ratio at Ground level for Europe, Asia and North America

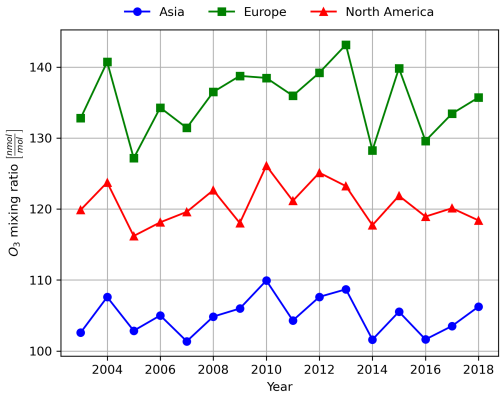

Figure 6.10: Comparison of the average annual O_3 mixing ratio at Flight altitudes for Europe, Asia and North America

Figure 6.8, Figure 6.9 and Figure 6.10 do however show that there is a difference in the O_3 mixing ratio between regions in different altitude domains. For the flight altitudes it can be seen that Europe has the largest O_3 mixing ratio fluctuating between 130 nmol $\cdot$ mol^{-1} and 140 nmol $\cdot$ mol^{-1}. This is followed by North America with a O_3 mixing ratio that fluctuates around 120 nmol $\cdot$ mol^{-1}, followed by Asia which fluctuates around 105 nmol $\cdot$ mol^{-1}. On the other hand, at ground level the O_3 mixing ratio for Europe and Asia are similar which fluctuate around approximately 36 nmol $\cdot$ mol^{-1}, whereas the O_3 mixing ratio fluctuates around 35.5 nmol $\cdot$ mol^{-1}. At the ground level the region with the highest O_3 mixing ratio initially alternates between Europe and Asia, but from 2014 onwards, Asia always has the

higher O_3 mixing ratio at ground level. The average O_3 mixing ratio for the whole troposphere, however, follows a similar trend as the flight altitudes, with the European O_3 mixing ratio fluctuating around 82.5 nmol $\cdot$ mol^{-1}, followed by North America which fluctuates around 76 nmol $\cdot$ mol^{-1}, while the O_3 mixing ratio for Asia fluctuates around 70 nmol $\cdot$ mol^{-1}

Looking at the differences between the regions, shows that for the whole troposphere and at flight altitudes, the O_3 mixing ratio is always highest for Europe, followed by North America and the mixing ratio in Asia is always the lowest. Tropospheric O_3 column measurements shown by Elshorbany et al. (2024), suggest that the tropospheric O_3 column values for the east of North America and the west of Europe are similar in magnitude, with the tropospheric O_3 column of east Asia, being the lowest. Assuming, that these subregions listed by Elshorbany et al. (2024) are representative of the regions considered in this thesis, the results shown in Figure 6.8 and Figure 6.10 do not fully match measurements. In both figures, the mixing ratios above Europe are approximately 10% larger than the mixing ratios above North America. These differences in the results could be due to differences between the used emission inventories used for the EMAC simulation and the actual emissions which led to the measured O_3 values. Furthermore, Jöckel et al. (2016) have shown that the EMAC model overestimate the O_3 levels across large parts of the globe. This in combination with the mismatch of emission inventories, could lead to results which vary from the measurement data presented by Elshorbany et al. (2024).

Butler et al. (2020) show that the annual average surface level mixing ratio of O_3 is just under 40 ppb for Asia, while it is about 35 ppb for Europe and about 33 ppb for North America. Comparing these results to the results shown in Figure 6.9, shows that the results for Asia are underestimated. Butler et al. (2020) suggests that Asia, as defined in this thesis, has a higher O_3 mixing ratio at surface level due to the fact that more of Asia's O_3 is produced from local emissions rather than from transported emissions from different regions. Furthermore, the authors also show that south Asian surface level emissions do not get transported to the surface of other parts of the northern hemisphere. Instead, these either form O_3 locally, or they are transported efficiently to higher altitudes in the free troposphere, where they have a larger contribution to the global tropospheric O_3 levels. On the other hand, the surface level emissions of Europe and North America are spread more globally across the surface level of the Northern Hemisphere. The fact that the surface O_3 level results shown for Asia are lower in Figure 6.9 when compared to the research done by Butler et al. (2020) might be due to the impact of different emission inventories. Additionally, it is also important to note that Jöckel et al. (2016) have shown that the EMAC model underestimates tropospheric O_3 levels in the east of Asia, which could be contributing towards the underestimation of the O_3 levels for Asia.

6.4 Spatial Distribution of Ozone

Figure 6.11, Figure 6.12 and Figure 6.13 show the spatial distribution of the average annual O_3 mixing ratio for 2018 for the whole troposphere, ground level and flight altitudes. Here it is important to note that the spatial distributions are only shown for 2018, because the spatial distributions do not change visibly between 2003 and 2018.

Figure 6.11 shows a strong difference in the O_3 mixing ratio between the northern and southern hemisphere. In the northern hemisphere the mixing ratio can get as high as 120 nmol $\cdot$ mol^{-1}, whereas in the southern hemisphere, the maximum mixing ratio is around 80 nmol $\cdot$ mol^{-1}. Furthermore, it can be seen that the southern hemisphere has a more uniform distribution of the O_3 mixing ratio compared to the northern hemisphere. Looking at the values in Figure 6.11 it is important to note that in Figure A.1, the average global mixing ratio of O_3 for 2018 was seen to be approximately 63.50 nmol $\cdot$ mol^{-1}. Comparing this with the large spatial distribution seen in Figure 6.11 further suggests that the year on year fluctuations seen in Figure 6.8 are not significant. This is because the overall difference between successive years in Figure A.1 is less than 2 nmol $\cdot$ mol^{-1}, whereas across the global grid the range of mixing ratio values is more than 80 nmol $\cdot$ mol^{-1} as seen in Figure 6.11. Furthermore, Figure 6.11 shows that the highest O_3 mixing ratios are found at mid to high latitudes with O_3 mixing ratio peaks in

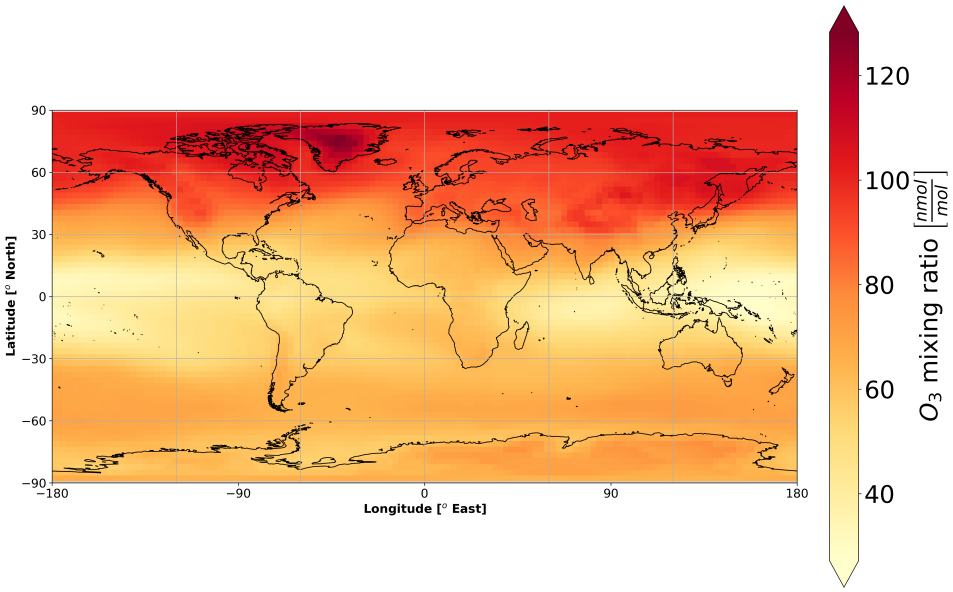

Figure 6.11: Cartograph of the average annual O_3 mixing ratio for the whole Troposphere in 2018

the arctic region, whereas the tropical and equatorial regions have the lowest mixing ratios.

The larger O_3 mixing ratios across the northern hemisphere are expected and these occur due to Europe, North America and Asia having the largest anthropogenic emissions (J. Liu et al., 2022). These emissions act as precursors for the formation of O_3 and are transported across mainly the northern hemisphere (Dahlmann et al., 2011). Figure 6.11 shows a latitudinal pattern, with O_3 mixing ratios increasing with increasing latitudes. This pattern is partially expected due to the Brewer Dobson circulation and the upwards motion it creates in the tropical regions and the downwards motion it creates in mid to high latitudes. This leads to air containing O_3 to be transported from the troposphere to the stratosphere in the tropical regions, while air containing O_3 is transported from the the stratosphere to the troposphere at the mid to high latitudes. Additionally, the local minima over the tropics are also due to the high local solar radiation and the abundant water vapor content in the air. Together these form OH which lead to the depletion of local O_3. Furthermore, these oceanic areas are around regions that have low emissions of O_3 precursors. Together the high rate of depletion of O_3, the low rate of formation of O_3 and the updraft motions lead to local minima in the tropical regions.

Figure 6.11, however, also shows an impact of the definition of the troposphere that is used in this thesis. Local maxima can be seen in Figure 6.11 close to the polar regions, which are not seen in literature (Dahlmann et al., 2011). As was discussed in Section 6.2, the definition which is used for the troposphere in this thesis captures more and more stratospheric air at higher latitudes and the poles. Thus, in Figure 6.11, the local maxima peaks in the polar latitudes are being caused by the stratospheric air that is being captured and the large mixing ratios of O_3, which occur in the stratosphere. Similarly Figure 6.3, also shows that in the tropical regions, the troposphere definition based on air pressure does not capture the whole troposphere. This means that Figure 6.11 under-represents the tropospheric O_3 in the tropical regions between 30^o South and 30^o North. The overestimation of tropospheric O_3 in the polar regions and the underestimation in the tropical regions, subsequently leads to the strong latitudinal gradient that is observed in Figure 6.11.

In Figure 2 of their paper, J. Liu et al. (2022) show the global distribution of the tropospheric O_3 column, which shows a similar distribution as observed in Figure 6.11. The distribution presented by J. Liu et al. (2022) is based on OMI/MLS measurement data, averaged for the time period between 2005 and 2018. It is important to note that the measurement data, only shows the distributions between 60^o

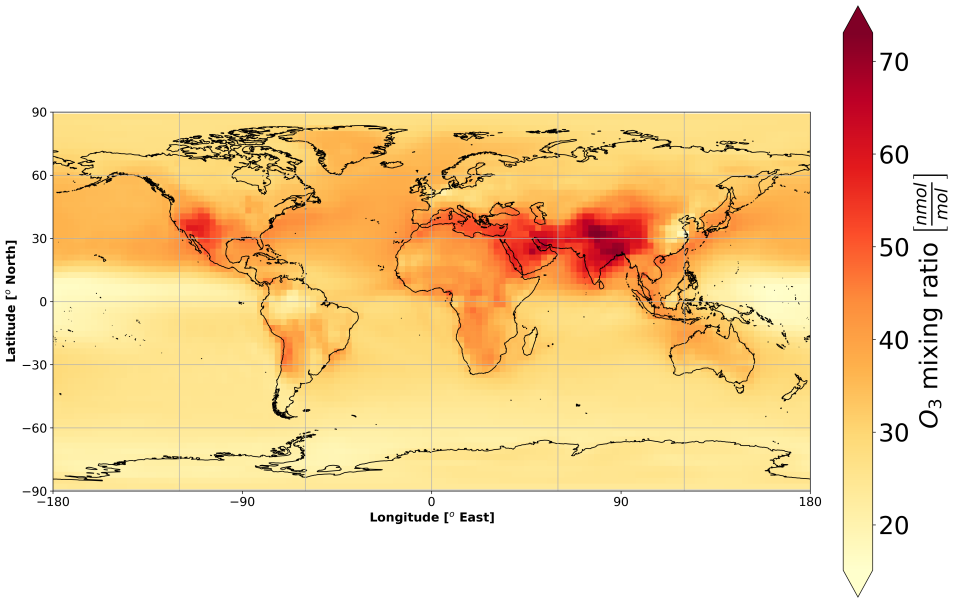

Figure 6.12: Cartograph of the average annual O_3 mixing ratio at Ground level in 2018

South and 60^o North. The measurement data presented shows local minima in the tropical region in the Pacific Ocean close to Indonesia and Papua New Guinea. On the other hand, the measurement data also shows local maxima in the Eastern parts of China and Asia, in the Northern Parts of India, in the Middle East and in the Mediterranean Sea. This means that Figure 6.11 aligns with measurement data on the location of local minima, but it does not align on the location of local maxima. Overall, the measurement data shows that the Northern hemisphere has a larger tropospheric O_3 burden and that the highest burden occurs between 30^o North and 60^o North. These results, provide further evidence on how the troposphere definition in this thesis, drives the latitudinal gradient which is seen in Figure 6.11. It should be noted that a direct quantitative comparison with the empirical results shown by J. Liu et al. (2022) is not made, as it beyond the scope of this thesis.

Figure 6.12 shows that the spatial distribution of the O_3 mixing ratio at ground level is very different compared to the distribution for the whole troposphere. Figure 6.12 still shows that the O_3 levels are higher in the northern hemisphere, however, Figure 6.12 does not show the strong latitudinal gradient that can be seen for the whole troposphere. Instead, the O_3 peaks are seen in northern India, western China, western United States and the middle East. These also coincide with some observable local peaks in Figure 6.11. Looking more closely at these regions in Figure 6.12 and Figure 6.11 it can be noted that these local maxima in O_3 mixing ratios occur in areas with elevation, showing that topography also impacts the O_3 mixing ratio. As, explained earlier, at higher altitudes both O_3 and NO_x lifetimes are higher, leading to higher O_3 mixing ratios. Thus, the highest O_3 mixing ratios at ground level occur over large mountain ranges, with the highest being over the Himalayan Mountains. Similarly, some of these maxima can also be identified in Figure 6.11, since the results in Figure 6.11 are simply the average values across the vertical column between the ground level and the troposphere boundary at 150 hPa. Thus, higher ground level values and topography above these mountain ranges, will lead to higher tropospheric O_3 mixing ratio averages.

Butler et al. (2020) look at the source attribution of O_3 at ground level in their paper and the authors show a total surface O_3 distribution that is similar to what can be seen in Figure 6.12. The Cartograph shown by Butler et al. (2020) shows the same peaks in the west of the North America, over India, over the Mediterranean ocean and over the Middle East. Butler et al. (2020) also show the spatial distributions of the different tagged NO_x sources. From these distributions it can be inferred that most of the local O_3 hotspots that can be seen in Butler et al. (2020) are due to high local anthropogenic emissions along with high anthropogenic emissions in neighbouring regions, in addition to the topography effect

mentioned earlier. The peak in the west of USA and central America is due to American anthropogenic emissions along with the O_3 due to shipping in the Pacific Ocean. The peak over India, is primarily due to local anthropogenic emissions in addition to some shipping emissions in the Indian ocean. As mentioned earlier, the O_3 formed due to South Asian (primarily Indian) anthropogenic emissions does not spread strongly longitudinally, but instead is efficiently transported to higher altitudes due to efficient convection. The local hotspots around and in the Middle East are shown to be due to the ”Rest of the World” tag set by Butler et al. (2020). This tag represents the anthropogenic emissions of South East Asia, Northern Africa, the Middle East, Central America and Central Asia. The high levels of O_3 seen in the Mediterranean region in Figure 6.12 are due to a combination of local shipping emissions and due to a southward transport of the anthropogenic emissions across mainland Europe.

The magnitudes of the spatial distribution in Figure 6.12 are similar in value to the results of Butler et al. (2020) and to results shown by Mertens et al. (2024). The previously identified local hotspots have O_3 levels of about 50 nmol $\cdot$ mol^{-1} to 60 nmol $\cdot$ mol^{-1} according to Butler et al. (2020) and Mertens et al. (2024). These values are similar to the values that can be seen in Figure 6.12. The local minima across the pacific are seen to be under 20 nmol $\cdot$ mol^{-1} in Figure 6.12, which is similar to the 10 nmol $\cdot$ mol^{-1} to 20 nmol $\cdot$ mol^{-1} range that is seen in the results shown by Butler et al. (2020) and Mertens et al. (2024). In general, the authors find that their model data agrees with the data of other models. However, when comparing their model data to the Tropospheric Ozone Assessment Report (TOAR) database, Butler et al. (2020) found that, similar to the EMAC model, their model also tends to have a positive O_3 bias (Schultz et al., 2017).

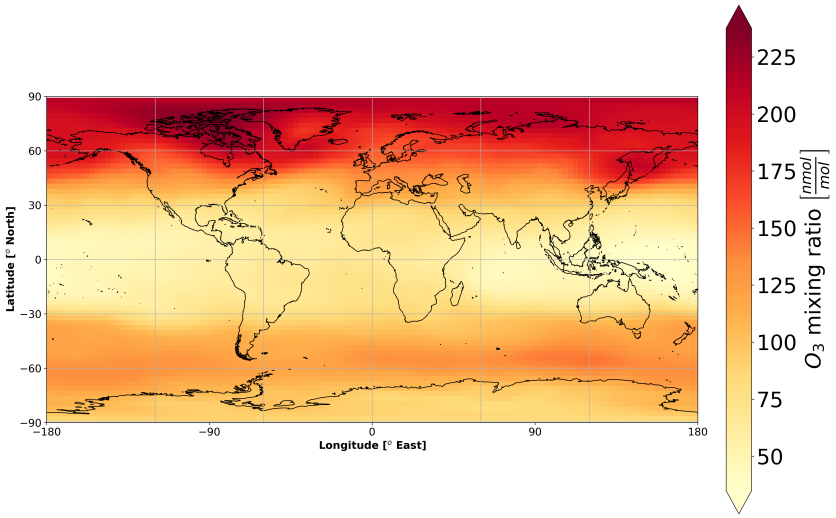

Figure 6.13: Cartograph of the average annual O_3 mixing ratio at Flight altitudes in 2018

The spatial distribution for the flight altitudes in Figure 6.13 is similar to the spatial distribution for the whole troposphere shown in Figure 6.11. This is to be expected, because most of the troposphere consists of the free troposphere (including the flight altitudes), where long range transport has a more predominant impact on O_3 levels than local anthropogenic emissions (Butler et al., 2018; Fowler, 2008). Figure 6.13 shows that the latitudinal gradient is more amplified compared to what can be seen in Figure 6.11. There is a much larger difference between the mid to high latitude and equatorial O_3 mixing ratios in the Northern Hemisphere than what is depicted in Figure 6.11. This is caused by the fact that at flight altitudes (200 hPa to 300 hPa), at latitudes higher than 40^o, a large portion of the air, consists of stratospheric air with stratospheric O_3, whereas up to latitudes of 40^o, the air is purely tropospheric and thus has lower O_3 mixing ratios. Thus, Figure 6.13 shows a stronger jump between the polar and mid to high latitude regions.

Figure 6.13 does not show any localised hotspots, but rather shows smooth distributions. At the higher latitudes (larger than 60^o North) the O_3 mixing ratios are upwards of 200 nmol $\cdot$ mol^{-1}, whereas around

the equator these mixing ratios are about 50 nmol $\cdot$ mol^{-1}. In the Southern Hemisphere, at latitudes higher than 30^o, the O_3 mixing ratio is seen to be higher than 100 nmol $\cdot$ mol^{-1}, also displaying a consistent latitudinal variability, just smaller in magnitude in comparison to the Northern Hemisphere. This latitudinal variability in Figure 6.13 is also driven by the large scale transport of air that is present in the upper troposphere and lower stratosphere. This Brewer Dobson circulation as depicted in Figure 2.5 shows that in the equatorial regions, air containing little O_3 is transported from the upper troposphere towards the stratosphere, whereas air containing larger concentrations of O_3 (including stratospheric O_3) is transported from the stratosphere to the troposphere close to the poles. This effect in the Northern Hemisphere is simply stronger due to the larger anthropogenic emissions across the Northern Hemisphere which leads to more O_3 that is transported towards the North Pole.

7

Aviation Contribution to Tropospheric Ozone

Having previously looked at the total tropospheric O_3 level in Chapter 6, further analysis can now be done to determine the contribution of aviation and to compare it to the contribution of other sources. This analysis is first conducted on a global scale in Section 7.1, which is followed by an analysis on a regional scale in Section 7.2.

7.1 Global Overview of Aviation Contribution to Ozone

This section looks at the global aviation contribution to O_3. This analysis is broken down into two parts. Firstly, the contribution of aviation to O_3 is compared across altitudes in Section 7.1.1, looking at how the global average of ${O_3}^{air}$ varies across the altitudes. This is followed by a comparison of ${O_3}^{air}$ to the contribution of other sources across the different altitude domains in Section 7.1.2

7.1.1. Comparing Aviation Contribution to Ozone across Altitude Domains

Figure 7.1 shows the trend in the aviation contribution to ozone (${O_3}^{air}$) averaged across the horizontal grid for the whole troposphere, the ground level and the flight altitudes. Figure 7.2 shows the same data, but as percentage of the total O_3 mixing ratios for those specific altitude domains.

Figure 7.1 shows that the absolute values of ${O_3}^{air}$ are highest for the flight altitudes at values between 1.2 nmol $\cdot$ mol^{-1} and 1.4 nmol $\cdot$ mol^{-1}, followed by the whole troposphere, with values between 1.0 nmol $\cdot$ mol^{-1} and 1.2 nmol $\cdot$ mol^{-1} and the ground level with values between 0.6 nmol $\cdot$ mol^{-1} and 0.75 nmol $\cdot$ mol^{-1}. All three lines in Figure 7.1 show that despite some inter-annual variability, the overall trend for ${O_3}^{air}$ across the three altitude domains is an increasing one. Figure 7.1 shows that at the flight altitudes, the increase between 2003 and 2018 is about 0.2 nmol $\cdot$ mol^{-1}. For the whole troposphere, the increase is slightly lower and for the ground level the increase is about 0.15 nmol $\cdot$ mol^{-1}. The increasing trend in ${O_3}^{air}$ suggests that there may be an increase in aviation NO_x emissions across the years, or there may be an increase in the O_3 burden efficiency for aviation due to changing background NO_x or VOC levels.

Figure 7.1 shows that there is a strong decrease in ${O_3}^{air}$ across all altitude domains between 2008 and 2009. This decline is primarily attributable to the global economic recession that occurred during this

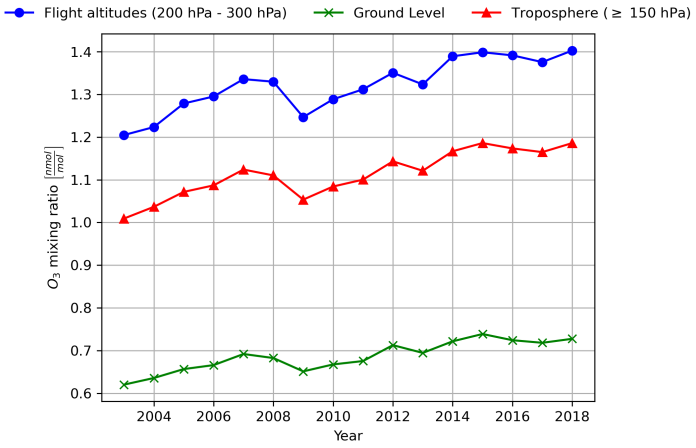

Figure 7.1: Comparison of the temporal evolution in the global annual molar mixing ratio averages of $O_3{}^{air}$ of the whole troposphere, the ground level and the flight altitudes.

time period. This recession led to substantially reduced air travel, thus reducing aviation NO_x emissions and their contributions toward tropospheric O_3 (Tong et al., 2016).

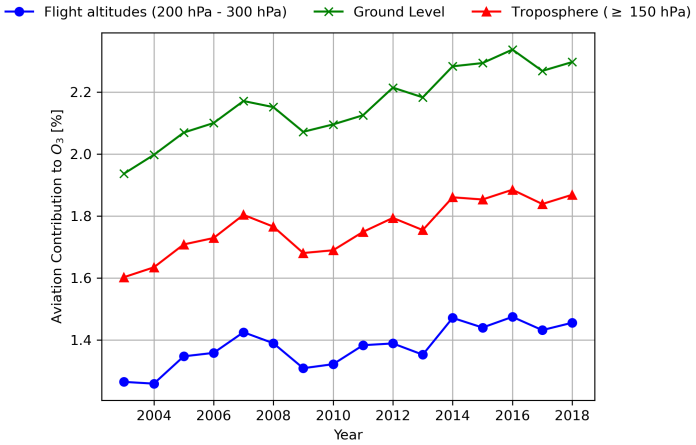

Figure 7.2: Comparison of the temporal evolution in the global annual mean percentage contribution of $O_3{}^{air}$ to O_3 of the whole troposphere, the ground level and the flight altitudes.

Looking at the percentage contribution of aviation in Figure 7.2 shows that for the whole troposphere the aviation contribution is between 1.6% and 1.9% across the time period between 2003 and 2018. These values are significantly lower than the values reported by Butler et al. (2018) and Nalam et al. (2025), who find that aviation contributes approximately 4.2% and 3.8% to tropospheric O_3, respectively. Firstly, it is important to note that both Butler et al. (2018) and Nalam et al. (2025) use different climate chemistry models, with different reanalysis data and different emissions inventories, which can lead to differences between their findings and the findings of this thesis. Additionally, in the EMAC model used in this thesis, NO_x and VOCs are tagged concurrently, whereas in the work by Butler et al. (2018) and Nalam et al. (2025), both sets of precursors are tagged individually across two different simulations. In the past, authors have seen that concurrent tagging of VOCs and NO_x leads to lower contribution estimates for sectors which have high NO_x and low VOC emissions, when comparing the results to contribution studies, where the two groups of precursors are tagged individually (Butler et al., 2018; Kilian et al., 2024; Mertens et al., 2018, 2024). This effect contributes towards the lower aviation contribution in Figure 7.2, when comparing to the results by Butler et al. (2018) and Nalam et al. (2025). Additionally, since the troposphere definition used in this thesis also captures a large amount of stratospheric air, the total O_3 mixing ratios are elevated, due to the larger proportion of stratospheric O_3, that is now being included in the tropospheric values. This, then reduces the percentage contribution of other emission

sectors such as aviation, especially when comparing the values to the results of Butler et al. (2018) and Nalam et al. (2025), who define their troposphere based on a maximum O_3 mixing ratio of 150 nmol $\cdot$ mol^{-1}.

Looking at the percentage contribution of aviation in Figure 7.2 shows that the contribution is largest for the ground level and smallest for the flight altitudes, which is opposite to the trend in Figure 7.1. In Figure 7.2 the contribution of aviation at ground level is between 1.9% and 2.3% and for the flight altitudes, the aviation contribution is between 1.25% and 1.45%. Looking at both Figure 7.1 and Figure 7.2 together shows that the absolute value for $O_3{}^{air}$ is larger at flight altitudes compared to the ground level, however, due to the larger O_3 mixing ratio at flight altitudes the percentage value of $O_3{}^{air}$ is lower at flight altitudes compared to the ground level. This larger O_3 level at flight altitudes is caused by the extended O_3 lifetimes at higher altitudes and the large contribution of stratospheric air as discussed earlier in Chapter 6. This larger total O_3 mixing ratio, thus makes the percentage contribution of aviation at flight altitudes smaller than the contribution at ground level, despite aviation having a larger absolute contribution at flight altitudes. In general, these results suggest that more O_3 from aviation is produced at flight altitudes, but its relative impact is greatest at the surface level, where the background O_3 levels are low.

Also, the aviation contribution to ground level O_3 is found to be lower than what has been previously reported in literature. Butler et al. (2020) find a contribution of aviation to ground level O_3 of around 1.13 nmol $\cdot$ mol^{-1}, which equates to approximately 3.7%, whereas Nalam et al. (2025) find a contribution of aviation to ground level O_3 of 0.99 nmol $\cdot$ mol^{-1}, which equates to about 3.9%. On the other hand, the analysis using the EMAC data shows that the aviation contribution to ground level O_3 is between 0.6 nmol $\cdot$ mol^{-1} and 0.75 nmol $\cdot$ mol^{-1}, which equates to approximately 1.9% to 2.3%. Similar to the earlier discussion, the differences between the findings in literature and this thesis could be due to the differences in the used models, emissions inventories and reanalysis data. These in addition to the fact that both Butler et al. (2020) and Nalam et al. (2025) conduct VOC and NO_x tagging individually give rise to the differences that are seen.

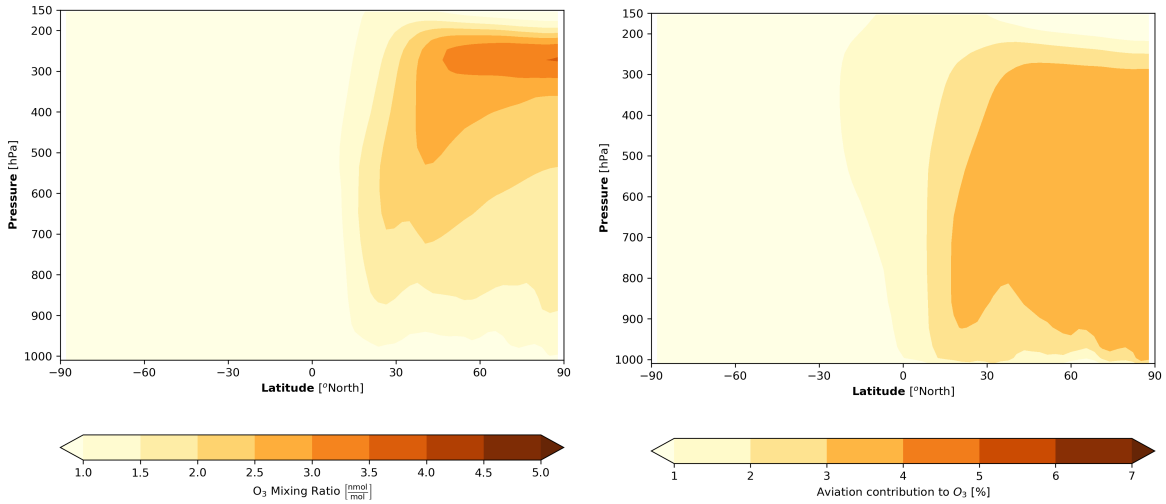

Figure 7.3: Zonal annual mean of $O_3{}^{air}$ for 2003 with the left figure showing the absolute contributions, while the right figure shows the percentage contributions.

Together, Figure 7.3, Figure 7.4 and Figure 7.5 show the annual zonal means of $O_3{}^{air}$ for the years 2003, 2011 and 2018 respectively, showing both the absolute and percentage contributions. The plots showing the absolute contributions show that the peak absolute O_3 contribution of aviation occurs at the flight altitudes (200 hPa to 300 hPa) between 60^o North and 90^o North, close to where most aviation NO_x is emitted.

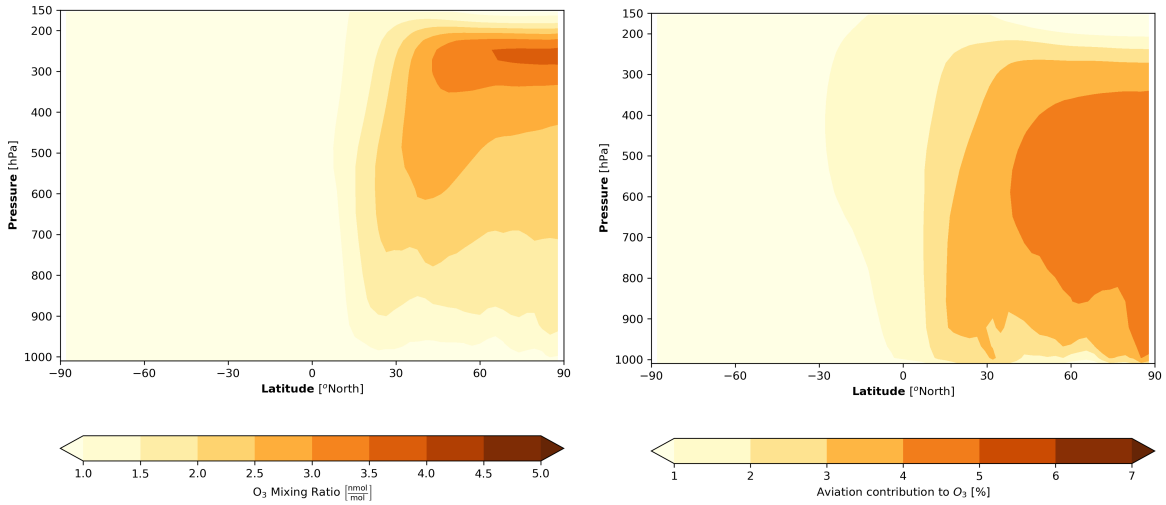

Figure 7.4: Zonal annual mean of $O_3{}^{air}$ for 2011 with the left figure showing the absolute contributions, while the right figure shows the percentage contributions.

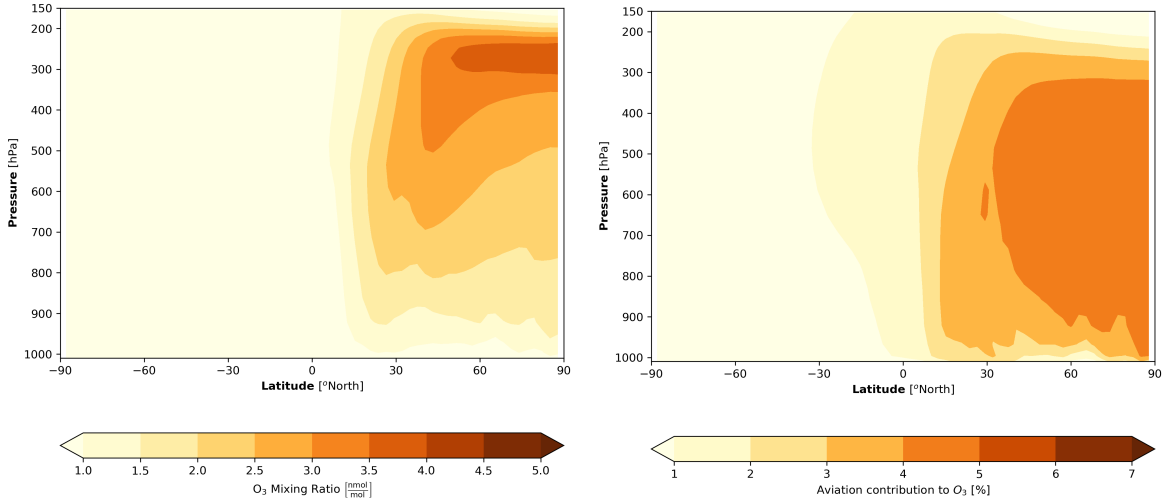

Figure 7.5: Zonal annual mean of $O_3{}^{air}$ for 2018 with the left figure showing the absolute contributions, while the right figure shows the percentage contributions.

Maruhashi et al. (2022) investigate the transport patterns of aviation NO_x particles where they model the transport paths of NO_x emissions. The authors show that aviation NO_x emitted in North America and Eurasia spends around 35% to 40% of its lifetime in the northern mid-latitudes (between 35^o North and 65^o North), 10% to 15% of its time in the Arctic (between 65^o North and 90^o North) and about 20% to 25% in the tropics (between 23.5^o South and 23.5^o North). The authors also show that for these two regions, the aviation NO_x particles tend to descend, with most of the NO_x ending up between 200 hPa to 800 hPa.

The transportation phenomena of aviation NO_x emissions as described by Maruhashi et al. (2022) can be used to explain the distributions in the absolute contributions seen in Figure 7.3, Figure 7.4 and Figure 7.5. The $O_3{}^{air}$ that is formed as a result of the aviation NO_x emissions is not only found at flight altitudes, but is spread vertically across the whole free troposphere. However, Maruhashi et al. (2022) do state that the largest O_3 mixing ratio impact from aviation NO_x emissions does occur at the higher flight altitudes. Similarly, Figure 7.3, Figure 7.4 and Figure 7.5 show that the $O_3{}^{air}$ mixing ratios increase with increasing altitude up to 200 hPa, which is primarily caused by the increasing lifetimes of O_3, leading to more $O_3{}^{air}$ accumulation. In general, Maruhashi et al. (2022) show that the transportation

of the aviation NO_x emitted in the northern hemisphere leads to a higher increase in the O_3 levels at higher altitudes and at higher northern latitudes, which aligns with the O_3^{air} distributions seen across Figure 7.3, Figure 7.4 and Figure 7.5. The low contribution in the southern hemisphere, is primarily, due to the lower aviation emissions in the southern hemisphere. However, Maruhashi et al. (2022) also showed that the aviation NO_x emitted in the Southern hemisphere has a tendency to move towards the tropics and equatorial regions. From these equatorial regions, the O_3^{air} undergoes upwards motion due to the large scale Brewer-Dobson circulation.

Looking at the percentage contributions in Figure 7.3, Figure 7.4 and Figure 7.5, shows that the peak O_3^{air} percentage contribution values primarily occur across 300 hPa to 800 hPa between approximately 40^o North and 90^o North. These peaks effectively come down to the high local absolute values of O_3^{air} along with the lower values of total O_3, when compared to flight altitude values, as described previously. Looking at the evolution of O_3^{air} across the years clearly shows that there is an increasing trend. In 2003 the peak absolute contributions are about 3 $nmol \cdot mol^{-1}$ and by 2018 these increase to approximately 4 $nmol \cdot mol^{-1}$. Similarly, the percentage contribution peaks increases from about 3% to about 4%. These trends in the zonal means of O_3^{air} support the general increasing trends seen in Figure 7.1 and Figure 7.2 suggesting that there is a clear increase of O_3^{air} in the northern hemisphere. The zonal mean plots show that this increase in O_3^{air} is primarily driven by the increase between 40^o North and 90^o North between 200 hPa and 800 hPa.

Grewe et al. (2017) and Mertens et al. (2024), show similar plots for the aviation contribution to O_3 and both publications show that the percentage contribution of aviation peaks at around 4% to 5% as is the case in Figure 7.3, Figure 7.4 and Figure 7.5. The plot presented by Mertens et al. (2024) shows an altitudinal pattern similar to what can be seen across Figure 7.3, Figure 7.4 and Figure 7.5. Here it is important to note that both Grewe et al. (2017) and Mertens et al. (2024) use similar simulation setups compared to this thesis, however, the emissions inventories used, vary compared to each other and this thesis. The variation in the emissions inventory may be the source for slight differences that may be present, but otherwise, the results shown in across the zonal mean plots agree with literature.

7.1.2. Comparing Aviation Contribution and Other Sources

Figure 7.6 and Figure 7.7 compare the different contributions to O_3 for the whole troposphere, with Figure 7.6 showing the absolute contribution in terms of mixing ratio, while Figure 7.7 shows the percentage contribution [1]. Both figures, compare the aviation contribution to the contribution of lightning, CH_4 degradation, shipping emissions, N_2O degradation, biomass burning, land emissions and biogenic emissions.

Figure 7.6 and Figure 7.7 show that the largest contributors to tropospheric O_3 are biogenic emissions with an absolute contribution of about 11 $nmol \cdot mol^{-1}$, which translates to about 17% of the total tropospheric O_3. This is followed by lightning, which contributes about 10 $nmol \cdot mol^{-1}$ (equivalent to about 16 %) to the total tropospheric O_3. CH_4 degradation and land emissions show a modest but consistent increase over the years, with the CH_4 contribution increasing from around 8 $nmol \cdot mol^{-1}$ to about 9 $nmol \cdot mol^{-1}$, while the contribution of land emissions increases from about 7.5 $nmol \cdot mol^{-1}$ to around 8.5 $nmol \cdot mol^{-1}$. Both of these sources account for approximately 12% to 14% of total tropospheric O_3. Shipping emissions and biomass burning both show an overall decreasing trend across the years. A decrease from about 3.5 $nmol \cdot mol^{-1}$ to about 3 $nmol \cdot mol^{-1}$ can be seen for shipping, while for biomass burning the decrease is from 3.5 $nmol \cdot mol^{-1}$ to 2.5 $nmol \cdot mol^{-1}$. Both of these sources account for 4% to 6% of the O_3. The smallest contributions to O_3 come from N_2O degradation and aviation emissions, both contributing around 1 $nmol \cdot mol^{-1}$, which is equivalent to a 2% contribution.

Looking at the year on year fluctuations in Figure 7.6 and comparing these to the fluctuations in Fig-

[1] Figure 7.6 and Figure 7.7 exclude the contribution of stratospheric O_3. The same figures with the contribution of stratospheric O_3 are shown in Figure A.4

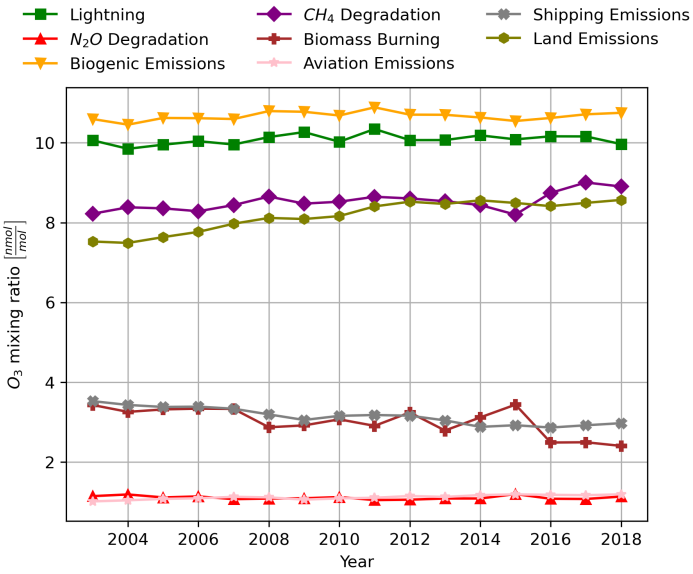

Figure 7.6: Comparison of the temporal evolution in the contribution to O_3 of different tagged sources for the whole troposphere. The individual plots for the different sources are given in Figure A.7.

ure 7.7, shows that the trends for all contributions behave exactly the same in both plots. This further strengthens the argument that there is no significant trend in the global O_3 mixing ratio. If there were a significant trend in the global O_3 mixing ratio, then it would be expected that the trends in Figure 7.6 and Figure 7.7 would not fully match.

Looking at the contribution of land emissions, a slight decrease can be seen between 2008 and 2009. This decline can be seen a bit more clearly in Figure A.7. This decrease is consistent with the decrease in the aviation contribution to O_3 that is seen during the same time period and was discussed earlier. The global recession which took place during this time period, led to reductions in industrial and road transport emissions, reducing the accompanying land NO_x emissions and the subsequent contribution to O_3 [2].

Looking at the contribution of CH_4 degradation between 2014 and 2016 shows that between 2014 and 2015 there is a steep decline, followed by a steep increase in the contribution between 2015 and 2016. At the same time between 2014 and 2015 there is an increase in the contribution of biomass burning, which is followed by a steep decrease between 2015 and 2016. These patterns for the contributions of CH_4 degradation and biomass burning to tropospheric O_3, are related and occurred due to the El Niño weather event across this time period. The El Niño weather event is a phenomena that has occurred on multiple occasions and alters global temperatures, precipitation and circulation patterns (Doherty et al., 2006). The El Niño event between 2014 and 2016 led to a decrease in the concentrations of OH, which acts as the primary sink of CH_4 and subsequently starts the chain to form O_3 via CH_4 degradation as shown in Equation (R21) (Nisbet et al., 2019). Thus, a decrease in the global OH concentrations leads to a decrease in the contribution of CH_4 degradation to O_3 in 2015. Once the OH concentrations were restored again in 2016, the contribution of CH_4 degradation to O_3 was also restored. Additionally, the El Niño weather event led to widespread warm and dry conditions in 2015, particularly in tropical regions such as Indonesia and South America. These conditions, led to increased wildfires, thereby increasing the contribution of biomass burning to tropospheric O_3 in 2015. However, in 2016, when the El Niño event subsided, rainfall returned to the affected regions, leading to a sharp decrease in wildfires and subsequently biomass burning contributions.

[2] https://www.eea.europa.eu/highlights/recession-contributes-to-air-pollutant Date accessed 2nd September 2025

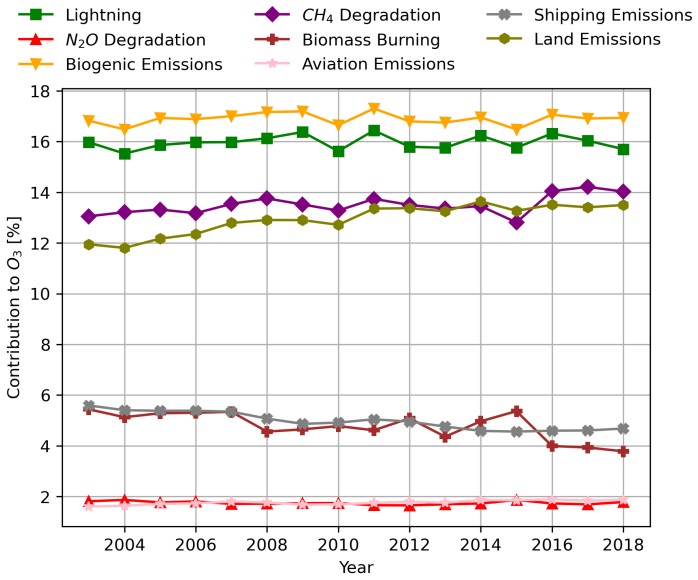

Figure 7.7: Comparison of the temporal evolution in the percentage contribution to O_3 of different tagged sources for the whole troposphere

Table 7.1: Comparison between the results of Butler et al. (2018), Nalam et al. (2025) and this thesis for the contributions of various sources towards tropospheric O_3.

Source	EMAC Model 2018 Results	Butler et al. (2018) Results	Nalam et al. (2025) Results
Stratosphere	27.5%	24%	29%
Land Emissions	13.5%	35%	37%
Lightning	16.0%	25%	22%
Biogenic Emissions	16.8%	26%	17%
Aviation Emissions	1.9%	4%	4%
Biomass Burning	3.8%	4%	4%
CH_4 Degradation	14.0%	35%	40%
Shipping Emissions	4.7%	N/A	7%

Butler et al. (2018) and Nalam et al. (2025) look at the contribution to tropospheric O_3 of various tagged sources and their findings are summarised in Table 7.1. In their analysis Butler et al. (2018) look at the year 2010, while Nalam et al. (2025) present the averaged values across their analysed time period of 2000 to 2018. The findings of Butler et al. (2018) and Nalam et al. (2025) are compared to the findings of the EMAC model used in this thesis for the year 2018 in Table 7.1. It is also important to note that the analyses done by Butler et al. (2018) and Nalam et al. (2025) apply VOC and NO_x tagging separately, across two different simulations, which leads to two sets of results. This is why, the contributions for both Butler et al. (2018) and Nalam et al. (2025) shown in Table 7.1 add up to more than 100%, as for sources where the emissions are NO_x dominated, the NO_x tagging results are shown, whereas for sources where the emissions are dominated by Carbon species, the VOC tagging results are shown. This means that for and emissions, lightning emissions, aviation emissions and shipping emissions the results of the NO_x tagging simulations are shown for Butler et al. (2018) and Nalam et al. (2025) in Table 7.1, while the VOC tagging results are shown for biogenic emissions, biomass burning and CH_4 degradation. In this thesis, the tagging of NO_x and VOCs is done concurrently. Especially for sources that have high NO_x emissions and low VOC emissions, or high VOC emissions and low NO_x emissions, the tagging approach used in this thesis will lead to lower contributions compared to the tagging approaches where NO_x and carbon based species are tagged separately (Butler et al., 2018; Kilian et al., 2024; Mertens et al., 2018, 2024)

Looking at the comparison in Table 7.1 shows that in general, the results of the EMAC model lead

to lower contributions when compared to values found in literature. Part of this result comes from the differences in how the tagging is applied to the NO_x and VOC species as mentioned earlier. This means that the values reported by Butler et al. (2018) and Nalam et al. (2025) are expected to be larger than the values found using the EMAC model. Additionally, differences also arise due to the use of different emissions inventories, different chemistry climate models and different meteorology for different years. Furthermore, differences also arise due to the definition of the troposphere that is used in this thesis, which captures a large amount of stratospheric air, leading to a high contribution of stratospheric O_3 to the tropospheric O_3 budget.

As mentioned previously, the contribution of CH_4 degradation, land emissions, aviation emissions to tropospheric O_3 show increasing trends, while the contribution of shipping emissions, and biomass burning, show decreasing trends in Figure 7.6 and Figure 7.7. In their analysis Nalam et al. (2025) see that there is a significant positive trend in the contribution of aviation, shipping, biogenic and land emissions and CH_4 degradation. For these four sources, the authors also find a significant increasing trend in the emissions of the NO_x or Reactive Carbon precursors, On the other hand, Nalam et al. (2025) also see a decreasing trend in the contribution of lightning emissions and biomass burning. The increasing trends in the contribution of aviation, shipping, biogenic and land emissions are seen to be due to increasing emissions of NO_x (or Reactive Carbon for Biogenic emissions). Of these increasing precursor trends, however, Nalam et al. (2025) only report medium certainty (90%) for the increasing trend in biogenic reactive carbon emissions, whereas the increasing trend in aviation, shipping and land NO_x emissions is seen to have 95% certainty. A decreasing trend is seen in the emission of biomass burning, but this trend also only has medium certainty (90%). For lightning NO_x emissions and CH_4 emissions, Nalam et al. (2025) see a negative trend with high certainty. These trends in the emissions of aviation, shipping, land, biogenic, lightning, biomass burning and CH_4 explain the respective trends in the related O_3 contributions. Since the authors report their O_3 trends in Tg $(O_3) \cdot \text{yr}^{-1}$, a quantitative comparison of their trends and the ones seen in Figure 7.6 and Figure 7.7 is not made, since this is beyond the scope of this thesis.

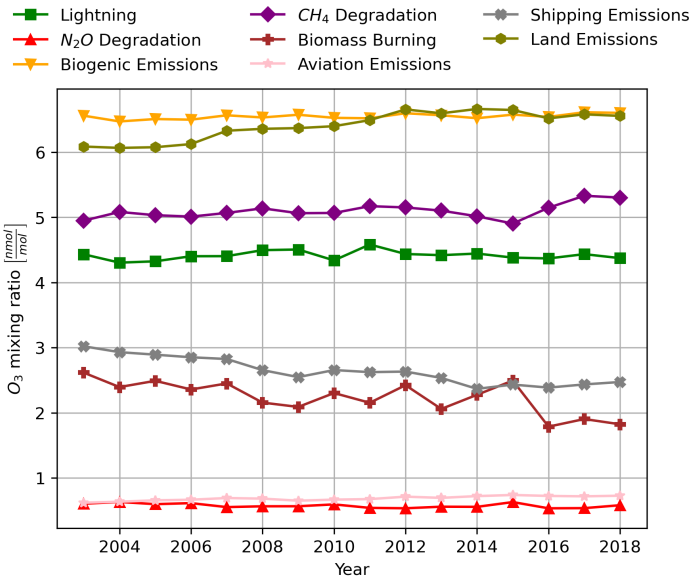

Figure 7.8: Comparison of the temporal evolution in the contribution to O_3 of different tagged sources at ground level. The individual plots for the different sources are given in Figure A.8.

Figure 7.8 and Figure 7.9 show the trends of different contributions to O_3 for the ground level, with Figure 7.8 showing the absolute contribution in terms of mixing ratio, while Figure 7.9 shows the percentage contribution[3]. Again, the figures, compare the aviation contribution to the contribution of light-

[3]Figure 7.8 and Figure 7.9 exclude the contribution of stratospheric O_3. The same figures with the contribution of stratospheric O_3 are shown in Figure A.5

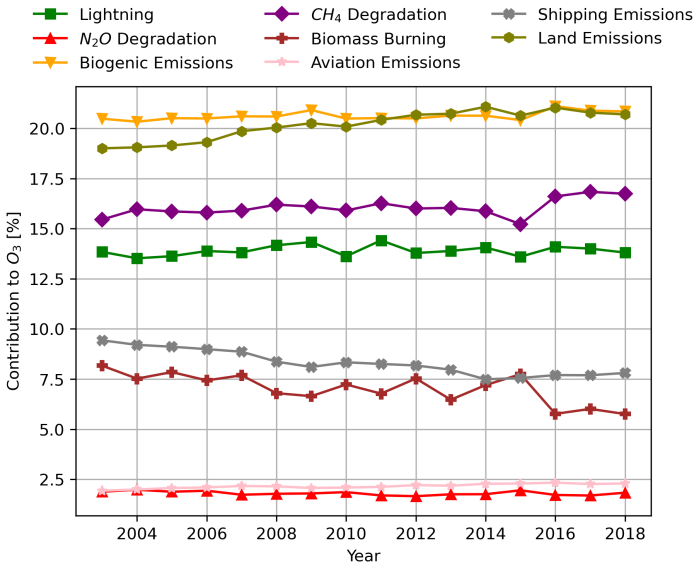

Figure 7.9: Comparison of the temporal evolution in the percentage contribution to O_3 of different tagged sources at ground level

ning, CH_4 degradation, shipping emissions, N_2O degradation, biomass burning, land emissions and biogenic emissions.

In Figure 7.8 and Figure 7.9 it can be seen that the largest contribution to O_3 at ground level across the years comes from biogenic emissions at about 6.6 nmol $\cdot$ mol^{-1}, which is equivalent to a contribution of about 21 %. This is followed by land emissions, where the contribution increases from about 6 nmol$\cdot$mol^{-1} to 6.5 nmol$\cdot$mol^{-1} at ground level between 2003 to 2018. This means that the contribution of land emissions grows from 19% to approximately 21%. CH_4 degradation shows an increasing trend at ground level increasing from about 5 nmol$\cdot$mol^{-1} to about 5.5 nmol$\cdot$mol^{-1}, leading to an increase in the contribution from about 15% to about 17.5%. Lightning emissions have a much lower contribution at ground level than they do for the whole troposphere, with a contribution of around 4.5 nmol $\cdot$ mol^{-1}, which translates to approximately 14%. Shipping emissions contribute around 3 nmol $\cdot$ mol^{-1} and this contribution decreases to about 2.5 nmol $\cdot$ mol^{-1} across the years, meaning that the percentage contribution decreases from 9.5% to about 7.5%. A similar decreasing trend is seen for biomass burning, which decreases from about 2.6 nmol $\cdot$ mol^{-1} (approximately 8%) to just under 2 nmol $\cdot$ mol^{-1} (approximately 6%). N_2O degradation and aviation contribute between 0.5 nmol $\cdot$ mol^{-1} to 0.75 nmol $\cdot$ mol^{-1} which is equivalent to 2.25% to 2.5%.

Butler et al. (2020) and Nalam et al. (2025) look at the attribution of ground level O_3 by separately tagging NO_x and carbon species as mentioned earlier. Their results are summarised in Table 7.2, where the results of the NO_x tagging simulations are shown for the NO_x dominant emissions sources and the the Carbon species tagging results are shown for the VOC dominant emissions sources. This means that the contribution results shown for Butler et al. (2020) and Nalam et al. (2025) add up to more than 100%. Additionally, Butler et al. (2020) look at the year 2010, while Nalam et al. (2025) present the average values for the period across 2000 to 2018. The results shown in Table 7.2 are based on the ground level mixing ratios values that are presented by the authors. For this it is important to note that Butler et al. (2020) present mixing rations that are averaged over the northern hemisphere only, however they do not clearly specify the weighting methodology. Since, area based averaging is the most common practice in literature, it is assumed that the results shown by Butler et al. (2020) employ area based weighting to calculate their average northern hemisphere mixing ratios. On the other hand, Nalam et al. (2025) clearly state that they use grid area based averaging. Thus, for the comparison between the results found by Butler et al. (2020), Nalam et al. (2025) and this thesis it is important to

Table 7.2: Comparison between the results of Butler et al. (2020), Nalam et al. (2025) and this thesis for the contributions of various sources towards ground level O_3.

Source	EMAC Model 2018 Results	Butler et al. (2020) Results	Nalam et al. (2025) Results
Stratosphere	11.0%	10.3%	19.7%
Land Emissions	21.0%	44.9%	48.1%
Lightning	14.0%	10.2%	13.8%
Biogenic Emissions	21.0%	23.5%	16.0%
Aviation Emissions	2.5%	3.7%	3.9%
Biomass Burning	5.0%	4.7%	5.2%
CH_4 Degradation	17.0%	40.4%	47.2%
Shipping Emissions	7.5%	17.4	6.6%

remember that this thesis employs grid air mass based averaging, which therefore also accounts for the topography and its impact on air density and pressure.

Comparing the results shown in Table 7.2 highlights some strong differences between the results found using the EMAC model and the results found by Butler et al. (2020) and Nalam et al. (2025). As was the case for the differences in Table 7.1, a big part of the differences in Table 7.2 can be attributed to the differences in the tagging methodologies which have already been discussed. Furthermore, comparing the results of Butler et al. (2020) and Nalam et al. (2025), a strong difference between the results can be seen despite both sets of authors using similar models. The main differences between the models used by Butler et al. (2020) and Nalam et al. (2025) are that Nalam et al. (2025) uses updated emissions inventories, except for Biogenic emissions, where the same inventories are used. Furthermore, Nalam et al. (2025) also makes use of a newer chemistry dynamics model, along with considering different meteorology as a different time period is analysed. Additionally, Butler et al. (2020) tag VOC species in addition to NO_x, while Nalam et al. (2025) tag reactive carbon species along with NO_x, meaning that Nalam et al. (2025) consider a broader range of carbon species in their analysis. These strong differences between the results of Butler et al. (2020) and Nalam et al. (2025), despite small differences in methodologies, shows how sensitive chemistry climate model simulations can be to the model setup, the emissions inventory and the considered meteorology in contribution studies. Comparing the results from literature to the results of the EMAC model in Table 7.2, shows that there is no clear systematic difference as was the case for the contributions to tropospheric O_3 shown in Table 7.1, where the values for the different sources were always lower for the EMAC model compared to the literature values, excluding stratospheric O_3. In some instances the results found using the EMAC model are higher than the contributions reported in literature, whereas in other instances the contributions found by the EMAC model are lower. The differences are highest for the contributions of land emissions and CH_4 degradation. These large differences are most likely being driven by the fact that the tagging method used in this thesis as described by Grewe et al. (2017) tags both NO_x and VOC at the same time, whereas in the research done by Butler et al. (2020) and Nalam et al. (2025) the tagging is conducted separately. Additionally, these difference amongst these two publications and this thesis could also be driven by the three different weighted averaging methods that are used to calculate the ground level mixing ratio, as discussed earlier.

Figure 7.10 and Figure 7.11 show the trends of different contributions to O_3 at flight altitudes, with Figure 7.10 showing the absolute contribution in terms of mixing ratio, while Figure 7.11 shows the percentage contribution[4]. The figures compare the aviation contribution to the contribution of lightning, CH_4 degradation, shipping emissions, N_2O degradation, biomass burning, land emissions and biogenic emissions.

Figure 7.10 and Figure 7.11 show that the largest contributions at flight altitudes come from lightning

[4]Figure 7.10 and Figure 7.11 exclude the contribution of stratospheric O_3. The same figures with the contribution of stratospheric O_3 are shown in Figure A.6

with around 15 nmol · mol^{-1}, equivalent to about 15.5%, closely followed by biogenic emissions with a contribution of about 14.5 nmol · mol^{-1}, equivalent to about 15%. CH_4 degradation is the third largest contribution, with a contribution that increases from about 11 nmol · mol^{-1} to about 12 nmol · mol^{-1} over the years, equivalent to an increase from about 12% to about 13%. The contribution of land emissions to O_3 increases from about 8 nmol · mol^{-1} to about 10 nmol · mol^{-1}, which represents an increase from about 8.5% to about 10 % across 2003 to 2018. The contribution of shipping to O_3 at flight altitudes decreases across the years from about 4 nmol · mol^{-1} to 3.5 nmol · mol^{-1} which is equivalent to a percentage contribution change from just over 4% to just over 3.5%. The contribution of biomass burning to O_3 in 2003 has a similar value to the shipping contribution, but decreases to about 3 nmol · mol^{-1} in 2018, which represents about 3% of the total O_3 at flight altitudes. At flight altitudes the contributions of N_2O degradation and aviation are between 1 nmol · mol^{-1} and 2 nmol · mol^{-1} representing about 1% to 2% of the total O_3 at flight altitudes.

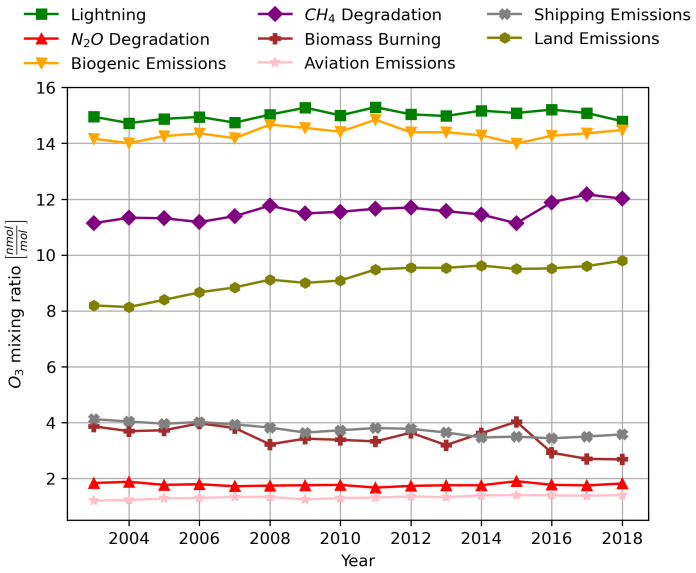

Figure 7.10: Comparison of the temporal evolution in the contribution to O_3 of different tagged sources at flight level. The individual plots for the different sources are given in Figure A.9.

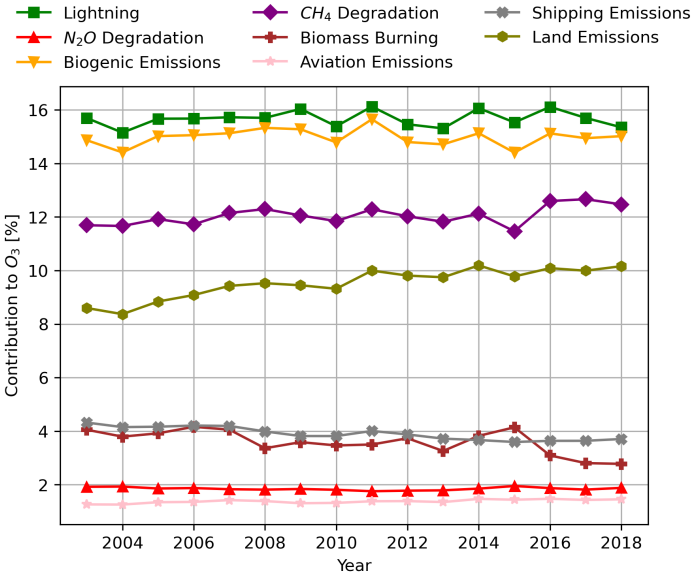

Figure 7.11: Comparison of the temporal evolution in the percentage contribution to O_3 of different tagged sources at flight level

Literature that looks at the contribution of different sources to O_3 at flight altitudes was not found. How-

ever, Grewe et al. (2017) and Butler et al. (2018) look at the variation of contributions to O_3 across different altitudes. Grewe et al. (2017) show multiple zonal mean plots as shown in Figure 7.3 showing different contributions, while Butler et al. (2018) compare contributions at ground level to contributions at 400 hPa. In general, similar differences to the ones seen between Figure 7.9 and Figure 7.11 are shown by Grewe et al. (2017) and Butler et al. (2018) when looking at how contributions vary with altitude. In most cases the percentage contribution at ground level is higher than at flight altitudes, even though the absolute contributions are higher at flight altitudes. As was explained specifically for the aviation contribution in Section 7.1.1, this is because in the upper troposphere, there is a much higher proportion of stratospheric O_3 than at ground level, which leads to an increase in the total O_3 levels. This means that despite larger absolute concentrations at higher altitudes, percentage contributions are reduced. However, for stratospheric O_3 and O_3 due to lightning NO_x emissions, the percentage contribution at flight altitudes is larger than at ground altitudes. For stratospheric O_3 this is the case, because in the upper troposphere STE is enhanced. For lightning attributed O_3, this is the case because lightning emissions take place at high altitudes, primarily in the tropics. Most of the subsequent O_3 formed, then disperses vertically with the majority ending up between 300 hPa and 600 hPa (Grewe et al., 2017).

Looking at the contributions of sources across the whole troposphere, the ground level and flight altitudes, in Figure 7.6, Figure 7.8 and Figure 7.10 respectively, shows that the increasing or decreasing trends seen in the contribution of a specific tagged source in one altitude domain, can be seen across all altitudinal domains. For example, a steady and consistently increasing trend can be seen for the contribution of land emissions to O_3 across the whole troposphere, the ground level and at flight altitudes. This similarity of trends in the contribution of different emission sources across ground level, the whole troposphere and the flight altitudes shows the strong coupling of the chemical and transport processes which drive tropospheric O_3. For example, land emissions are primarily emitted at ground level, yet their influence is not constrained to just ground level O_3. In fact, largs scale circulation and convection redistribute precursors and the subsequently formed O_3 vertically. At higher altitudes, the longer lifetimes promote more accumulation and thus higher mixing ratios, whereas at ground level the mixing ratios are kept low due to deposition. This phenomena leads to a homogeneity in the trends of different contributions across different altitude domains, reflecting the coupled nature of tropospheric O_3 levels. Thus, perturbations in emissions at ground level are seen to propagate through vertical transport, becoming present in the whole troposphere and at flight altitudes.

7.2 Regional Distribution and Trends

So far in this chapter, the analysis has looked at global averages of the aviation contribution to O_3 and how this has compared to other sources. In this section, the analysis is further broken down into regions, where Section 7.2.1 compares the contribution of aviation to O_3 across regions, which is followed by a comparison of O_3^{air} to other sources for the same regions in Section 7.2.2.

7.2.1. Comparing Aviation Contribution to Ozone across Regions

Figure 7.12 shows the aviation contribution to O_3 over Asia, Europe and North America across the whole troposphere. Figure 7.12 shows that O_3^{air} is consistently the highest for Europe with the contribution increasing from about 2.1 nmol $\cdot$ mol^{-1} to over 2.5 nmol $\cdot$ mol^{-1}. A similar increasing trend is seen for North America, which increases from about 1.8 nmol $\cdot$ mol^{-1} to over 2.1 nmol $\cdot$ mol^{-1}. Similarly the aviation contribution to O_3 increases for Asia from approximately 1.5 nmol $\cdot$ mol^{-1} to just under 1.8 nmol $\cdot$ mol^{-1}.

Figure 7.13, which shows the aviation contribution to O_3 for Asia, Europe and North America at ground level, shows a similar trends to Figure 7.12. Overall, all three regions see an ever increasing trend, despite some inter-annual variability. The aviation contribution for Europe increases from approximately 1.2 nmol $\cdot$ mol^{-1} to 1.5 nmol $\cdot$ mol^{-1}. For North America the contribution increases from just under 1.2 nmol $\cdot$ mol^{-1} to 1.4 nmol $\cdot$ mol^{-1} and for Asia the contribution increases from 0.95 nmol $\cdot$ mol^{-1} to approximately 1.1 nmol $\cdot$ mol^{-1}. Comparing Figure 7.13 and Figure 7.12 shows that at ground level the

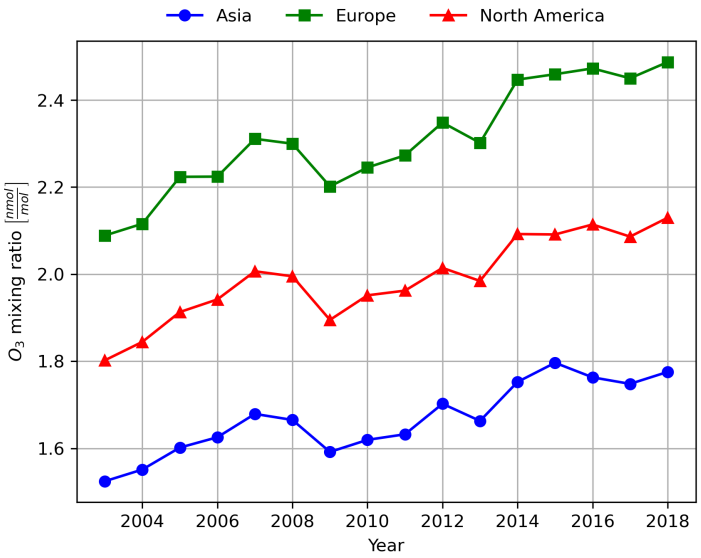

Figure 7.12: Comparison of Aviation contribution to O_3 for the whole troposphere for Asia, Europe and North America

difference in contribution of aviation to O_3 between Europe and North America is much smaller than for the whole troposphere.

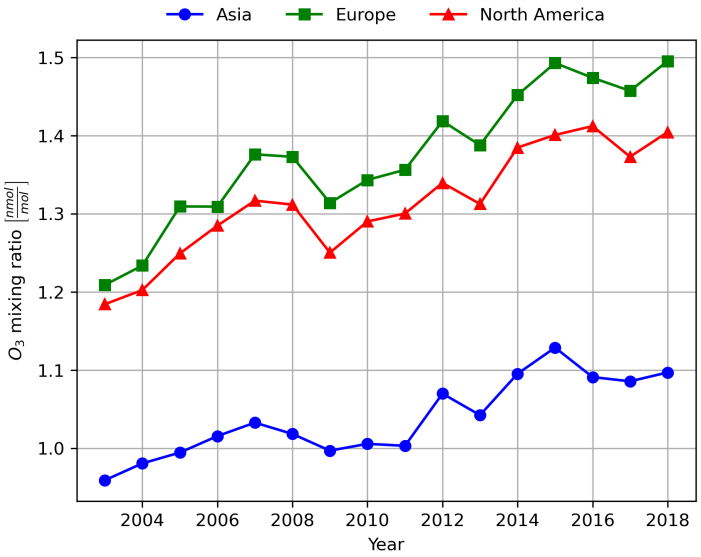

Figure 7.13: Comparison of Aviation contribution to O_3 at ground level for Asia, Europe and North America

A similar analysis for the flight altitudes shown in Figure 7.14, shows that the aviation contribution for Europe increases from about 2.6 nmol $\cdot$ mol^{-1} to about 3.0 nmol $\cdot$ mol^{-1}. Similar increasing trends are seen for North America and Asia again, with the contribution increasing from 2.1 nmol $\cdot$ mol^{-1} to just over 2.4 nmol $\cdot$ mol^{-1} for North America and from 1.8 nmol $\cdot$ mol^{-1} to 2.1 nmol $\cdot$ mol^{-1} for Asia.

7.2.2. Comparing Aviation Contribution and Other Sources across Regions

Europe

Figure 7.15 compares the trends the of different considered contributions to O_3 for the whole troposphere for the region of Europe. Figure 7.15 shows that for the region of Europe, land emissions have the largest contribution staying mostly constant at a value of around 12 nmol $\cdot$ mol^{-1} to 13 nmol $\cdot$ mol^{-1}. This is followed by biogenic emissions which also stay constant and contribute around 11 nmol $\cdot$ mol^{-1}.

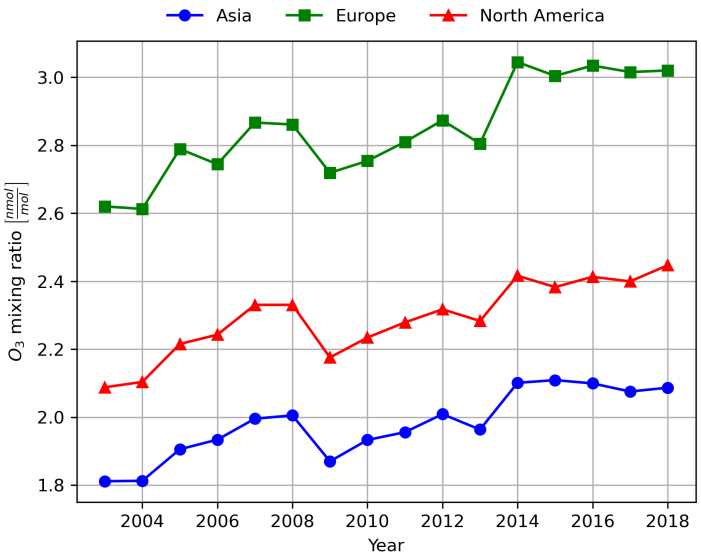

Figure 7.14: Comparison of Aviation contribution to O_3 at flight altitudes for Asia, Europe and North America

The contribution of CH_4 degradation increases from around 9 nmol $\cdot$ mol^{-1} in 2003 to approximately 10 nmol $\cdot$ mol^{-1} in 2018. The contribution of lightning stays constant at about 9 nmol $\cdot$ mol^{-1}. The shipping contributions show a slight decrease from about 4 nmol $\cdot$ mol^{-1} to about 3.5 nmol $\cdot$ mol^{-1}. The contribution of biomass burning also decreases from about 3.5 nmol $\cdot$ mol^{-1} in 2003 to around 2 nmol $\cdot$ mol^{-1} in 2018. The contribution of aviation in this case is just over 2 nmol $\cdot$ mol^{-1} and the contribution of N_2O degradation is the smallest, with a value of around 1 nmol $\cdot$ mol^{-1}.

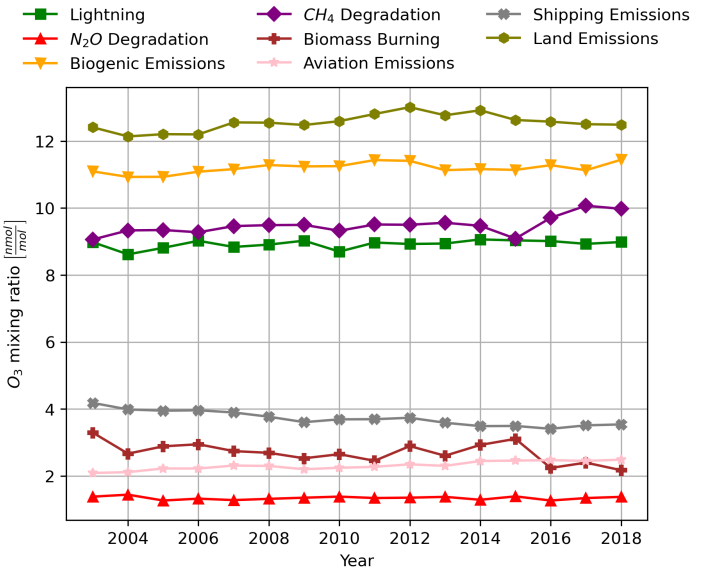

Figure 7.15: Comparison of the temporal evolution in the contribution to O_3 of different tagged sources for the whole troposphere above Europe.

Figure 7.16 compares the trends of the different contributions to O_3 for the ground level in Europe. Again, the land emissions have the largest contribution, which across the years decreases slightly from about 10 nmol $\cdot$ mol^{-1} in 2003 to 9.5 nmol $\cdot$ mol^{-1} in 2018. The contribution of biogenic emissions stays constant just under 7 nmol $\cdot$ mol^{-1}. At ground level, the CH_4 degradation also sees a slight increase in the contribution from around 5 nmol $\cdot$ mol^{-1} to just under 6 nmol $\cdot$ mol^{-1}. On the other hand, the contribution of shipping emissions decreases from just under 4 nmol $\cdot$ mol^{-1} in 2003 to around

3 nmol · mol^{-1} in 2018. The contribution of lightning emissions to ground level O_3 stays constant at about 3 nmol · mol^{-1}. The contribution of biomass burning decreases from about 2 nmol · mol^{-1} to approximately 1 nmol · mol^{-1}. The contribution of aviation is around 1 nmol · mol^{-1} as mentioned previously and the contribution of N_2O degradation is around 0.5 nmol · mol^{-1}.

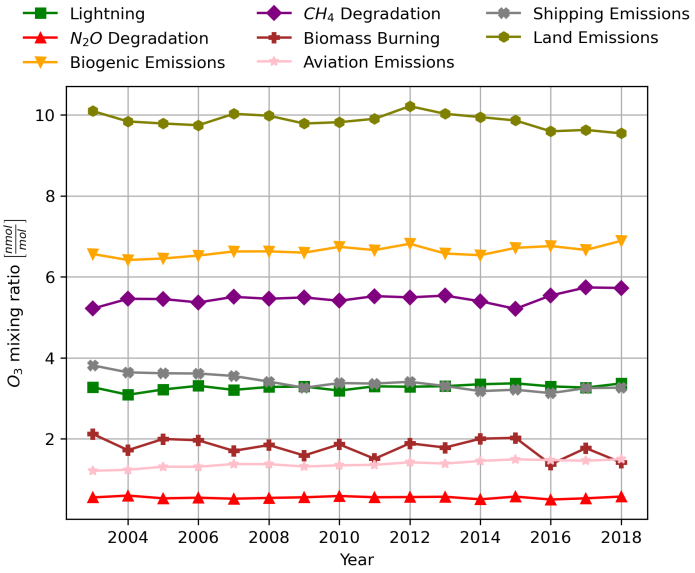

Figure 7.16: Comparison of the temporal evolution in the contribution to O_3 of different tagged sources at ground level in Europe.

Figure 7.17 shows the trends in the various contributions to O_3 for the flight altitudes in Europe. At the flight altitudes the contribution of biogenic emissions is the largest and it increases from about 15 nmol · mol^{-1} in 2003 to about 16 nmol · mol^{-1} in 2018. This is followed by the contribution of lightning which fluctuates around 14.5 nmol · mol^{-1}. Both land emissions and CH_4 degradation show an increase from about 13 nmol · mol^{-1} in 2003 to around 14 nmol · mol^{-1} in 2018. The contribution of shipping emissions decreases from about 5 nmol · mol^{-1} to about 4 nmol · mol^{-1}. The biomass burning contribution decreases from about 4 nmol · mol^{-1} to about 2.5 nmol · mol^{-1}. As mentioned previously, the contribution of aviation is around 2.6 nmol · mol^{-1} to 3 nmol · mol^{-1} and the contribution of N_2O degradation is around 1 nmol · mol^{-1}.

Comparing Figure 7.15, Figure 7.16 and Figure 7.17 to the global trends in Section 7.1.2 shows that there are key differences between the global trends and the trends for Europe. Firstly, it can be seen that the contribution of all tagged sources are higher in Europe than in the global average, which is consistent with Europe's higher O_3 mixing ratio. Furthermore, it can be seen that the for the whole troposphere and at ground level, the contribution of land emissions becomes more important in Europe, as in Europe, the land emissions are the largest contributor, whereas in the global average, the biogenic emissions are the largest contributor. In general it can be seen that the anthropogenic sources become more prominent in Europe than they are globally. This effect is most likely driven by the fact that Europe has a larger concentration of emissions, which leads to more local O_3, whereas the global values also include regions in the southern Hemisphere, which are known to have low emissions and thus subsequently lower concentration of O_3.

Asia

Figure 7.18 shows the various trends for the different contributions to O_3 for the whole troposphere for the region of Asia. Figure 7.18 shows that for Asia, the contribution of land emissions increases from about 11 nmol · mol^{-1} to about 12.5 nmol · mol^{-1}. The contribution of biogenic emissions fluctuates around 11 nmol · mol^{-1} and the contribution of lightning fluctuates around approximately 9 nmol · mol^{-1}. The contribution of CH_4 degradation increases from about 9 nmol · mol^{-1} to just under 10 nmol · mol^{-1}. The contribution of shipping emissions decreases from around 4.5 nmol · mol^{-1} in 2003 to just under

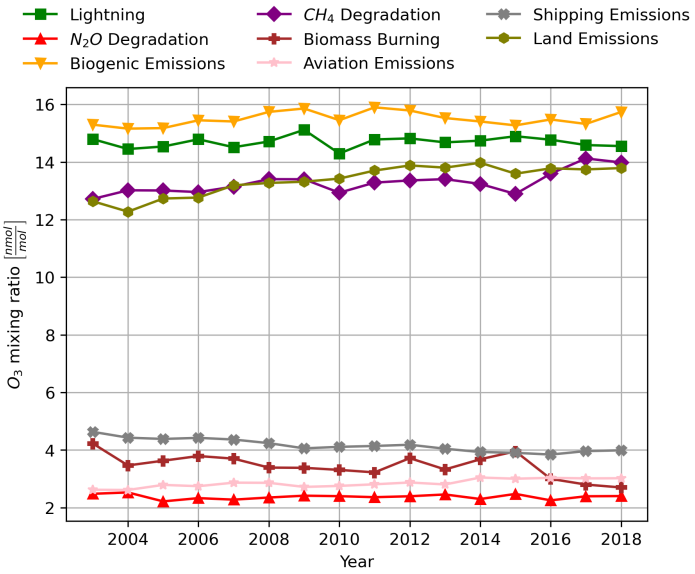

Figure 7.17: Comparison of the temporal evolution in the contribution to O_3 of different tagged sources at flight altitudes above Europe.

4 nmol · mol^{-1} in 2018. The contribution of biomass burning decreases from about 3 nmol · mol^{-1} to about 2 nmol · mol^{-1}. The aviation contribution is under 2 nmol · mol^{-1} throughout the years, while the N_2O contribution is around 1 nmol · mol^{-1}.

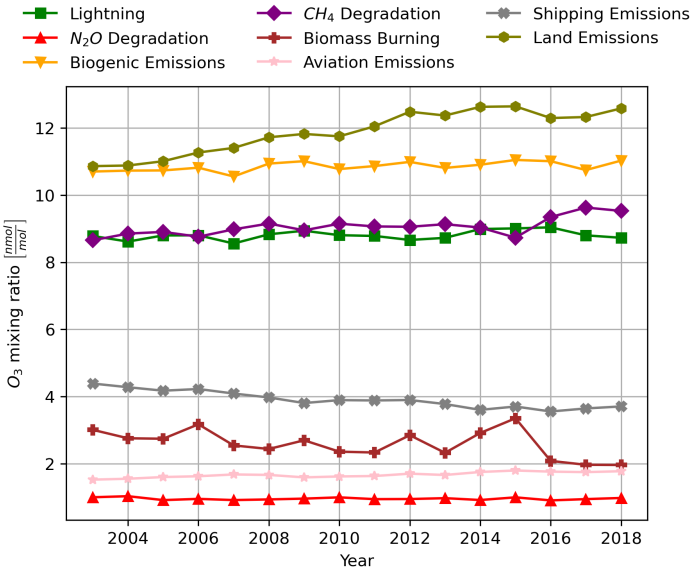

Figure 7.18: Comparison of the temporal evolution in the contribution to O_3 of different tagged sources for the whole troposphere above Asia.

Figure 7.19 shows the trends in the O_3 contributions for various tagged source at ground level for Asia. Again, the land emissions contribute the most with the contribution increasing from about 9.5 nmol · mol^{-1} in 2003 to about 10.5 nmol · mol^{-1} in 2018. The biogenic emissions' contribution remains mostly constant around 7 nmol · mol^{-1}. The contribution of CH_4 degradation increases from about 5.5 nmol · mol^{-1} to about 6 nmol · mol^{-1} between 2003 and 2018. The contribution of shipping emissions decreases from just over 4 nmol · mol^{-1} to just over 3 nmol · mol^{-1}. The contribution due to biomass burning decreases from about 2.5 nmol · mol^{-1} in 2003 to about 1.5 nmol · mol^{-1}. The contribution of aviation is around 1 nmol · mol^{-1}, while the contribution of N_2O degradation stays constant at around

0.5 nmol · mol^{-1}.

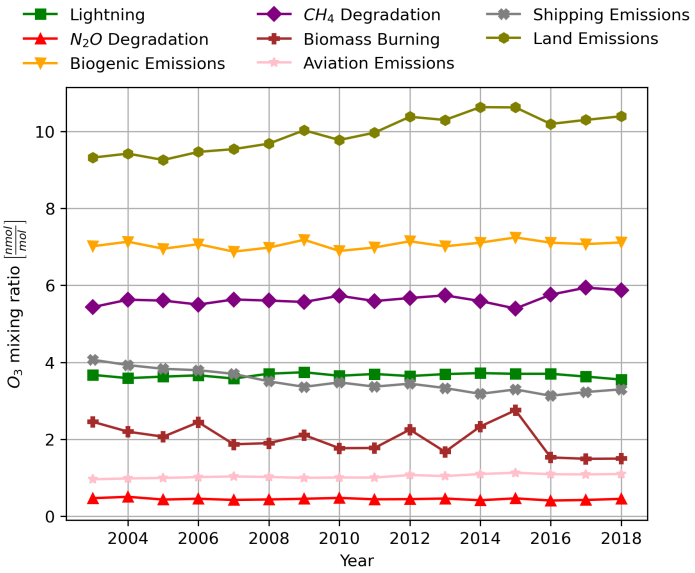

Figure 7.19: Comparison of the temporal evolution in the contribution to O_3 of different tagged sources at ground level above Asia.

In Figure 7.20 the biggest contribution to O_3 at flight levels in Asia comes from biogenic emissions, which fluctuate around 14 nmol·mol^{-1}. This is closely followed by lightning contributions which fluctuate around 13.5 nmol · mol^{-1}. The contribution of land emissions is again seen to increase from around 11 nmol · mol^{-1} in 2003 to about 13.5 nmol · mol^{-1} in 2018. The contributions of CH_4 degradation increase from about 11.5 nmol · mol^{-1} in 2003 to about 12.5 nmol · mol^{-1} in 2018. The O_3 resulting from shipping emissions is again shown to decrease from about 5 nmol · mol^{-1} to 4 nmol · mol^{-1}. Biomass burning contributions decrease from 3.5 nmol · mol^{-1} to about 2 nmol · mol^{-1}. The aviation contribution is around 2 nmol · mol^{-1}, while the contribution of N_2O degradation is just over 1.5 nmol · mol^{-1} across the years.

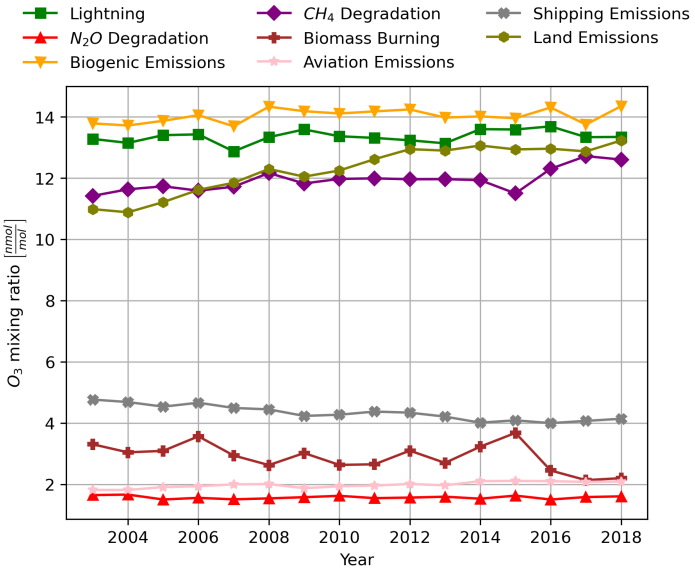

Figure 7.20: Comparison of the temporal evolution in the contribution to O_3 of different tagged sources at flight altitudes above Asia.

North America

Figure 7.21 shows the trends in the O_3 contribution for various tagged sources for the whole atmosphere above North America. The largest contribution to O_3 in this region for the whole atmosphere comes from land emissions which slightly increase from around 11.5 nmol $\cdot$ mol^{-1} to approximately 12 nmol $\cdot$ mol^{-1} across the years. The contribution of biogenic emissions fluctuates around 10.5 nmol $\cdot$ mol^{-1}, while the contribution of North America fluctuates around 9 nmol $\cdot$ mol^{-1}. The contribution of CH_4 degradation increase from around 9 nmol $\cdot$ mol^{-1} to about 10 nmol $\cdot$ mol^{-1}. The contribution of shipping emissions decreases from about 4 nmol $\cdot$ mol^{-1} to about 3.5 nmol $\cdot$ mol^{-1}, while the contribution of biomass burning decreases from about 3.5 nmol $\cdot$ mol^{-1} to about 2 nmol $\cdot$ mol^{-1}. The contribution of aviation is around 2 nmol $\cdot$ mol^{-1} across the years, whereas the contribution of N_2O degradation is around 1 nmol $\cdot$ mol^{-1} across the years.

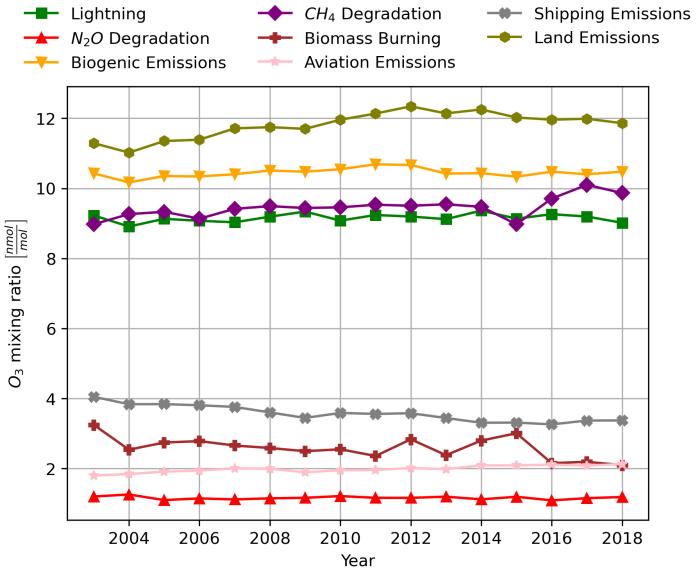

Figure 7.21: Comparison of the temporal evolution in the contribution to O_3 of different tagged sources for the whole troposphere in North America.

Figure 7.22 shows the trends in the various contributions at ground level for North America. Figure 7.22 shows that the largest contribution of O_3 comes from land emissions which decreases from approximately 9.5 nmol $\cdot$ mol^{-1} to 9 nmol $\cdot$ mol^{-1}. The contribution of biogenic emissions is constant at around 6 nmol $\cdot$ mol^{-1}, while the contribution of lightning emissions is around 3.5 nmol $\cdot$ mol^{-1}. The contribution of shipping decreases from about 3.5 nmol $\cdot$ mol^{-1} to about 3 nmol $\cdot$ mol^{-1}, while the contribution of biomass burning decreases from about 2.5 nmol $\cdot$ mol^{-1} to about 1.5 nmol $\cdot$ mol^{-1}. The contribution of aviation is around 1.5 nmol $\cdot$ mol^{-1} and the contribution of N_2O degradation is around 0.5 nmol $\cdot$ mol^{-1}.

Figure 7.23 shows the trends in the contribution of various O_3 sources to the O_3 levels at flight altitudes in North America. The largest contributors to O_3 are biogenic and lightning emissions, which both contribute between 14 nmol $\cdot$ mol^{-1} and 14.5 nmol $\cdot$ mol^{-1}. The contribution of CH_4 degradation increases from about 12 nmol $\cdot$ mol^{-1} to about 13.5 nmol $\cdot$ mol^{-1}. Similarly the contribution of land emissions increase from about 11.5 nmol $\cdot$ mol^{-1} to about 13 nmol $\cdot$ mol^{-1}. The contribution of shipping emissions decreases from about 4.5 nmol $\cdot$ mol^{-1} to just under 4 nmol $\cdot$ mol^{-1}, while the contribution of biomass burning decreases from about 4 nmol $\cdot$ mol^{-1} to about 2 nmol $\cdot$ mol^{-1}. The contribution due to aviation emissions is between 2 nmol $\cdot$ mol^{-1} and 2.5 nmol $\cdot$ mol^{-1} and the contribution of N_2O degradation is around 2 nmol $\cdot$ mol^{-1}.

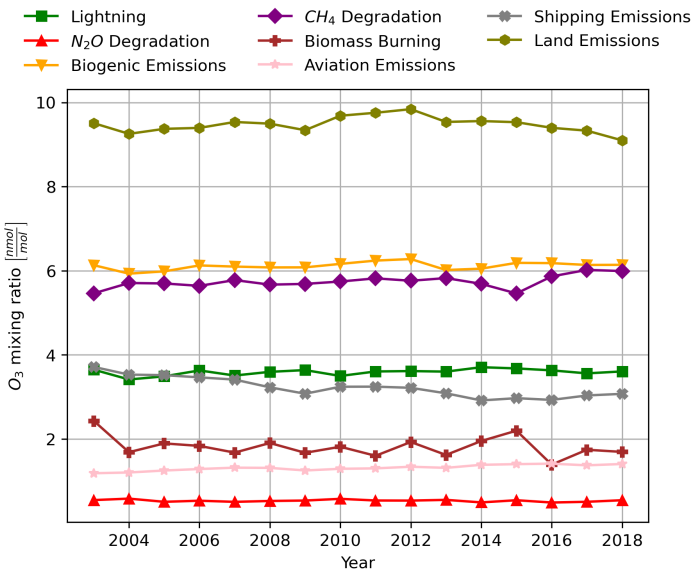

Figure 7.22: Comparison of the temporal evolution in the contribution to O_3 of different tagged sources at ground level in North America.

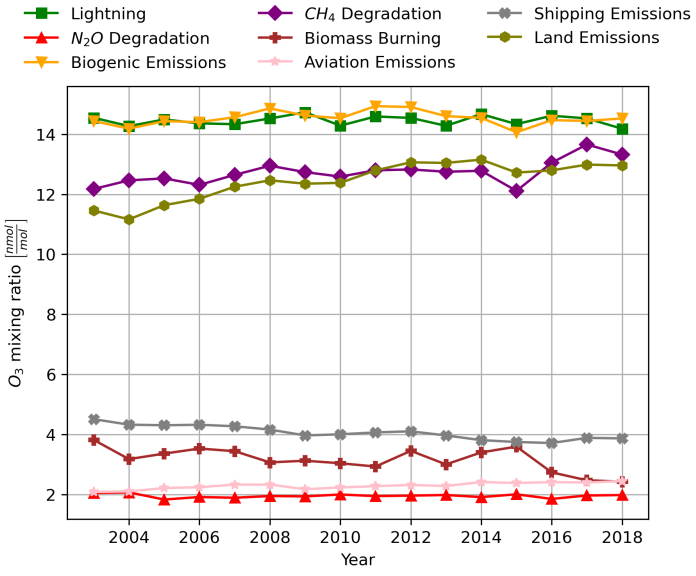

Figure 7.23: Comparison of the temporal evolution in the contribution to O_3 of different tagged sources at flight altitudes in North America.

8

Ozone Burden Efficiency of Aviation Emissions

This chapter looks at the Ozone Burden Efficiency of aviation NO_x emissions and tries to analyse them to explain the trends in Chapter 7. Similar to the analysis in Chapter 7, first the analysis is conducted on a global scale in Section 8.1 followed by an analysis on a regional scale in Section 8.2. Both parts of this analysis of the OBE aim to link the OBE results to the results in O_3 mixing ratios seen previously in this thesis.

8.1 Global Overview of Aviation's Ozone Burden Efficiency

This section looks at the Ozone Burden Efficiency (OBE) of aviation on a global scale, by analysing averages of the whole horizontal grid. The first part of this section in Section 8.1.1 compares the OBE of aviation across the various altitude domains that are analysed in this thesis. This is followed by an analysis where the OBE of aviation is compared to the OBE of other sources in Section 8.1.2.

8.1.1. Aviation's Ozone Burden Efficiency across Altitude Domains

Figure 8.1 shows the trends in the OBE of aviation across the whole troposphere, the ground level and the flight altitudes. Figure 8.1 shows that the highest value of the OBE of aviation is the average for the whole troposphere which decreases from about 4.65 Tg $(O_3) \cdot$ Tg^{-1} (NO_x) [1] to about 4.45 Tg $(O_3) \cdot$ Tg^{-1} (NO_x), with the range of values being similar to the findings of Mertens et al. (2024). Figure 8.1 shows that the OBE in the planetary boundary layer decreases from about 2.6 Tg $(O_3) \cdot$ Tg^{-1} (NO_x) to 2.4 Tg $(O_3) \cdot$ Tg^{-1} (NO_x) across the years whereas, the OBE at flight altitudes decreases from around 1.31 Tg $(O_3) \cdot$ Tg^{-1} (NO_x) to 1.23 Tg $(O_3) \cdot$ Tg^{-1} (NO_x). Since the OBE for the whole troposphere is higher than the OBEs at flight altitudes and in the planetary boundary layer, the OBE must be highest either between the planetary boundary layer and the flight altitudes, or between the flight altitudes and the tropopause. Looking at the distribution of O_3^{air} as shown in Figure 7.3, Figure 7.4 and Figure 7.5, the peak OBE is most likely to present between the flight altitudes and the planetary boundary layer, as this is where the bulk of O_3^{air} is present, but little aviation NO_x is emitted.

This is further evident from the O_3^{air} burden distribution shown in Figure 8.2 which shows that the total O_3^{air} burden in the whole troposphere increases from about 8 Tg to over 9 Tg. However, the O_3^{air} burden of the flight altitudes is less than 1.5 Tg, whereas the burden in the planetary boundary layer is around

[1] It is important to note that Tg^{-1} (NO_x) is defined as Tg^{-1} (NO) in this thesis

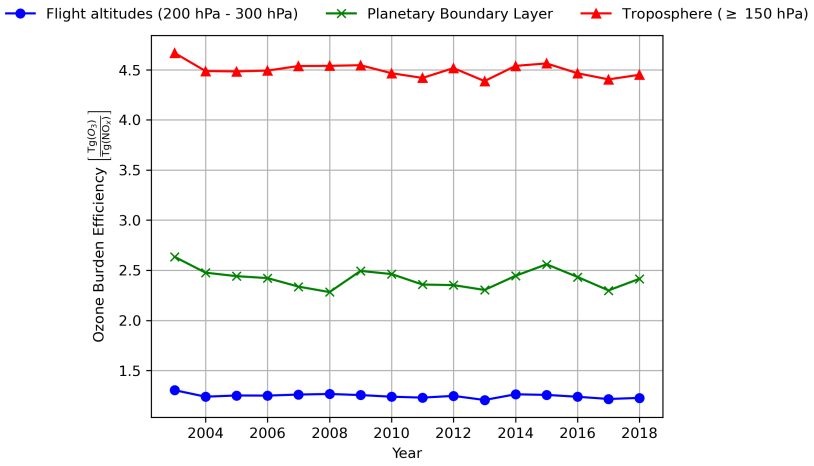

Figure 8.1: Comparison of the temporal evolution in global annual O_3 Burden efficiency of aviation of the whole troposphere, the planetary boundary layer and the flight altitudes

0.1 Tg. This means that more than 7 Tg of $O_3{}^{air}$ must be present between the planetary boundary layer and the flight altitudes. Additionally, Figure 8.3 shows that approximately 60% of aviation NO_x is emitted at flight altitudes and that approximately 2% are emitted within the planetary boundary layer. The remaining 38% of the NO_x must be present between the flight altitudes and the planetary boundary layer. Combining the results of the Figure 8.2 and Figure 8.3 would suggest that the OBE of aviation between the flight altitudes and the planetary boundary layer is between 8 Tg $(O_3) \cdot$ Tg^{-1} (NO_x) and 9 Tg $(O_3) \cdot$ Tg^{-1} (NO_x).

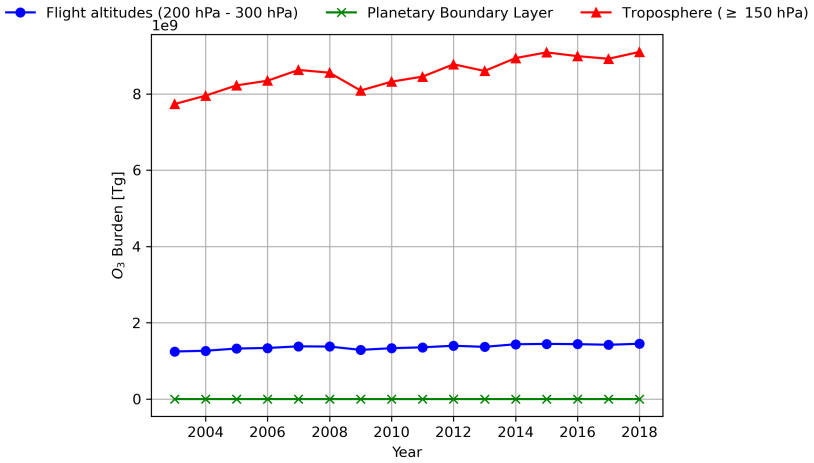

Figure 8.2: Comparison of the temporal evolution in the global annual $O_3{}^{air}$ burden of the whole troposphere, the planetary boundary layer and the flight altitudes.

This result is most likely, mainly driven by downward transport of aviation NO_x emissions at flight altitudes and $O_3{}^{air}$ formed at the flight altitudes. However, it is important to note that it is quite interesting that only about 60% of the NO_x emissions occur at cruise flight altitudes, where aircraft spend most of their time during flight. This could potentially, also suggest a distribution error in the aviation NO_x emissions inventory. Here it is important to note that more exact documentation on the CAMS emissions inventory used for this thesis could not be found. However, the newest version of the CAMS aviation emissions inventory (version 6.1) is based on the Community Earth atmospheric Data System (CEDS) emissions inventory for aircraft emissions. Thor et al. (2023) found that the CEDS emissions inventory has an inconsistency in the latitudinal variation, however, they authors did not look at the variation of the emissions inventory across different altitudes. Therefore, further analysis of the accuracy of the CEDS aviation emissions inventory should be conducted, especially looking at the variation across altitudes,

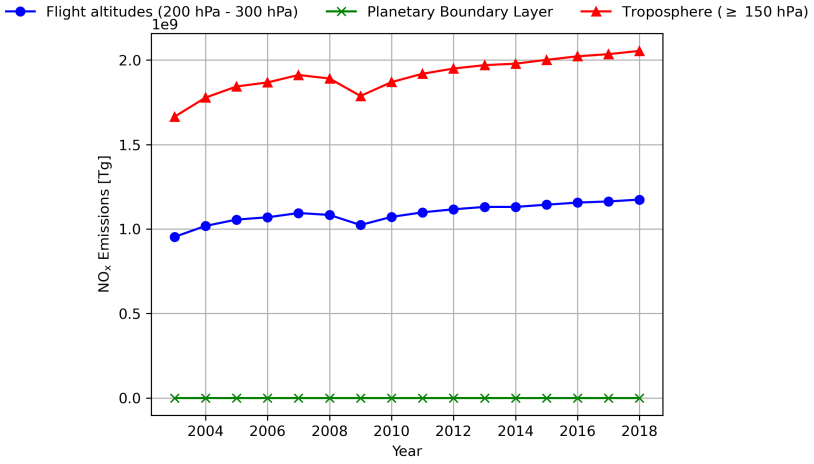

Figure 8.3: Comparison of the temporal evolution in global annual aviation NO_x emissions in the whole troposphere, ground level and flight altitudes.

which might explain the unexpected vertical distribution seen in Figure 8.3.

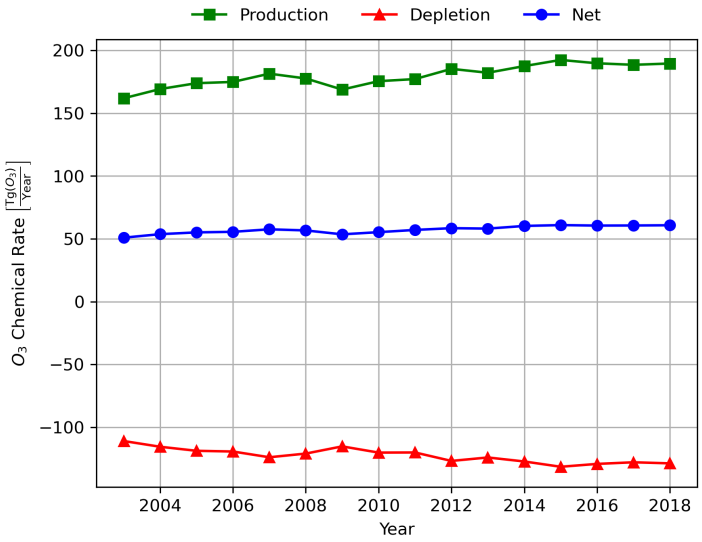

Figure 8.4: The trends in the production, depletion and net chemical rates for $O_3{}^{air}$ for the whole troposphere. The depletion values are shown to be negative.

Figure 8.4 shows the chemical rates for the production, depletion and net production of $O_3{}^{air}$ for the whole troposphere. Figure 8.4 shows that the magnitude of all three rates increases over the years. The increase in the chemical production rates of $O_3{}^{air}$ can be explained by the increasing NO_x emissions as seen in Figure 8.3. With a higher NO_x concentration there is a higher likelihood that the photolysis of NO_2 occurs which subsequently leads to the formation of O_3 via Reaction R2. On the other hand, a larger presence of NO_x also means that more OH is formed, which can happen across many pathways such as the depletion of O_3 leading to Reaction R7 or NO reacting with HO_2 to form OH as shown in Reaction R11. This larger presence means that O_3 depletion reactions are also more likely, which is why the rate of depletion also increases in magnitude in Figure 8.4.

Looking back at Figure 8.1, it can be seen that across the years the overall trend is a slight decrease in the OBE of aviation across the whole troposphere, the planetary boundary layer and the flight altitudes. This slight decrease in the OBE values is consistent with the fact that there is approximately a 23% increase in the NO_x emissions across the years as shown by Figure 8.3, while the increase in the $O_3{}^{air}$

burden is about 17% for the whole troposphere. Since the percentage increase in the O_3^{air} burden is smaller across the years than the percentage increase in the total aviation NO_x emissions Figure 8.2 and Figure 8.3 show that the efficiency of each NO_x molecule to form O_3 is decreasing with the increasing NO_x levels. This translates to a decreasing OBE. This lower efficiency occurs because the NO_x - O_3 chemistry is highly non-linear. This means that by increasing NO_x levels, chemical pathways such as the depletion of O_3 or the formation of HNO_3 start becoming more and more important, leading to the decrease of the OBE.

The OBE of aviation across the whole troposphere, the flight altitudes and the planetary boundary layer all show a decreasing behaviour. The OBE for the whole troposphere and for the flight altitudes decrease by a factor of about 5% across the years. However, the OBE for aviation for the planetary boundary layer, decreases by a factor of about 8%. This larger decrease in the OBE in the planetary boundary layer most likely occurs because the planetary boundary layer has a much larger background NO_x level than the free troposphere due to the emissions of other sectors. This makes the chemistry less efficient in the planetary boundary layer compared to the free troposphere. Furthermore, the increase of the aviation NO_x emissions in the planetary boundary layer, could also lead to an increase in NO_x titration and strengthening of deposition processes, which further reduce the ability of the planetary boundary layer to efficiently produce an aviation O_3 burden.

8.1.2. Comparing the OBE of Aviation and other Sources

Figure 8.5 shows the trends in the OBEs of the different tagged sources for the whole troposphere. Figure 8.5 shows that the global OBE is largest for lightning NO_x emissions at a values of around 17.5 $Tg\,(O_3) \cdot Tg^{-1}\,(NO_x)$. This is followed by the OBE of biogenic emissions which is around 6.0 $Tg\,(O_3) \cdot Tg^{-1}\,(NO_x)$. As mentioned previously the OBE for aviation is slightly higher than 4 $Tg\,(O_3) \cdot Tg^{-1}\,(NO_x)$. The OBE of biomass burning fluctuates around 1.6 $Tg\,(O_3) \cdot Tg^{-1}\,(NO_x)$ across the years. The OBE of shipping emissions increases from about 1.55 $Tg\,(O_3) \cdot Tg^{-1}\,(NO_x)$ to about 1.70 $Tg\,(O_3) \cdot Tg^{-1}\,(NO_x)$. The OBE of land emissions fluctuates just under 1 $Tg\,(O_3) \cdot Tg^{-1}\,(NO_x)$. The corresponding trends in the O_3 burden and the NO_x emissions are shown in Figure 8.5 and Figure 8.7, respectively.

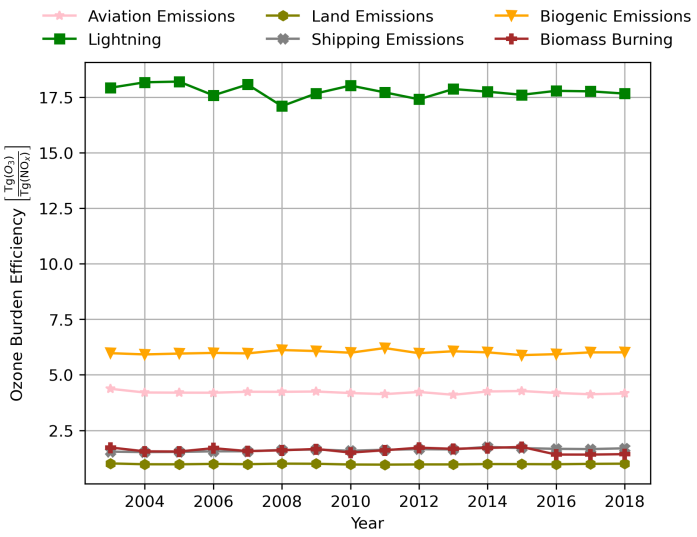

Figure 8.5: Comparison of the temporal evolution in the OBEs of different tagged sources for the whole troposphere.

As mentioned previously, the increase in O_3 burden due to aviation is driven by the increase in NO_x emissions, however, there is also a decrease in the OBE of aviation across the years. Similar increasing trends in the O_3 burden and NO_x emissions due to land emission can be seen in Figure 8.5 and Figure 8.7, but Figure 8.5, shows that there is no significant change in the OBE of the land emissions. For Biomass burning it can be seen that both the O_3 burden and NO_x emissions decrease, but there is no signification change in the corresponding OBE. These stagnant OBE values for land emissions

and biomass burnings, are most likely driven by the fact that most of these emissions take place at ground level in areas, that are already highly polluted and often have high background NO_x. Thus the respective changes in the NO_x emissions seen in Figure 8.7 are incremental compared to the overall background NO_x levels, leading to effectively no change in the efficiency of these NO_x molecules to produce a O_3 burden. On the other hand a decrease in the O_3 burden and NO_x emissions can be seen for shipping across the years. However, since shipping emissions primarily take place over secluded ocean regions where the background NO_x levels are low and the environment is less polluted, the decrease in the shipping emissions leads to an increase of shipping's OBE, as the chemistry becomes more NO_x limited. For biogenic emissions and lightning, since the NO_x levels stay consistent, the OBE values also do not change over time.

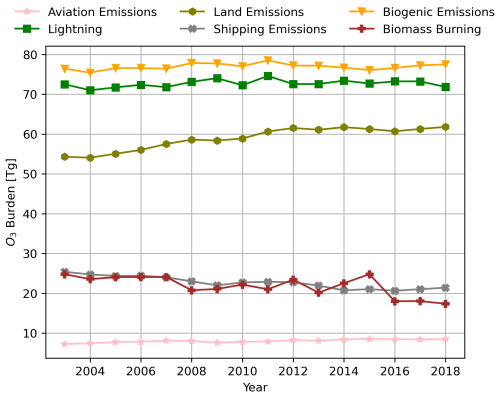

Figure 8.6: Comparison of the temporal evolution in the O_3 Burdens of different tagged sources for the whole troposphere.

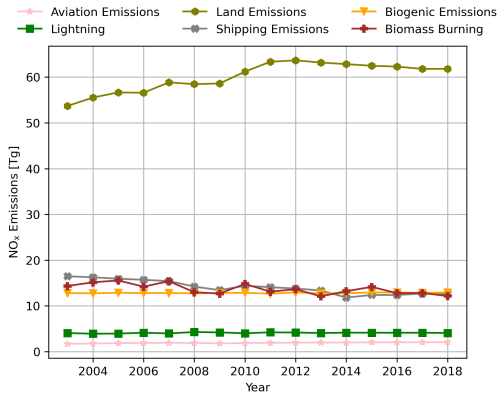

Figure 8.7: Comparison of the temporal evolution in the NO_x emitted by the different tagged sources across the whole troposphere.

Comparing the OBEs of the different tagged sources for the whole troposphere, to the OBEs for the same sources at the flight altitudes and the planetary boundary layer shows that the OBEs for the whole troposphere are always the largest. For ground based emission sources, this is driven by the fact that emissions and subsequently formed O_3 is transported to higher altitudes. On the other hand, for aviation O_3 and NO_x emissions, these are transported downwards to lower altitudes from the original flight altitudes where most of the emissions take place. A similar thing is true for lightning, however, lightning shows a very high OBE of around 80 $\mathrm{Tg}\,(O_3) \cdot \mathrm{Tg}^{-1}\,(NO_x)$ in the planetary boundary layer. This very high OBE is driven by the fact that the NO_x emitted in the planetary boundary layers is miniscule, but comparatively the subsequent O_3 burden due to lightning is very high. This highlights that the OBE as a metric is only meaningful when calculated for sufficiently large NO_x emissions magnitudes. At miniscule emission levels, like in the case of lightning NO_x emissions in the planetary boundary layer, the OBE becomes artificially inflated, yielding a value that is not an accurate representation of the atmospheric chemistry. This is why, future work looking at the OBE should make use of a lower NO_x emission threshold below which the OBE is not calculated, as it is not physically meaningful. This prevents false interpretation of very high efficiencies and makes sure that comparing OBEs across different sources remains numerically robust and representative of the background chemistry conditions.

To fully understand the trends given in Figure 7.6 and Figure 7.7 which show the absolute and percentage contributions of different tagged sources to tropospheric O_3, Figure 8.5 needs to be combined with information on the net chemical production rates shown in Figure 8.8. Here it is important to note that Figure 8.8 only takes into account chemical production and loss rates, and that deposition is not taken into account in these rates.

The large contribution of biogenic emissions in Figure 7.6 and Figure 7.7 is driven by the fact that the net production rate of O_3 due to biogenic emissions is really high compared to other sources, while the OBE of biogenic emissions is also really high. The high OBE suggests that the biogenic emissions are chemically effective at producing large amounts of O_3 with little NO_x emitted. This is to be expected for

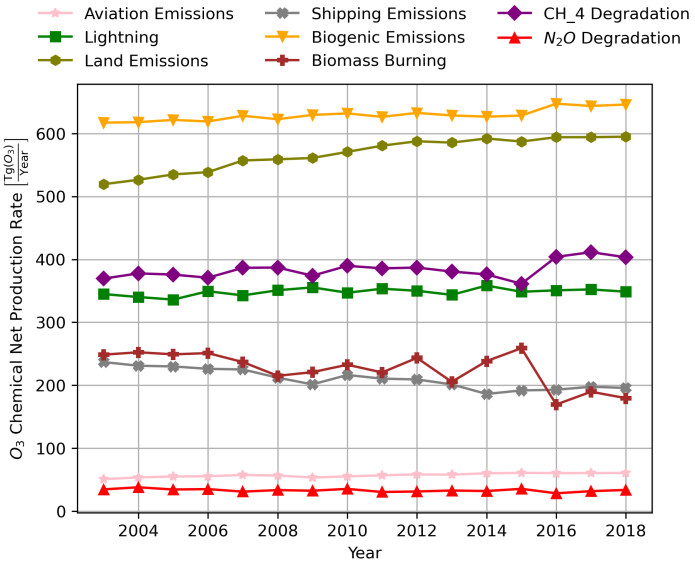

Figure 8.8: Comparison of the temporal evolution in the net production rate of O_3 of the different tagged sources for the whole troposphere

two reasons. Firstly, biogenic emissions mostly take place in rural areas or in areas with a lot of vegetation, such as forests. This means that biogenic emissions are emitted into less polluted air, which leads to a higher chemical efficiency to produce O_3 (Guenther et al., 2012). However, biogenic emissions are dominated by VOCs rather than NO_x. The VOCs react with OH to form radicals which cycle NO to NO_2 subsequently leading to O_3 formation. Thus, even a small amount of biogenic NO_x emissions can be very effective at creating a high O_3 burden. Thus, the high O_3 burden due to biogenic VOC emissions and the comparatively small NO_x emissions, lead to a high OBE, which does not necessarily reflect a larger chemical efficiency of the emitted biogenic NO_x. This shows that the OBE needs to be used carefully when comparing different emission sectors, where the emissions of precursors of O_3 vary greatly in composition. The OBE as a metric will lead to artificially inflated values for sources which emit low NO_x but abundant amounts of VOCs. This shows that the OBE is most robust when applied to emission sectors that are NO_x dominated.

The large contribution of lightning NO_x is driven primarily by the high OBE of lightning NO_x emissions. Since this NO_x is emitted primarily in a cleaner NO_x limited environment, each NO_x molecule is very efficient at producing O_3 (Dahlmann et al., 2011). Additionally, the fact that this NO_x is emitted at high altitudes, means that the lifetimes of the NO_x are longer making the NO_x even more efficient at producing O_3. Since the O_3 is produced at high altitudes, the lifetime of the O_3 is also longer, which means that it contributes towards larger O_3 mixing ratios as seen in Figure 7.6 and Figure 7.7. Here it is also important to note that the long lifetimes of both NO_x and O_3 are also driven by the low deposition rates at higher altitudes.

No OBE data is given for stratospheric O_3 and O_3 due to CH_4 and N_2O degradation. This is because no NO_x emissions take place which are attributed to these three sources of O_3. This represents a fundamental limitation of the OBE as a metric. Large contributors to tropospheric O_3 such as stratospheric O_3 and CH_4 degradation have to be excluded from OBE based comparisons, meaning that reliance on OBE alone as metric to describe variation in contributions to O_3 is not possible.

Looking at Figure 8.8 shows that land emissions have the second highest net production rate. But Figure 7.6 and Figure 7.7 show that land emissions only have the fourth highest contribution to O_3, while Figure 8.5 show that they have the lowest OBE. The production rates for land emissions are high due to their very high NO_x emissions, leading to subsequently high tagged NO_x concentrations.

However, these emissions mostly take place in highly polluted regions, where the background NO_x is already high. Furthermore, these emissions also take place in the planetary boundary layer, where deposition can remove a lot the NO_x emissions and the O_3 contribution. All in all, this leads to a very low chemical efficiency of the NO_x molecules, with the chemical regimes being NO_x saturated. The high production rate due to the high emissions, along with the very low OBE combine to produce a contribution that is significant, but not proportionate to the emissions levels.

Figure 7.6 and Figure 7.7 show that the contribution of shipping emissions to tropospheric O_3 decreases. This is primarily driven by the decrease in NO_x emissions which can be seen in Figure 8.7 and also in Figure 8.8 by the decreasing net production rate. As mentioned earlier, the decrease in shipping NO_x emissions and shipping's contribution to O_3 comes with an increase in shipping's OBE, as the O_3 formation becomes more and more NO_x limited, making any NO_x emissions more efficient at forming O_3. Since shipping NO_x emissions occur in less polluted regions compared to land emissions, the OBE of shipping is higher than that of land emissions (Mertens et al., 2024). However, the sheer amount of NO_x that comes from land emissions, makes them a larger contributor towards tropospheric O_3 compared to shipping.

Figure 7.6 and Figure 7.7 show that the contribution of biomass burning to tropospheric O_3 decreases over time and Figure 8.7 shows that this is primarily driven by the decrease in the NO_x emissions. Additionally, Figure 8.5 shows that the OBE of biomass burning stays constant across the years. This means that the NO_x - O_3 chemistry is not heavily impacted by the decrease in biomass burning emissions. This would suggest that background NO_x levels in the regions of biomass burning emissions are high such that small NO_x emissions changes have a minor impact on the chemical regime. However, this goes against the findings of Dahlmann et al. (2011) who find that biomass burning emissions primarily take place in low background NO_x environments. These divergent findings could be due to the fact that different emissions inventories are used for this thesis and the work conducted by Dahlmann et al. (2011). Varying emission inventories can impact the O_3 mixing ratios differently and this can subsequently lead to varying background chemistry, where the effect of changes in emission can diverge.

Figure 7.6 and Figure 7.7 show that the contribution of aviation NO_x emissions to tropospheric O_3 is approximately 2%. This relatively small contribution is primarily due to the low aviation NO_x emissions. However, due to the fact that the NO_x emissions occur in a cleaner environment, the NO_x molecules are more efficient at producing O_3. Additionally, the emission of aviation NO_x and the formation of aviation O_3 occurring at high altitudes has the impact that the lifetimes are longer. This further increases the chemical efficiency of aviation NO_x to form O_3. The OBE of aviation is found to be around 4.5 $\mathrm{Tg}\,(O_3) \cdot \mathrm{Tg}^{-1}\,(NO_x)$ showing that globally, aviation emissions play a in important role in the formation of tropospheric O_3.

8.2 Regional Distribution and Trends

This section looks at the OBE on a regional scale. Firstly, the OBE of aviation is compared across the regions that have been analysed in this thesis in Section 8.2.1. This is followed by a comparison of the OBE of aviation to the OBEs of other sources in Section 8.2.2 across the same regions.

8.2.1. Comparing Aviation's Ozone Burden Efficiency across Regions

Figure 8.9, Figure 8.11 and Figure 8.13 show the trends in the OBE of aviation for Europe, North America and Asia respectively. Figure 8.9, Figure 8.11 and Figure 8.13 show a decreasing trend in the OBE of aviation for all three regions, with the OBE being largest for Asia, followed by North America and Europe. The OBE for Asia drops from around 5.75 $\mathrm{Tg}\,(O_3) \cdot \mathrm{Tg}^{-1}\,(NO_x)$ to about 5.45 $\mathrm{Tg}\,(O_3) \cdot \mathrm{Tg}^{-1}\,(NO_x)$. The aviation OBE for North America drops from about 3.1 $\mathrm{Tg}\,(O_3) \cdot \mathrm{Tg}^{-1}\,(NO_x)$ to about 2.975 $\mathrm{Tg}\,(O_3) \cdot \mathrm{Tg}^{-1}\,(NO_x)$ and the aviation OBE for Europe drops from around 2.525 $\mathrm{Tg}\,(O_3) \cdot \mathrm{Tg}^{-1}\,(NO_x)$ to about 2.450 $\mathrm{Tg}\,(O_3) \cdot \mathrm{Tg}^{-1}\,(NO_x)$. Similarly, Figure 8.10, Figure 8.12 and Figure 8.14 show the net chemical production rates of O_3^{air}, along with the production and depletion contributions for Europe, North

America and Asia respectively. All three chemical net production plots show a slight increase in the net chemical production $O_3{}^{air}$ for the whole troposphere for all three regions. However, here North America, shows the highest values followed by Europe and then Asia.

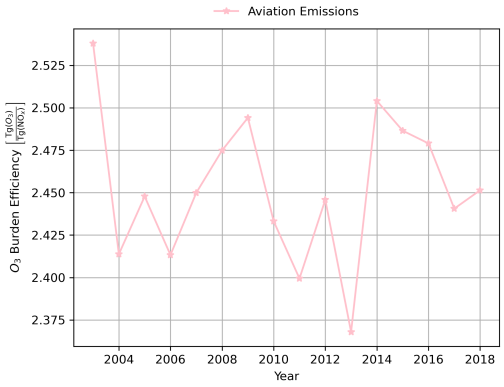

Figure 8.9: Trend in the O_3 Burden Efficiency of Aviation over Europe for the whole troposphere.

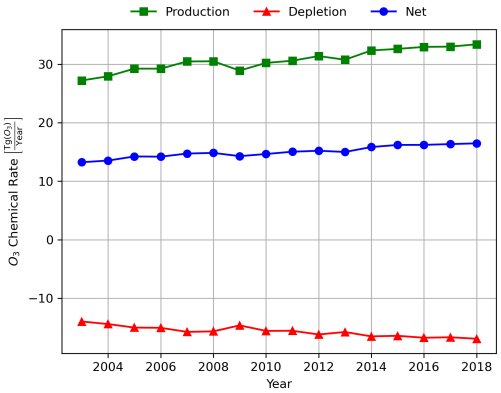

Figure 8.10: Trend in the net chemical production of $O_3{}^{air}$ over Europe for the whole troposphere

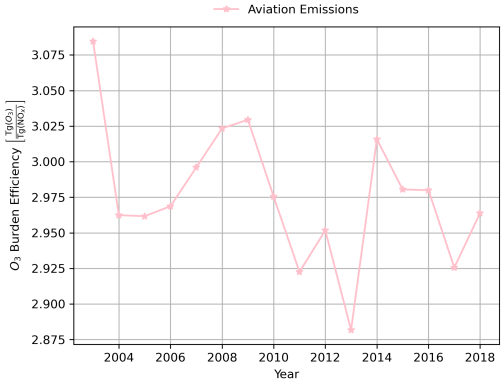

Figure 8.11: Trend in the O_3 Burden Efficiency of Aviation over North America for the whole troposphere.

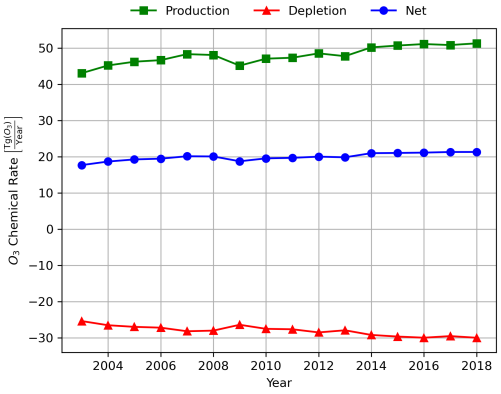

Figure 8.12: Trend in the net chemical production of $O_3{}^{air}$ over North America for the whole troposphere

Figure 7.12 shows that the mixing ratio above Europe is the largest, but Figure A.10 and Figure A.12 show that the burden over North America is the largest. This difference comes from the fact that the horizontal grid area covered by North America is larger than the one covered by Europe as shown in Figure 5.4. This means that North America has a slightly lower $O_3{}^{air}$ mixing ratio over a much larger mass of air, which leads to a larger burden. Despite having the lowest OBE, Europe has the highest mixing ratio, which suggests that a lot of O_3 accumulation occurs over Europe as a results of horizontal transport. The results of Maruhashi et al. (2022) show that a lot of the O_3 formed from local NO_x emissions North America is transported towards the East ending up over the northern Atlantic Ocean and mainland Europe. This shows, why despite having a larger OBE, North America has a lower mixing ratio of $O_3{}^{air}$. The high OBE over Asia suggests that within the troposphere over Asia, NO_x molecules are more chemically efficient than over Europe and North America. This means that at higher altitudes in the troposphere, Asia has a more NO_x limited chemical environment, with comparatively long effective lifetimes, meaning that once $O_3{}^{air}$ is formed in this region, it tends to stay there longer. However, despite the high OBE, the $O_3{}^{air}$ mixing ratios are lowest over Asia and this is driven primarily by the amount of aviation NO_x emitted in this region, subsequently leading to a low $O_3{}^{air}$ burden compared to Europe and North America.

Comparing the aviation OBEs for Europe, North America and Asia, across the planetary boundary layer and the flight altitudes, shows the exact same distribution as for the whole troposphere, as expected. This again, comes down to the distribution of NO_x emissions across the regions, with altitudinal

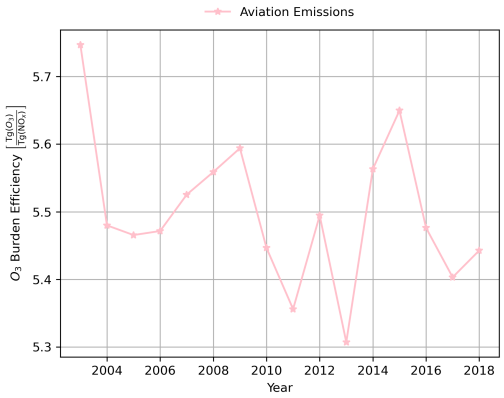

Figure 8.13: Trend in the O_3 Burden Efficiency of Aviation over Asia for the whole troposphere.

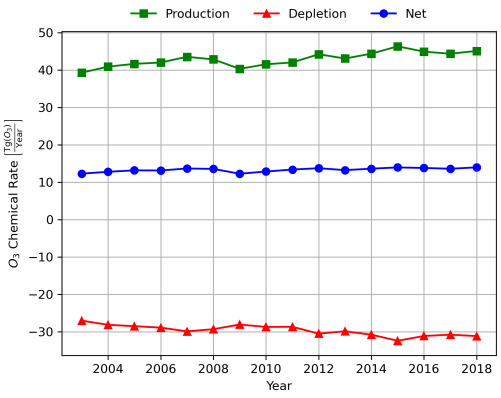

Figure 8.14: Trend in the net chemical production of $O_3{}^{air}$ over Asia for the whole troposphere

differences being the same as described earlier in Section 8.1.1.

8.2.2. Comparing Ozone Burden Efficiency of Aviation and other Sources across Regions

Europe

Comparing the global annual average OBEs of the different tagged sources shown in Figure 8.5 to the OBEs of the same tagged sources above Europe, as shown in Figure 8.15, shows that there are some differences between the O_3 production. The first two major differences are the large increases in the OBE of lightning emissions and biomass burning emissions. Comparing Figure 8.8 and Figure 8.16 shows that these increases in the OBEs of biomass burning and lightning are caused by the fact that the local NO_x emissions from these sources are very low, whereas the corresponding O_3 levels are not as low, due to long range transport. This effectively increases the OBE values of lightning and biomass burning, compared to the global average values, again highlighting the numerical weaknesses of the OBE as a metric.

As was the case for the global average annual OBE of shipping, the OBE of shipping in Europe also increases over time. The values of the shipping OBE in Europe are lower than the global shipping OBE values. This suggests that over Europe, the background NO_x is higher, which is expected since the Europe region includes the Atlantic ocean, which as shown by Mertens et al. (2024), has the largest shipping contribution to O_3. Additionally, it can also be seen that the OBE of land emissions increases from about 0.8 $\mathrm{Tg}\,(O_3) \cdot \mathrm{Tg}^{-1}\,(NO_x)$ to about 1.1 $\mathrm{Tg}\,(O_3) \cdot \mathrm{Tg}^{-1}\,(NO_x)$. Looking at the trend for land emissions in Figure 8.16 shows that the net production rate decreases, which suggests a decreasing trend in the NO_x emissions. This decreasing trend in the local NO_x emissions over Europe, drives an increase in the OBE, as the background NO_x levels decrease and the NO_x emissions subsequently become more chemically efficient at producing O_3. The decrease in the land emissions NO_x is most likely driven by climate impact and air quality mitigation strategies employed in Europe over the past years (Elshorbany et al., 2024). The OBE of biogenic emissions over Europe is similar to the global OBE. In general it can be seen that even from a regional perspective, the OBE of aviation across the whole troposphere is higher than any other anthropogenic or transportation emission source. This highlights the importance of the fact aviation emissions take place at high altitudes where the NO_x is more chemically efficient in producing O_3.

Comparing the trends across the whole troposphere over Europe to the trends at flight altitudes or in the planetary boundary layer does not show major differences between the altitude domains. The main observation made is that the lightning OBE is significantly higher in the planetary boundary layer compared to the whole troposphere and the flight altitudes. As suggested in the previous section, this is due to the very low NO_x emissions in the planetary boundary layer, which artificially inflates the OBE.

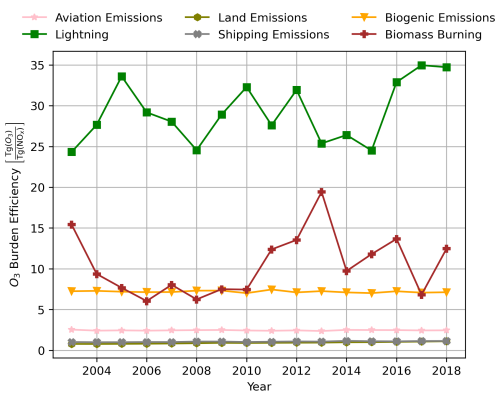

Figure 8.15: Comparison of the temporal evolution in the O_3 Burden Efficiency of different tagged sources over Europe for the whole troposphere.

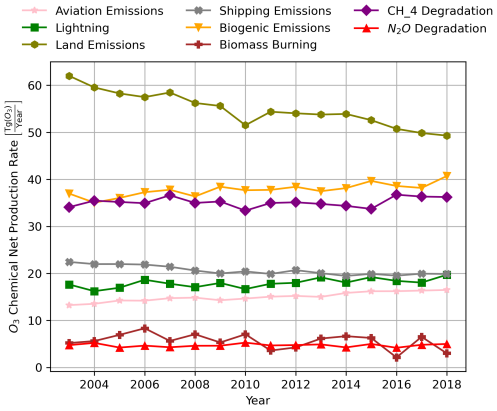

Figure 8.16: Comparison of the temporal evolution in the net chemical production of O_3 from different tagged sources over Europe for the whole troposphere.

North America

A similar analysis can be conducted for North America with the trends in the OBEs of various sources shown in Figure 8.17 and the corresponding net production rates shown in Figure 8.18. As was the case for the OBE values in Europe, an increase in the OBE values of biomass burning and lightning can be seen when comparing to the global values. However, for North America, these increases are not as high as they were for Europe. This is because, as seen from Figure 8.18, the net production rates are higher in North America than in Europe. This means, that in North America, the NO_x emissions of lightning and biomass burning are also higher, but so are the O_3 burdens. This effectively, leads to a lower OBE of lightning and biomass burning over North America, compared to Europe.

As was the case in Europe, the increasing trend in the shipping OBE over Europe is consistent with the increasing trend in the global OBE of shipping. In North America, the value is slightly higher than the global average, while it is much higher than the values over Europe. A similar thing is true for the OBE of land emissions. This suggests that at lower altitudes the background NO_x of North America is lower than the background NO_x levels over Europe, since the planetary boundary layer over Europe is more chemically efficient at producing O_3 from existing emissions. This is also evident from looking at Figure 8.16 and Figure 8.18, which show that for all tagged sources the net chemical production rate is higher in North America than Europe.

Comparing the trends across the whole troposphere over North America to the trends at flight altitudes and in the planetary boundary layer, shows no major differences between the altitude domains, as was also the case for Europe. Again, the only main observation is that the large local lightning OBE in the planetary boundary layer.

Asia

Figure 8.19 shows the comparison of OBE values for the whole troposphere over Asia, while Figure 8.20 shows the net production rates. Comparing the results for Asia, to the global OBE values for the different tagged sources, shows that the OBE values for biogenic emissions, shipping, land emissions, lightning and biomass burning are lower in Asia, with the OBE of aviation being larger compared to the global average. The lower OBEs of biogenic emissions, shipping, land emissions and biomass burning suggest that the background NO_x levels in the planetary boundary layer in Asia are higher compared to the global average, which leads to less chemical efficiency in terms of O_3 production, leading to lower OBEs. This finding is consistent with the findings of Elshorbany et al. (2024), who find an increasing trend in the NO_x concentration in Asia between 2005 and 2019. The decreased OBE of lightning emissions in Asia, suggests that even at higher altitudes, the background NO_x levels are higher than the global average. However, this is clearly not the case for the whole free troposphere, as the aviation OBE for Asia is higher than the global average, suggesting lower background NO_x levels at

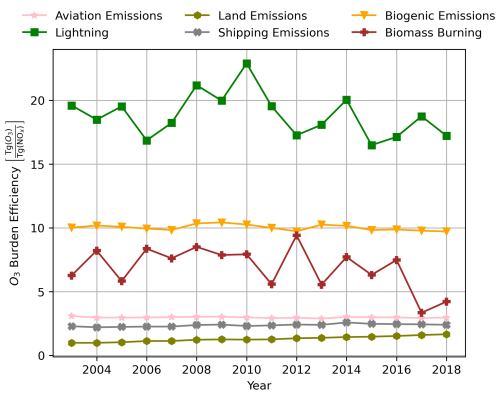

Figure 8.17: Comparison of the temporal evolution in the O_3 Burden Efficiency of different tagged sources over North America for the whole troposphere.

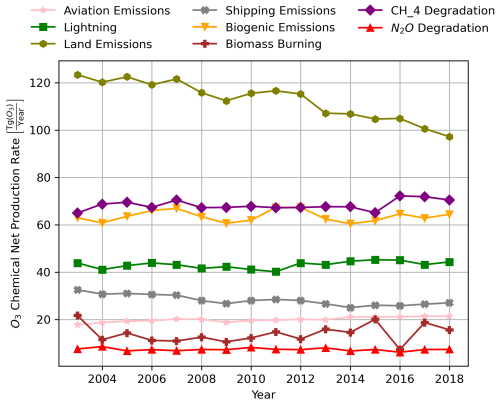

Figure 8.18: Comparison of the temporal evolution in the net chemical production of O_3 from different tagged sources over North America for the whole troposphere.

flight altitudes. Furthermore, Figure 8.19 also shows a trend in the land emission OBE. This decreases from about 0.675 $\mathrm{Tg}\,(O_3) \cdot \mathrm{Tg}^{-1}\,(NO_x)$ to 0.525 $\mathrm{Tg}\,(O_3) \cdot \mathrm{Tg}^{-1}\,(NO_x)$. This decreasing trend is driven by the increasing NO_x, which can be seen from the increasing net production rate in Figure 8.20. The increasing NO_x emissions subsequently lead to further decrease in the chemical efficiency of NO_x over Asia to produce O_3.

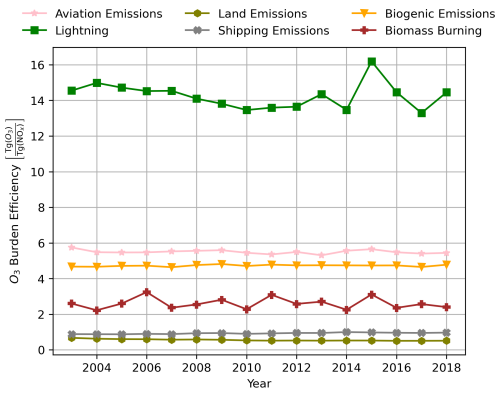

Figure 8.19: Comparison of the temporal evolution in the O_3 Burden Efficiency of different tagged sources over Asia for the whole troposphere.

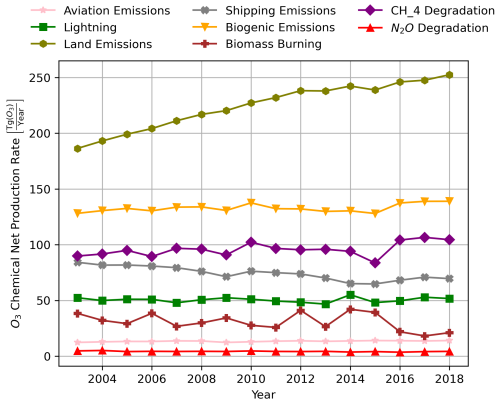

Figure 8.20: Comparison of the temporal evolution in the net chemical production of O_3 from different tagged sources over Asia for the whole troposphere.

Comparing the values for the whole troposphere over Asia shown in Figure 8.19 to the values at flight altitudes or in the planetary boundary layer over Asia, shows now major differences between the altitude domains. This was also the case for Europe and North America. As was the case previously, for Europe and North America, the main observation is the large local lightning OBE in the planetary boundary layer.

9

Conclusions and Recommendations

With increasingly more focus shifting towards mitigating climate change effects, anthropogenic emissions and their contribution towards the atmospheric concentrations of greenhouse gases have been gaining more attention. A major source of global anthropogenic emissions is aviation, a growing industry, which emits many greenhouse gases and precursors to greenhouse gases at high altitudes. One such precursor is Nitrogen Oxide (NO_x), which leads to the formation of Ozone (O_3). In the upper layers of the atmosphere, O_3 protects the surface from harmful ultraviolet radiation, but in the troposphere, O_3 acts as a pollutant. Furthermore, the chemistry that drives the formation of O_3 from NO_x is highly complicated and non-linear. Thus, this thesis aims to analyse the contribution of aviation NO_x emissions to tropospheric O_3 by answering the following research questions:

Q1 How do aviation NO_x emissions contribute towards tropospheric O_3 levels?

Q2 How does the ozone burden efficiency of aviation emissions vary in the troposphere?

Q3 Can the ozone burden efficiency trends be used to describe trends in tropospheric O_3 levels?

Simulation results of a ECHAM/MESSy Atmospheric Chemistry (EMAC) model were used to conduct the analysis and answer the research questions above. Evaluating the model showed that the model behaved as expected, with the EMAC model results showcasing a positive bias compared to measurement data and data from simulations of different models that have been used in literature. These results align with the findings of Jöckel et al. (2016). The analysis in this thesis looks at three different altitude domains which are the ground level, the flight altitudes (200 hPa to 300 hPa) and the whole troposphere. To simplify the analysis procedure the whole troposphere is defined as air where the air pressure is $\geq$ 150 hPa. Comparison of the analysis results showed that this troposphere definition leads to overestimates of the tropospheric O_3 burden, as this troposphere definition also captures considerable amounts of stratospheric air, which contains elevated levels of O_3. This has the impact that stratospheric O_3 contributions to tropospheric O_3 are artificially inflated in the calculated results.

An analysis of the average tropopause location showed that the definition of the troposphere commonly used in literature, as air where the O_3 mixing ratio is $\leq$ 150 nmol $\cdot$ mol^{-1}, matches the location of the tropopause much better than the definition used in this thesis. This analysis also showed that close

to the poles, the troposphere definition captures larger amounts of stratospheric air, whereas in the tropics, the troposphere definition does not capture all tropospheric air completely. This effect was later seen to cause elevated O_3 mixing ratios in the polar regions, along with very low mixing ratios in the tropics, leading to a very strong latitudinal gradient of O_3 across the globe.

To answer the first research question, variations in the contribution of aviation to tropospheric O_3 were analysed. The results of the EMAC model showed that for the troposphere, the global annular mixing ratio of the aviation contribution to O_3 increased from approximately 1 nmol $\cdot$ mol^{-1} to 1.2 nmol $\cdot$ mol^{-1} over the simulated period from 2003 to 2018. This represents an increase from approximately 1.6% to 1.9% of the total tropospheric O_3. The results showed that the contribution at flight altitudes (200 hPa to 300 hPa) is higher than at ground level, which was found to be due to the higher O_3 and NO_x lifetimes in the upper troposphere. At the same time, it was found that the aviation contribution to O_3 at ground level is higher as a percentage of the local O_3 mixing ratio compared to flight altitudes. This effect was found to be driven by the larger proportion of stratospheric O_3 at the flight altitudes, which also capture a large amount of stratospheric air and stratospheric O_3 especially in the polar regions. This inflates the total O_3 mixing ratios at flight altitudes, lowering the importance of aviation emissions. At ground level the percentage contribution of aviation to the O_3 levels was found to increase from 1.9% to 2.3% between 2003 and 2018, while at flight altitudes the increase was found to be around 1.25% to 1.45% across the same time period.

Zonal mean plots of the aviation contribution to O_3 showed that the peak absolute concentrations are primarily between 60^o North and 90^o North at flight altitudes (200 hPa to 300 hPa). This result is primarily driven by the increased lifetime of NO_x and O_3 at these altitudes, leading to larger O_3 accumulation. However, looking at percentage contributions, the peak occurs between 40^o North and 90^o at altitudes of 300 hPa to 800 hPa. In general the zonal mean plots show that the aviation contribution to O_3 is not only concentrated at flight altitudes, but that large scale vertical transport takes place, which leads to a vertical distribution across the free troposphere. Furthermore, the zonal mean plots show that the growth in the aviation contribution to O_3 is concentrated in the Northern hemisphere, between 300 hPa and 800 hPa, between 40^o North and 90^o.

Comparing the contribution of aviation emissions to tropospheric O_3 to the contribution of other sources, shows that aviation NO_x emissions are a relatively small contributor compared to land, biogenic, lightning, biomass burning and shipping emissions. This is true on both a global but also a regional scale, with the analysis looking at Europe, North America and Asia. Furthermore, the results showed that the aviation contribution to O_3 is highest over Europe with values of around 2.6 nmol $\cdot$ mol^{-1} to 3.0 nmol $\cdot$ mol^{-1}, while in North America the aviation contribution is 2.1 nmol $\cdot$ mol^{-1} to 2.4 nmol $\cdot$ mol^{-1} and in Asia it is 1.8 nmol $\cdot$ mol^{-1} to 2.1 nmol $\cdot$ mol^{-1}.

To explain the variations in the aviation contribution to O_3, this thesis looked at the Ozone Burden Efficiency (OBE). An analysis of the OBE showed that the average tropospheric OBE of aviation is about 4.5 Tg $(O_3) \cdot$ Tg^{-1} (NO_x). The analysis showed that in the planetary boundary layer the values of the OBE of aviation are around 2.5 Tg $(O_3) \cdot$ Tg^{-1} (NO_x), while at the flight altitudes these values are around 1.3 Tg $(O_3) \cdot$ Tg^{-1} (NO_x). Furthermore, the OBE of aviation for all three altitude domains showed decreasing trends over the analysed time period, driven by the increasing NO_x emissions. The analysis showed that downward transport of O_3 from the flight altitudes, must lead to a peak OBE value between the planetary boundary layer and flight altitudes. Here the aviation NO_x emissions are low but O_3 concentrations are high, which leads to an OBE value, estimated to be around 8 Tg $(O_3) \cdot$Tg^{-1} (NO_x).

In comparison, for the whole troposphere, the OBE of lightning emissions was found to be around 17.5 Tg $(O_3) \cdot$ Tg^{-1} (NO_x), while for biogenic emissions it was found to be around 6.0 Tg $(O_3) \cdot$ Tg^{-1} (NO_x). The OBE of biomass burning and shipping were both found to be around 1.5 Tg $(O_3) \cdot$ Tg^{-1} (NO_x), while the OBE of land emissions was found to be around 1.0 Tg $(O_3) \cdot$ Tg^{-1} (NO_x). The high OBE of aviation emissions suggests that aviation NO_x is emitted in an environment that is comparatively NO_x

limited, due to low background NO_x levels and that in this environment the lifetimes of NO_x and O_3 are high. This leads to the effect that a very small amount of NO_x emissions leads to a relatively high O_3 burden. To put this into perspective, land emissions are found to emit around 60 Tg of NO_x leading to a tropospheric O_3 burden of around 60 Tg. On the other hand about 2 Tg of NO_x are emitted by aviation leading to an O_3 burden of about 8.5 Tg. This shows that despite a comparatively small amount of emissions, aviation contributes disproportionately highly towards tropospheric O_3 levels due to the clean environment in which aviation emits NO_x.

The decreasing trend in the OBE of aviation is explained by the fact that the amount of aviation NO_x emitted increases over the analysed time period. This increase is found to be about 23% for the whole troposphere, and the accompanying O_3 burden increase is found to be about 17%. This shows that with increasing NO_x emissions and subsequently increasing background NO_x levels, the chemical efficiency of the troposphere to form O_3 decreases. Furthermore, the regional analysis shows that the OBE of aviation is highest over Asia being around 5.45 Tg $(O_3) \cdot Tg^{-1}$ (NO_x) in 2018, while over North America the OBE is around 2.96 Tg $(O_3) \cdot Tg^{-1}$ (NO_x) and 2.45 Tg $(O_3) \cdot Tg^{-1}$ (NO_x) over Europe.

This analysis shows that the OBE itself cannot be used to fully explain trends in the variations of O_3 and the aviation contribution to O_3. While the OBE itself provides important information about the efficiency of the NO_x - O_3 chemistry, the way the OBE has been applied in this thesis, it cannot give full clarity of tropospheric O_3 trends on its own. Having both the OBE and the NO_x emissions together can help provide a better understanding for certain trends that are seen. However, it is also important to note that the OBE cannot be used as metric for sources where the emissions are dominated by VOCs and limited in NO_x, such as biogenic emissions. Similarly, there are sources of O_3, which do not emit NO_x at all, such as CH_4 or N_2O degradation. This means that the OBE as a metric is inherently only suitable for emissions sources that are NO_x dominated. This means that using the OBE as a comparative metric between different emissions sources requires in depth knowledge of the emitted species. Thus, it might be worth investigating a metric similar to the OBE which also takes into account VOC emissions. Doing so, would allow for better understanding of O_3 variations and the reasons why these variations exist.

The OBE as a metric also has the weakness that it inflates the efficiency of a source, when the NO_x emissions are very small. This is specially true, when the global domain, is broken down into smaller regions, or when the whole atmosphere is broken down into smaller vertical domains. In these cases the NO_x emitted for specific sources can be very small, leading to very large OBE values, which do not translate into a valid representation of the background chemistry. Thus, future OBE analyses should make use of a lower NO_x emissions threshold, for which OBE values are computed.

In this thesis, the troposphere is defined to be air where the air pressure is $\geq$ 150 hPa. This is vastly different to the definition usually used in literature, which sets the tropopause at an O_3 mixing ratio of $\leq$ 150 nmol $\cdot$ mol^{-1}. To verify that the definition of the troposphere used in this thesis does not skew the results presented in this thesis, it is recommended that a sensitivity analysis is conducted, which looks at the effect of this definition. It is expected that for the values representing the average for the whole troposphere, that the mixing ratios found for the aviation contribution to O_3 will be lower than if the definition commonly found in literature would be used. However, the values for the flight altitudes and the ground level or planetary boundary layer should not be impacted by this definition.

A regional analysis has been conducted in this thesis. However, this regional analysis did not make use of regional source attribution markers, but instead the global grid was split into smaller subsets, to isolate trends within specific regions. However, Maruhashi et al. (2022) have shown that aviation NO_x and the subsequently formed O_3 undergoes many different transport patterns based on the original emissions region. A lot of this transportation occurs both in vertical direction but also in globally across different latitudes and longitudes. Thus, for future research it is recommended that both the vertical and global fird be split into multiple domains, which all receive a diagnostic tag. This way further analysis of transport patterns of aviation NO_x emissions can be conducted. Additionally, this will shed light

on to what extent aviation NO_x emitted at high altitudes contribute towards surface level O_3 and to what extent the aviation contribution of surface level O_3 comes from ascent and descent operations. Additionally, an analysis like this will also shed more light on how different flight corridors affect their neighbouring continents. Having this understanding would be vital to further understand the impact of aviation O_3 on local air quality but also on climate change. This understanding would then build the foundation towards further limiting the contribution of aviation NO_x to tropospheric O_3.

References

Butler, T., Lupascu, A., Coates, J., & Zhu, S. (2018). TOAST 1.0: Tropospheric Ozone Attribution of Sources with Tagging for CESM 1.2.2 [Publisher: Copernicus GmbH]. *Geoscientific Model Development*, *11*(7), 2825–2840. https://doi.org/10.5194/gmd-11-2825-2018

Butler, T., Lupascu, A., & Nalam, A. (2020). Attribution of ground-level ozone to anthropogenic and natural sources of nitrogen oxides and reactive carbon in a global chemical transport model [Publisher: Copernicus GmbH]. *Atmospheric Chemistry and Physics*, *20*(17), 10707–10731. https://doi.org/10.5194/acp-20-10707-2020

Dahlmann, K., Grewe, V., Ponater, M., & Matthes, S. (2011). Quantifying the contributions of individual NOx sources to the trend in ozone radiative forcing. *Atmospheric Environment*, *45*(17), 2860–2868. https://doi.org/10.1016/j.atmosenv.2011.02.071

Davis, S. M., Rosenlof, K. H., Hassler, B., Hurst, D. F., Read, W. G., Vömel, H., Selkirk, H., Fujiwara, M., & Damadeo, R. (2016). The Stratospheric Water and Ozone Satellite Homogenized (SWOOSH) database: A long-term database for climate studies [Publisher: Copernicus GmbH]. *Earth System Science Data*, *8*(2), 461–490. https://doi.org/10.5194/essd-8-461-2016

Doherty, R. M., Stevenson, D. S., Johnson, C. E., Collins, W. J., & Sanderson, M. G. (2006). Tropospheric ozone and El Niño–Southern Oscillation: Influence of atmospheric dynamics, biomass burning emissions, and future climate change. *Journal of Geophysical Research: Atmospheres*, *111*(D19). https://doi.org/10.1029/2005JD006849

Elshorbany, Y., Ziemke, J. R., Strode, S., Petetin, H., Miyazaki, K., De Smedt, I., Pickering, K., Seguel, R. J., Worden, H., Emmerichs, T., Taraborrelli, D., Cazorla, M., Fadnavis, S., Buchholz, R. R., Gaubert, B., Rojas, N. Y., Nogueira, T., Salameh, T., & Huang, M. (2024). Tropospheric ozone precursors: Global and regional distributions, trends, and variability [Publisher: Copernicus GmbH]. *Atmospheric Chemistry and Physics*, *24*(21), 12225–12257. https://doi.org/10.5194/acp-24-12225-2024

Fowler, D. (2008). *Ground-level ozone in the 21st century: Future trends, impacts and policy implications* [OCLC: 624958290]. The Royal Society.

Frömming, C., Ponater, M., Dahlmann, K., Grewe, V., Lee, D. S., & Sausen, R. (2012). Aviation-induced radiative forcing and surface temperature change in dependency of the emission altitude [_eprint: https://onlinelibrary.wiley.com/doi/pdf/10.1029/2012JD018204]. *Journal of Geophysical Research: Atmospheres*, *117*(D19). https://doi.org/10.1029/2012JD018204

Frömming, C., Grewe, V., Brinkop, S., Jöckel, P., Haslerud, A. S., Rosanka, S., van Manen, J., & Matthes, S. (2021). Influence of weather situation on non-CO_2 aviation climate effects: The REACT4C climate change functions [Publisher: Copernicus GmbH]. *Atmospheric Chemistry and Physics*, *21*(11), 9151–9172. https://doi.org/10.5194/acp-21-9151-2021

Gilmore, C. K., Barrett, S. R. H., Koo, J., & Wang, Q. (2013). Temporal and spatial variability in the aviation NOx-related O3 impact [Publisher: IOP Publishing]. *Environmental Research Letters*, *8*(3), 034027. https://doi.org/10.1088/1748-9326/8/3/034027

Grewe, V., Brunner, D., Dameris, M., Grenfell, J. L., Hein, R., Shindell, D., & Staehelin, J. (2001). Origin and variability of upper tropospheric nitrogen oxides and ozone at northern mid-latitudes. *Atmospheric Environment*, *35*(20), 3421–3433. https://doi.org/10.1016/S1352-2310(01)00134-0

Grewe, V., Champougny, T., Matthes, S., Frömming, C., Brinkop, S., Soevde, A., Irvine, E. A., & Halscheidt, L. (2014). Reduction of the air traffic's contribution to climate change: A REACT4C case study [Publisher: Elsevier]. *Atmospheric Environment*, *94*, 616–625. Retrieved January 30, 2025, from http://www.sciencedirect.com/science/article/pii/S1352231014004063

Grewe, V., Tsati, E., & Hoor, P. (2010). On the attribution of contributions of atmospheric trace gases to emissions in atmospheric model applications [Publisher: Copernicus GmbH]. *Geoscientific Model Development*, *3*(2), 487–499. https://doi.org/10.5194/gmd-3-487-2010

Grewe, V., Dahlmann, K., Matthes, S., & Steinbrecht, W. (2012). Attributing ozone to NOx emissions: Implications for climate mitigation measures. *Atmospheric Environment*, *59*, 102–107. https://doi.org/10.1016/j.atmosenv.2012.05.002

Grewe, V., Dameris, M., Fichter, C., & Lee, D. S. (2002). Impact of aircraft NOx emissions. Part 2: Effects of lowering the flight altitude [Publisher: Schweizerbart'sche Verlagsbuchhandlung]. *Meteorologische Zeitschrift*, 197–205. https://doi.org/10.1127/0941-2948/2002/0011-0197

Grewe, V., Tsati, E., Mertens, M., Frömming, C., & Jöckel, P. (2017). Contribution of emissions to concentrations: The TAGGING 1.0 submodel based on the Modular Earth Submodel System (MESSy 2.52). *Geoscientific Model Development*, *10*(7), 2615–2633. https://doi.org/10.5194/gmd-10-2615-2017

Griffiths, P. T., Murray, L. T., Zeng, G., Shin, Y. M., Abraham, N. L., Archibald, A. T., Deushi, M., Emmons, L. K., Galbally, I. E., Hassler, B., Horowitz, L. W., Keeble, J., Liu, J., Moeini, O., Naik, V., O'Connor, F. M., Oshima, N., Tarasick, D., Tilmes, S., … Zanis, P. (2021). Tropospheric ozone in CMIP6 simulations [Publisher: Copernicus GmbH]. *Atmospheric Chemistry and Physics*, *21*(5), 4187–4218. https://doi.org/10.5194/acp-21-4187-2021

Guenther, A. B., Jiang, X., Heald, C. L., Sakulyanontvittaya, T., Duhl, T., Emmons, L. K., & Wang, X. (2012). The Model of Emissions of Gases and Aerosols from Nature version 2.1 (MEGAN2.1): An extended and updated framework for modeling biogenic emissions [Publisher: Copernicus GmbH]. *Geoscientific Model Development*, *5*(6), 1471–1492. https://doi.org/10.5194/gmd-5-1471-2012

Haagen-Smit, A. J. (1952). Chemistry and Physiology of Los Angeles Smog [Publisher: American Chemical Society]. *Industrial & Engineering Chemistry*, *44*(6), 1342–1346. https://doi.org/10.1021/ie50510a045

IPCC. (2013). *Climate Change 2013: The Physical Science Basis. Contribution of Working Group I to the Fifth Assessment Report of the Intergovernmental Panel on Climate Change* (T. Stocker, D. Qin, G.-K. Plattner, M. Tignor, S. Allen, J. Boschung, A. Nauels, Y. Xia, V. Bex, & P. Midgley, Eds.). Cambridge University Press. https://doi.org/10.1017/CBO9781107415324

IPCC. (2018). *Global Warming of 1.5°C. An IPCC Special Report on the Impacts of Global Warming of 1.5°C Above Pre-Industrial Levels and Related Global Greenhouse Gas Emission Pathways, in the Context of Strengthening the Global Response to the Threat of Climate Change, Sustainable Development, and Efforts to Eradicate Poverty* (V. Masson-Delmotte, P. Zhai, H.-O. Pörtner, D. Roberts, J. Skea, P. Shukla, A. Pirani, W. Moufouma-Okia, C. Péan, R. Pidcock, S. Connors, J. Matthews, Y. Chen, X. Zhou, M. Gomis, E. Lonnoy, T. Maycock, M. Tignor, & T. Waterfield, Eds.). In Press.

Jöckel, P., Tost, H., Pozzer, A., Kunze, M., Kirner, O., Brenninkmeijer, C. A. M., Brinkop, S., Cai, D. S., Dyroff, C., Eckstein, J., Frank, F., Garny, H., Gottschaldt, K.-D., Graf, P., Grewe, V., Kerkweg, A., Kern, B., Matthes, S., Mertens, M., … Zahn, A. (2016). Earth System Chemistry integrated Modelling (ESCiMo) with the Modular Earth Submodel System (MESSy) version 2.51 [Publisher: Copernicus GmbH]. *Geoscientific Model Development*, *9*(3), 1153–1200. https://doi.org/10.5194/gmd-9-1153-2016

Kerkweg, A., Sander, R., Tost, H., & Jöckel, P. (2006). Technical note: Implementation of prescribed (OFFLEM), calculated (ONLEM), and pseudo-emissions (TNUDGE) of chemical species in the Modular Earth Submodel System (MESSy) [Publisher: Copernicus GmbH]. *Atmospheric Chemistry and Physics*, *6*(11), 3603–3609. https://doi.org/10.5194/acp-6-3603-2006

Kilian, M., Grewe, V., Jöckel, P., Kerkweg, A., Mertens, M., Zahn, A., & Ziereis, H. (2024). Ozone source attribution in polluted European areas during summer 2017 as simulated with MECO(n) [Publisher: Copernicus GmbH]. *Atmospheric Chemistry and Physics*, *24*(23), 13503–13523. https://doi.org/10.5194/acp-24-13503-2024

Koffi, B., Szopa, S., Cozic, A., Hauglustaine, D., & van Velthoven, P. (2010). Present and future impact of aircraft, road traffic and shipping emissions on global tropospheric ozone [Publisher: Copernicus GmbH]. *Atmospheric Chemistry and Physics*, *10*(23), 11681–11705. https://doi.org/10.5194/acp-10-11681-2010

Köhler, M., Rädel, G., Shine, K., Rogers, H., & Pyle, J. (2013). Latitudinal variation of the effect of aviation NOx emissions on atmospheric ozone and methane and related climate metrics. *Atmospheric Environment*, *64*, 1–9. https://doi.org/10.1016/j.atmosenv.2012.09.013

Lee, D., Fahey, D., Skowron, A., Allen, M., Burkhardt, U., Chen, Q., Doherty, S., Freeman, S., Forster, P., Fuglestvedt, J., Gettelman, A., De León, R., Lim, L., Lund, M., Millar, R., Owen, B., Penner, J., Pitari, G., Prather, M., … Wilcox, L. (2021). The contribution of global aviation to anthropogenic climate forcing for 2000 to 2018. *Atmospheric Environment (Oxford, England : 1994)*, *244*, 117834. https://doi.org/10.1016/j.atmosenv.2020.117834

Lee, D., Pitari, G., Grewe, V., Gierens, K., Penner, J., Petzold, A., Prather, M., Schumann, U., Bais, A., & Berntsen, T. (2010). Transport impacts on atmosphere and climate: Aviation. *Atmospheric Environment*, *44*(37), 4678–4734. https://doi.org/10.1016/j.atmosenv.2009.06.005

Liu, J., Strode, S. A., Liang, Q., Oman, L. D., Colarco, P. R., Fleming, E. L., Manyin, M. E., Douglass, A. R., Ziemke, J. R., Lamsal, L. N., & Li, C. (2022). Change in Tropospheric Ozone in the Recent Decades and Its Contribution to Global Total Ozone. *Journal of Geophysical Research: Atmospheres*, *127*(22), e2022JD037170. https://doi.org/10.1029/2022JD037170

Liu, S. C., Trainer, M., Fehsenfeld, F. C., Parrish, D. D., Williams, E. J., Fahey, D. W., Hübler, G., & Murphy, P. C. (1987). Ozone production in the rural troposphere and the implications for regional and global ozone distributions. *Journal of Geophysical Research: Atmospheres*, *92*(D4), 4191–4207. https://doi.org/10.1029/JD092iD04p04191

Maruhashi, J., Grewe, V., Frömming, C., Jöckel, P., & Dedoussi, I. C. (2022). Transport patterns of global aviation NO_x and their short-term O_3 radiative forcing – a machine learning approach [Publisher: Copernicus GmbH]. *Atmospheric Chemistry and Physics*, *22*(21), 14253–14282. https://doi.org/10.5194/acp-22-14253-2022

Maruhashi, J., Mertens, M., Grewe, V., & Dedoussi, I. C. (2024). A multi-method assessment of the regional sensitivities between flight altitude and short-term O3 climate warming from aircraft NOx emissions [Publisher: IOP Publishing]. *Environmental Research Letters*, *19*(5), 054007. https://doi.org/10.1088/1748-9326/ad376a

Mertens, M., Brinkop, S., Graf, P., Grewe, V., Hendricks, J., Jöckel, P., Lanteri, A., Matthes, S., Rieger, V. S., Righi, M., & Thor, R. N. (2024). The contribution of transport emissions to ozone mixing ratios and methane lifetime in 2015 and 2050 in the Shared Socioeconomic Pathways (SSPs). *Atmospheric Chemistry and Physics*, *24*(21), 12079–12106. https://doi.org/10.5194/acp-24-12079-2024

Mertens, M., Grewe, V., Rieger, V. S., & Jöckel, P. (2018). Revisiting the contribution of land transport and shipping emissions to tropospheric ozone [Publisher: Copernicus GmbH]. *Atmospheric Chemistry and Physics*, *18*(8), 5567–5588. https://doi.org/10.5194/acp-18-5567-2018

Nalam, A., Lupaşcu, A., Ansari, T., & Butler, T. (2025). Regional and sectoral contributions of NO_x and reactive carbon emission sources to global trends in tropospheric ozone during the 2000–2018 period [Publisher: Copernicus GmbH]. *Atmospheric Chemistry and Physics*, *25*(10), 5287–5311. https://doi.org/10.5194/acp-25-5287-2025

Nisbet, E. G., Manning, M. R., Dlugokencky, E. J., Fisher, R. E., Lowry, D., Michel, S. E., Myhre, C. L., Platt, S. M., Allen, G., Bousquet, P., Brownlow, R., Cain, M., France, J. L., Hermansen, O., Hossaini, R., Jones, A. E., Levin, I., Manning, A. C., Myhre, G., … White, J. W. C. (2019). Very Strong Atmospheric Methane Growth in the 4 Years 2014–2017: Implications for the Paris Agreement [_eprint: https://agupubs.onlinelibrary.wiley.com/doi/pdf/10.1029/2018GB006009]. *Global Biogeochemical Cycles*, *33*(3), 318–342. https://doi.org/10.1029/2018GB006009

Sander, R., Baumgaertner, A., Cabrera-Perez, D., Frank, F., Gromov, S., Grooß, J.-U., Harder, H., Huijnen, V., Jöckel, P., Karydis, V. A., Niemeyer, K. E., Pozzer, A., Riede, H., Schultz, M. G., Taraborrelli, D., & Tauer, S. (2019). The community atmospheric chemistry box model CAABA/MECCA-4.0 [Publisher: Copernicus GmbH]. *Geoscientific Model Development*, *12*(4), 1365–1385. https://doi.org/10.5194/gmd-12-1365-2019

Schultz, M. G., Schröder, S., Lyapina, O., Cooper, O. R., Galbally, I., Petropavlovskikh, I., von Schneidemesser, E., Tanimoto, H., Elshorbany, Y., Naja, M., Seguel, R. J., Dauert, U., Eckhardt, P., Feigenspan, S., Fiebig, M., Hjellbrekke, A.-G., Hong, Y.-D., Kjeld, P. C., Koide, H., … Zhiqiang, M. (2017). Tropospheric Ozone Assessment Report: Database and metrics data of global surface ozone observations (M. E. Chang & A. Lewis, Eds.). *Elementa: Science of the Anthropocene*, *5*, 58. https://doi.org/10.1525/elementa.244

Seinfeld, J. H. (2016). *Atmospheric Chemistry and Physics: From Air Pollution to Climate Change* (1st ed). John Wiley & Sons, Incorporated.

Skowron, A., Lee, D. S., & De León, R. R. (2015). Variation of radiative forcings and global warming potentials from regional aviation NO x emissions. *Atmospheric Environment*, *104*, 69–78. https://doi.org/10.1016/j.atmosenv.2014.12.043

Søvde, O. A., Matthes, S., Skowron, A., Iachetti, D., Lim, L., Owen, B., Hodnebrog, Ø., Di Genova, G., Pitari, G., Lee, D. S., Myhre, G., & Isaksen, I. S. (2014). Aircraft emission mitigation by changing route altitude: A multi-model estimate of aircraft NOx emission impact on O3 photochemistry. *Atmospheric Environment*, *95*, 468–479. https://doi.org/10.1016/j.atmosenv.2014.06.049

Stevenson, D. S., Doherty, R. M., Sanderson, M. G., Collins, W. J., Johnson, C. E., & Derwent, R. G. (2004). Radiative forcing from aircraft NO emissions: Mechanisms and seasonal dependence [_eprint: https://onlinelibrary.wiley.com/doi/pdf/10.1029/2004JD004759]. *Journal of Geophysical Research: Atmospheres*, *109*(D17). https://doi.org/10.1029/2004JD004759

Thor, R. N., Mertens, M., Matthes, S., Righi, M., Hendricks, J., Brinkop, S., Graf, P., Grewe, V., Jöckel, P., & Smith, S. (2023). An inconsistency in aviation emissions between CMIP5 and CMIP6 and the implications for short-lived species and their radiative forcing [Publisher: Copernicus

GmbH]. *Geoscientific Model Development*, *16*(5), 1459–1466. https://doi.org/10.5194/gmd-16-1459-2023

Tong, D., Pan, L., Chen, W., Lamsal, L., Lee, P., Tang, Y., Kim, H., Kondragunta, S., & Stajner, I. (2016). Impact of the 2008 Global Recession on air quality over the United States: Implications for surface ozone levels from changes in NOx emissions. *Geophysical Research Letters*, *43*(17), 9280–9288. https://doi.org/10.1002/2016GL069885

Tost, H., Jöckel, P., Kerkweg, A., Sander, R., & Lelieveld, J. (2006). Technical note: A new comprehensive SCAVenging submodel for global atmospheric chemistry modelling [Publisher: Copernicus GmbH]. *Atmospheric Chemistry and Physics*, *6*(3), 565–574. https://doi.org/10.5194/acp-6-565-2006

Turnock, S. T., Allen, R. J., Andrews, M., Bauer, S. E., Deushi, M., Emmons, L., Good, P., Horowitz, L., John, J. G., Michou, M., Nabat, P., Naik, V., Neubauer, D., O'Connor, F. M., Olivié, D., Oshima, N., Schulz, M., Sellar, A., Shim, S., … Zhang, J. (2020). Historical and future changes in air pollutants from CMIP6 models [Publisher: Copernicus GmbH]. *Atmospheric Chemistry and Physics*, *20*(23), 14547–14579. https://doi.org/10.5194/acp-20-14547-2020

Weidner, F. (2005). *Development and Application of a Versatile Balloon-Borne DOAS Spectrometer for Skylight Radiance and Atmospheric Trace Gas Profile Measurements* [PhD Thesis].

Young, P. J., Archibald, A. T., Bowman, K. W., Lamarque, J.-F., Naik, V., Stevenson, D. S., Tilmes, S., Voulgarakis, A., Wild, O., Bergmann, D., Cameron-Smith, P., Cionni, I., Collins, W. J., Dalsøren, S. B., Doherty, R. M., Eyring, V., Faluvegi, G., Horowitz, L. W., Josse, B., … Zeng, G. (2013). Pre-industrial to end 21st century projections of tropospheric ozone from the Atmospheric Chemistry and Climate Model Intercomparison Project (ACCMIP) [Publisher: Copernicus GmbH]. *Atmospheric Chemistry and Physics*, *13*(4), 2063–2090. https://doi.org/10.5194/acp-13-2063-2013

A

Additional Figures

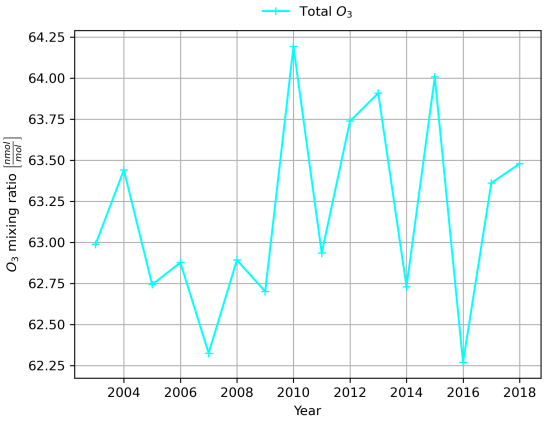

Figure A.1: The trend in the global annual molar mixing ratio average of O_3 of the whole troposphere

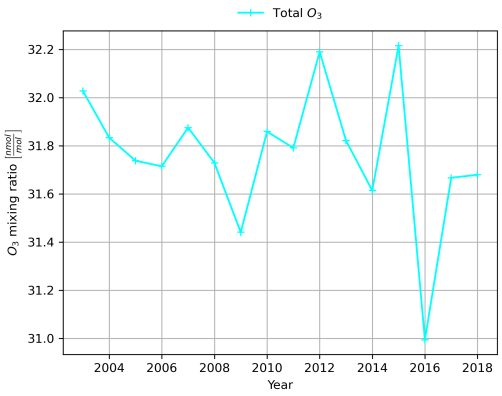

Figure A.2: The trend in the global annual molar mixing ratio average of O_3 at the ground level

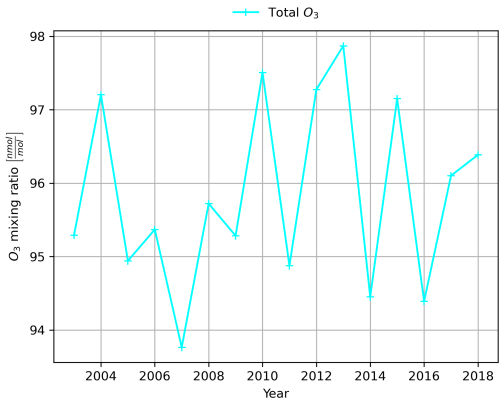

Figure A.3: The trend in the global annual molar mixing ratio average of O_3 at flight altitudes

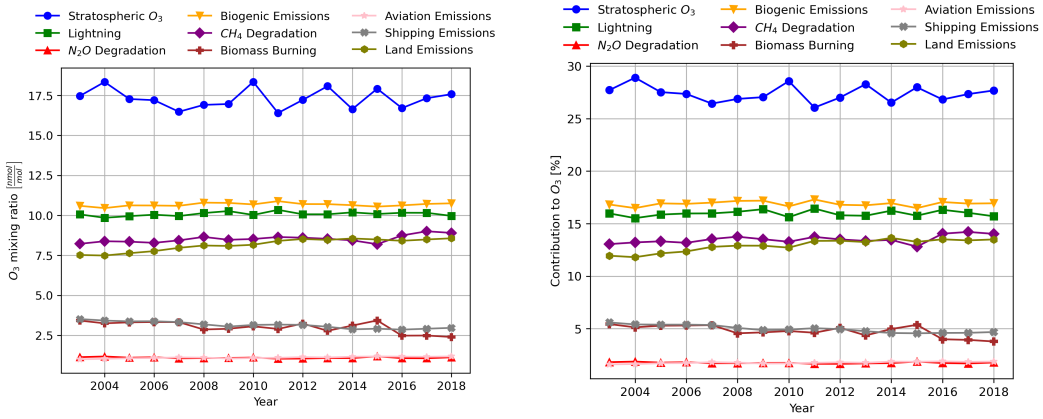

Figure A.4: Comparison of the temporal evolution in contribution to O_3 of different tagged sources for the whole troposphere in absolute values (left) and percentage contributions (right)

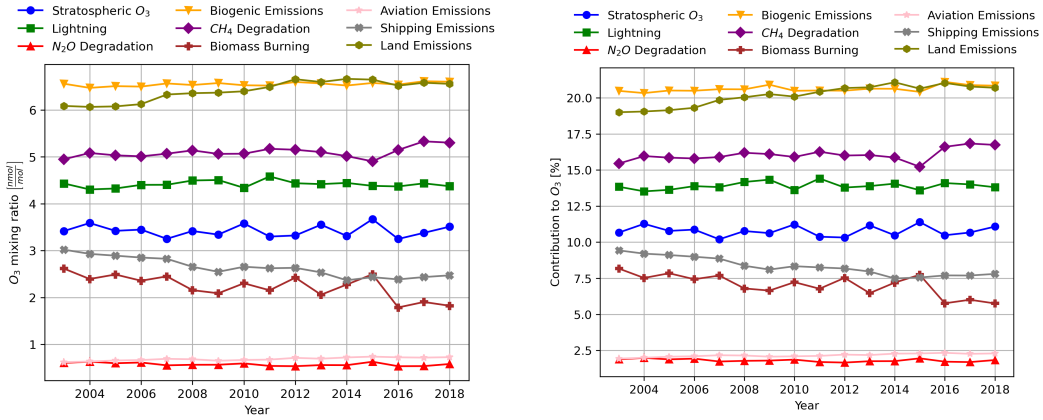

Figure A.5: Comparison of the temporal evolution in contribution to O_3 of different tagged sources for the ground level in absolute values (left) and percentage contributions (right)

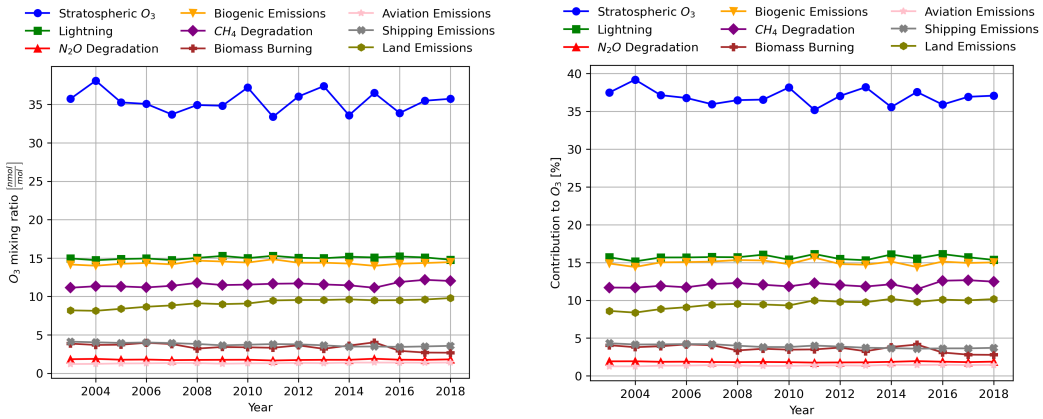

Figure A.6: Comparison of the temporal evolution in contribution to O_3 of different tagged sources at the flight altitudes in absolute values (left) and percentage contributions (right)

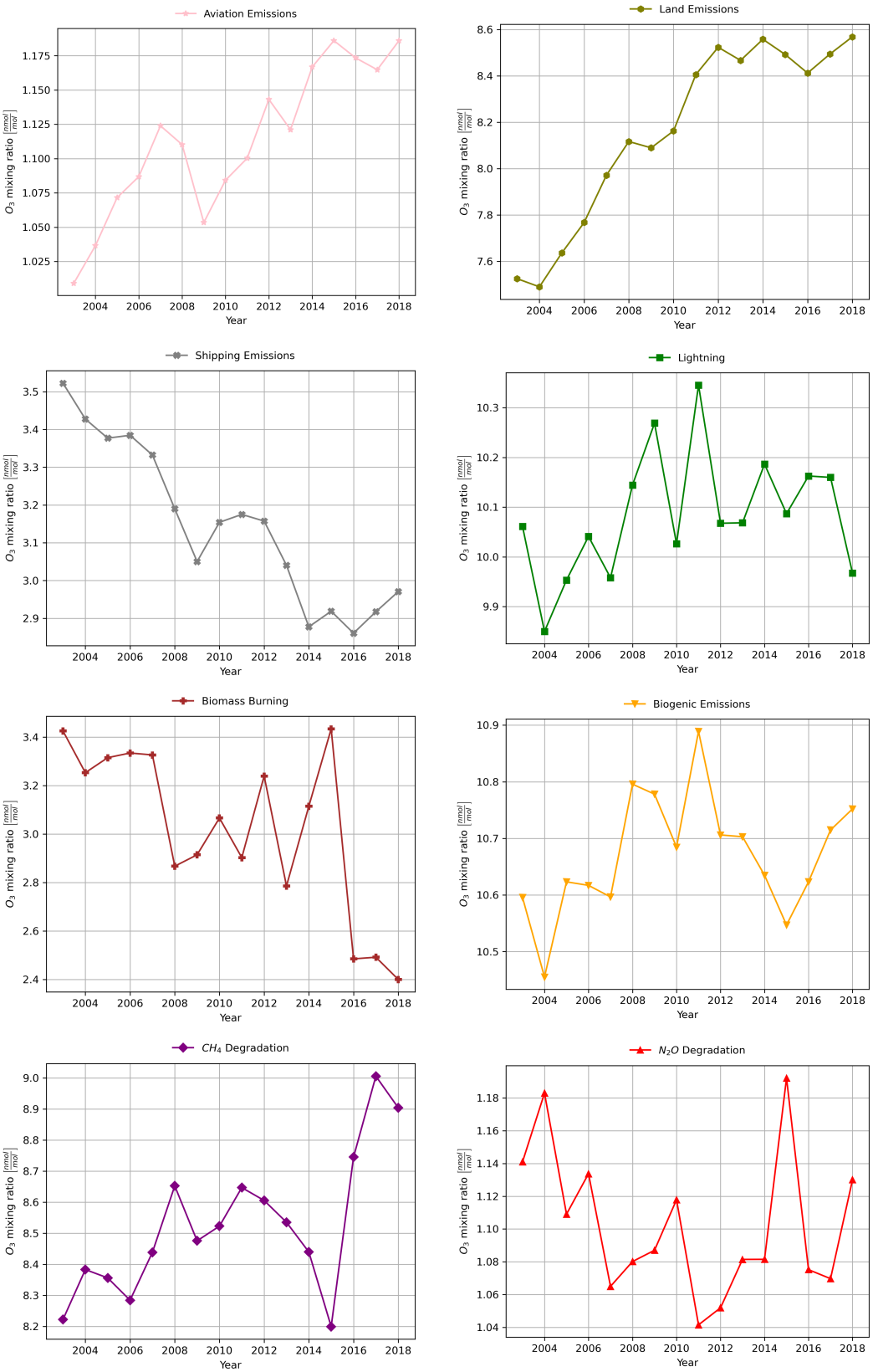

Figure A.7: Trends in contribution to O_3 of different tagged sources for the whole troposphere in absolute values

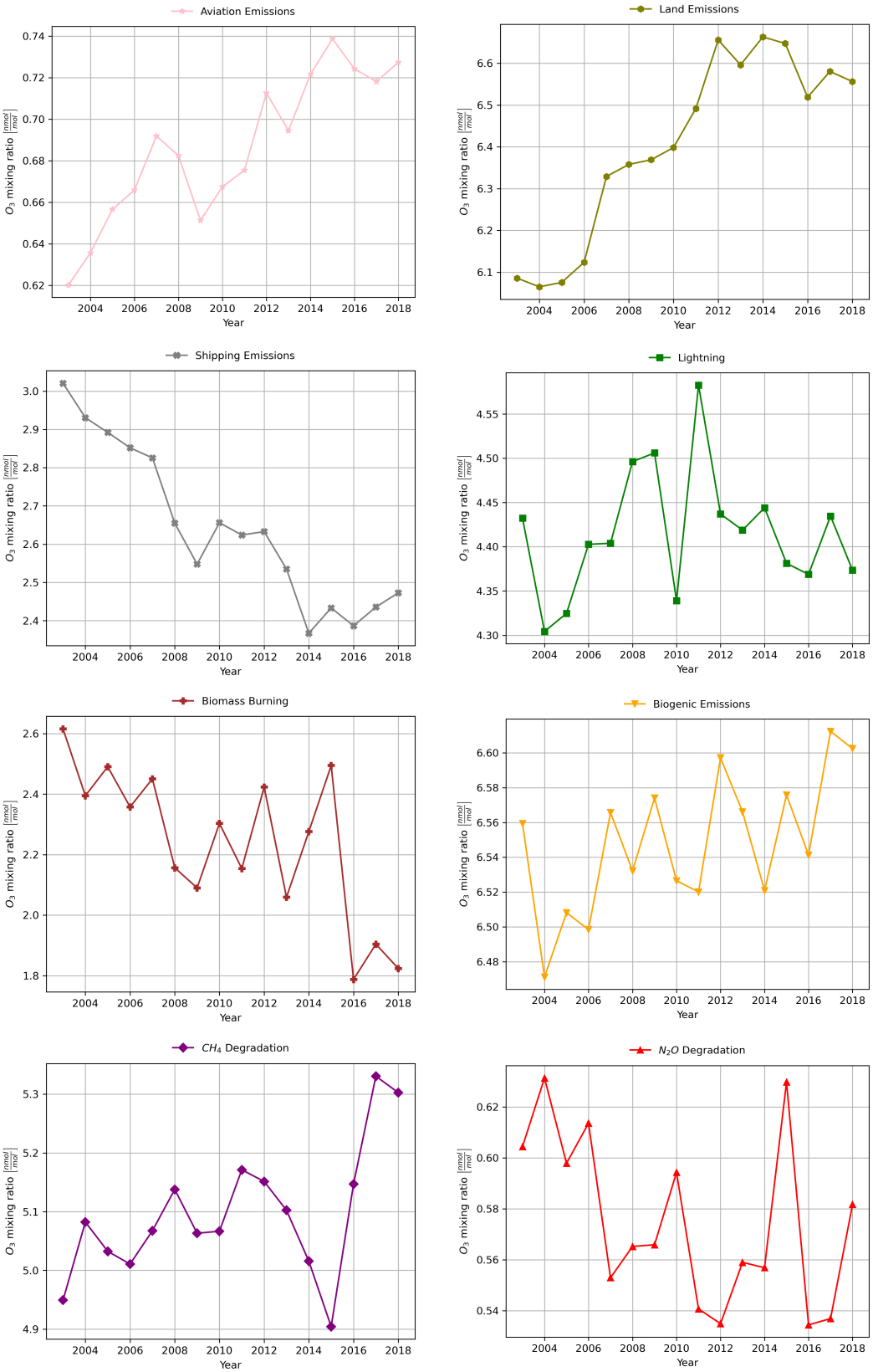

Figure A.8: Trends in contribution to O_3 of different tagged sources for the ground level in absolute values

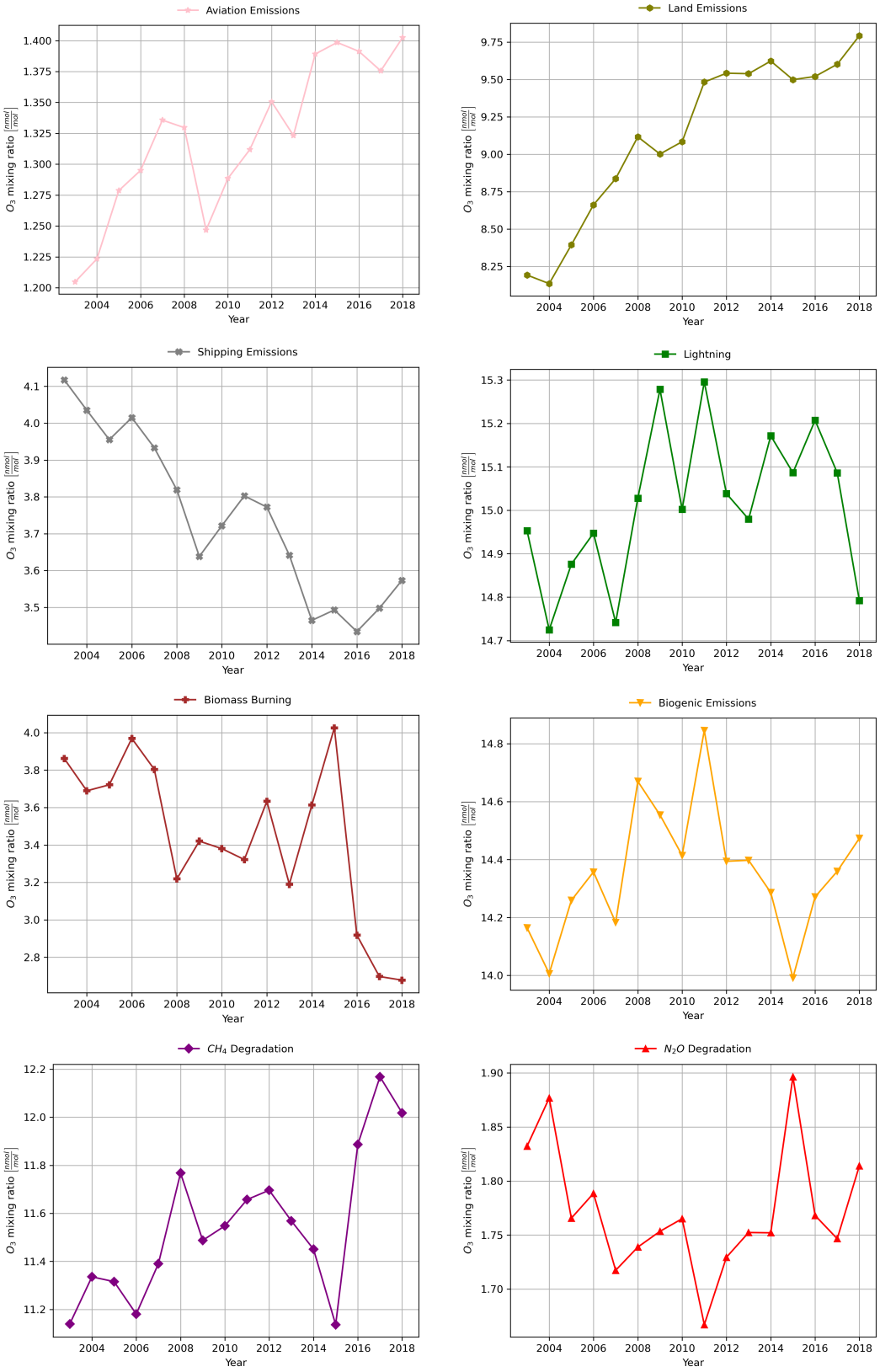

Figure A.9: Trends in contribution to O_3 of different tagged sources at flight altitudes in absolute values

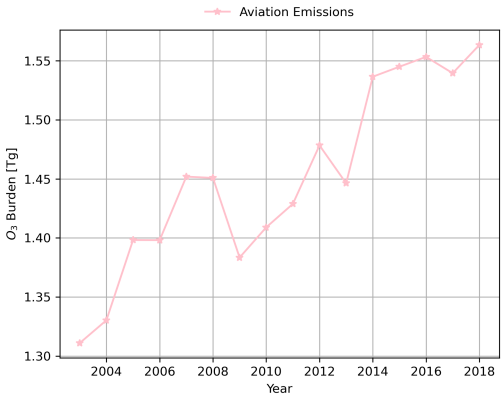

Figure A.10: Trend in the O_3 Burden of Aviation over Europe for the whole troposphere.

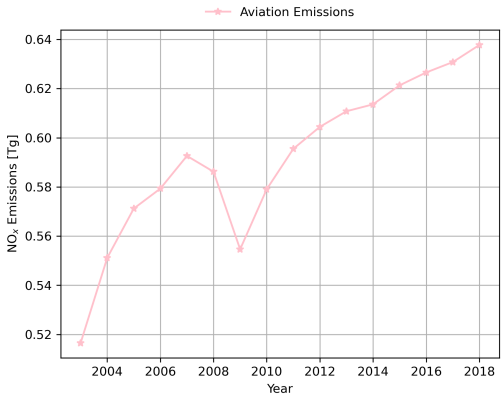

Figure A.11: Trend in the aviation NO_x emissions over Europe for the whole troposphere

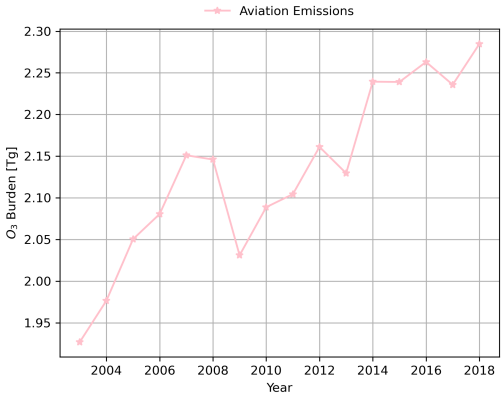

Figure A.12: Trend in the O_3 Burden of Aviation over North America for the whole troposphere.

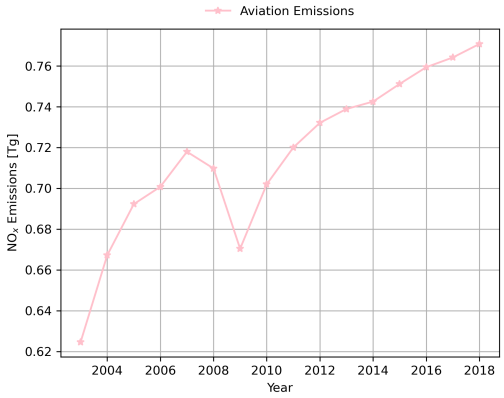

Figure A.13: Trend in the aviation NO_x emissions over North America for the whole troposphere

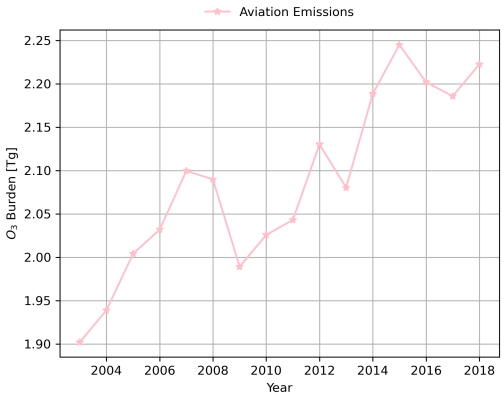

Figure A.14: Trend in the O_3 Burden of Aviation over Asia for the whole troposphere.

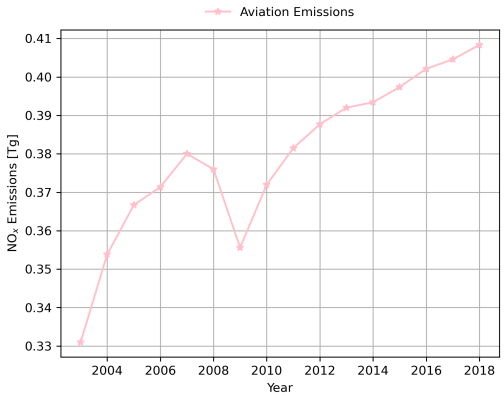

Figure A.15: Trend in the aviation NO_x emissions over Asia for the whole troposphere